11 Manganese: Predominant Role of Nodules and Crusts

Geoffrey P. Glasby

11.1 Introduction

The importance of manganese in the marine environment can be deduced from the fact that it is the tenth most abundant element in the Earth's crust (av. conc. 0.093%) and is available in two valency states whose stability boundary lies within the range of the natural environment (Glasby 1984). Manganese oxides also have a high adsorption capacity. δMnO_2, for example, has a surface area of about 260 $m^2 g^{-1}$ and a pH_{zpc} of 2.25 and can therefore adsorb cations such as Ni^{2+}, Cu^{2+} and Zn^{2+} from natural waters. By comparison, iron is the fourth most abundant element in the Earth's crust (av. conc. 5.17%) giving an average Mn/Fe ratio of 0.02. It also occurs in two valency states whose stability boundary lies within the range of the natural environment. Fe oxyhydroxides have a high adsorption capacity and large surface area. Goethite has a pH_{zpc} of 7.1 and can adsorb both cations (REE^{3+}) and anions (e.g. PO_4^{3-}, $MoO_4^{2-}$and WO_4^{2-}).

Both elements can therefore migrate under the influence of redox gradients. They can also fractionate from each other, particularly under acid or reducing conditions such as in lakes and shallow seas or in marine sediments. FeS_2 plays a major role in separating Mn and Fe in anoxic marine environments such as in Baltic Sea sediments where SO_4^{2-} ions are present. The reduced form of manganese, Ca-rhodochrosite ($CaMnCO_3$), is much rarer than FeS_2 but it is found in environments such as Gotland Deep sediments. Mn is more mobile than Fe. Mn therefore migrates more readily than Fe but Fe deposits more readily than Mn. This leads to the fractionation of Mn from Fe as, for example, in submarine hydrothermal systems or in anoxic environments such as Baltic Sea deeps.

The formation of huge quantities of manganese nodules and crusts on the deep-sea floor is a function of the fact that manganese and iron are relatively abundant in the Earth's crust and migrate from less oxidizing to more oxidizing environments. The increased glaciation of Antarctica about 12 Ma led to the initiation of Antarctic Bottom Water (AABW) flow and the increased ventilation of the deep ocean. The modern, well-oxygenated deep-sea has therefore become the ultimate repository for manganese. Deep-sea Mn nodules formed since the lower Miocene unconformity (12 Ma) hold about 10^{11} t of Mn (about 16 times the total Mn in terrestrial deposits) reflecting the importance of manganese nodules in the global cycle of manganese (Glasby 1988). The high contents of Co, Ni, Cu and Zn in manganese nodules and crusts make these deposits an important potential economic resource for these elements and are a function of the sorption characteristics of the manganese and iron oxyhydroxides.

11.2 Manganese, Iron and Trace Elements in Seawater

Manganese occurs in seawater mainly as Mn^{2+} or $MnCl^+$ (Bruland 1983). The dissolved Mn concentration in the open ocean is in range 0.2-3 nmol kg^{-1} which is above the equilibrium concentration with respect to MnO_2 or MnOOH. This situation reflects the slow rate of oxidation of Mn^{2+} in solution.

Figure 11.1 shows the vertical distribution of Mn in seawater at the VERTEX-IV site situated in the centre of the central North Pacific subtropical gyre, a region of low biological productivity (Bruland et al. 1994). The high content of Mn in the surface waters reflects the input of eolian material into this region from Asia. Photoreduction of particulate MnO_2 to Mn(II) takes place in the surface waters resulting in 99% of the Mn in the surface waters (0-100 m) being in the dissolved form. By contrast, only 80% of the Mn in the deep water (500-4,000 m) is in the dissolved form. Mn therefore

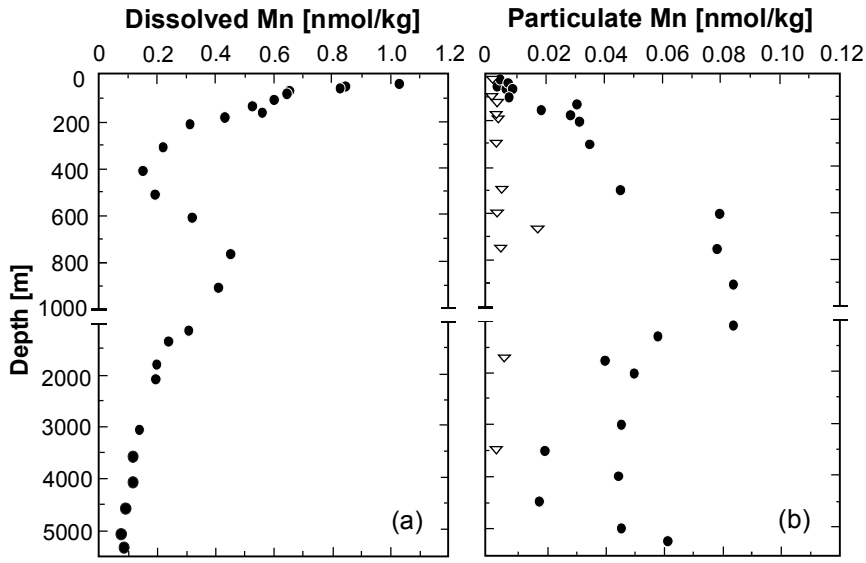

Fig. 11.1 Vertical profiles of (a) dissolved manganese (nmol kg^{-1}) and (b) particulate manganese (nmol kg^{-1}) at the VERTEX-IV site (after Bruland et al. 1994). For particulate manganese, filled circles represent the acetic acid leachable fraction and open triangles represent refractory manganese.

behaves in seawater as a scavenged-type metal. Bacterial mediation plays a key role in the scavenging and oxidation of dissolved Mn in intermediate and deep water. The higher concentration of particulate Mn in North Atlantic deep water (0.15 nmol kg^{-1}) than in central North Pacific deep water (0.05 nmol kg^{-1}) reflects the higher input of eolian material into the Atlantic compared to the Pacific Ocean.

Mn is also influenced by redox processes in the water column. Both dissolved and particulate Mn display maxima at the oxygen minimum zone which occurs at a depth of 500-1,000 m in the central North Pacific (Fig. 11.1). In this case, the maximum dissolved Mn concentration in the oxygen minimum zone is about 0.4 nmol kg^{-1}. This high concentration was considered to be the result of lateral transport of Mn from the continental margins to the open ocean along the oxygen minimum zone (Martin et al. 1985) and to be particularly important in the highly oxygen-deficient waters of the oxygen minimum zone in parts of the eastern North Pacific Ocean (Burton and Statham 1988). However, Johnson et al. (1996) have subsequently argued that a decrease in the oxidation rate of Mn (II) within the oxygen minimum zone is a more likely mechanism for the enrichment of manganese there, thus obviating the need for the lateral transport of Mn from the continental margins.

About 90% of the Mn introduced to the oceans has a hydrothermal origin (Glasby 1988). Hydrothermal Mn anomalies in seawater can be detected over 1,000 km from the source in the Pacific Ocean (Burton and Statham 1988). When hydrothermal fluids are discharged at the sea floor, a buoyant hydrothermal plume is formed on mixing of the hydrothermal fluid with seawater (Lilley et al. 1995; Lupton 1998; German and Van Damm 2004). The plume can rise tens to hundreds of meters above the sea floor to a level of neutral buoyancy where it forms a distinct hydrographic layer with a distribution extending tens to thousands of kilometers from the vent. The dilution factor of the vent fluid with respect to seawater is of the order of 10^4-10^5. In the first centimeters to meters above the vent, up to 50% of the iron is precipitated as sulfides. The chalcophile elements (Cu, Zn, Cd and Pb) tend to be incorporated in the sulfide minerals at this stage. The remaining Fe is precipitated over a longer time period as fine-grained iron oxyhydroxide particles. The half life for Fe (II) precipitation is 2-3 minutes. The iron oxyhydroxide particles scavenge anionic species such as HPO_4^{2-}, CrO_4^{2-}, VO_4^{2-} and $HAsO_4^{2-}$ as well as the rare earth elements (REE). Precipitation of particulate Mn oxides takes place much more slowly, mainly in the neutrally buoyant plume where the oxidation is bacterially mediated. Because of the slow precipitation rate, particulate Mn concentrations increase in the plume to a maximum 80-150 km from the vent. 80% of the hydrothermal Mn is deposited on the sea floor within several hundred km of the vent field but the remaining Mn still raises the background concentration of Mn in seawater several-fold (Lavelle et al. 1992). The residence time of hydrothermal Mn in seawater is several years. German and Angel (1995) have estimated that the total hydrothermal Mn flux to the oceans is $6.85 \cdot 10^9$ kg yr^{-1}. This

compares with the flux of Mn from the rivers of $0.27 \cdot 10^9$ kg yr^{-1} (Elderfield and Schulz 1996) confirming the original calculation of Glasby (1988).

The predominance field of Mn in seawater (Glasby and Schulz 1999) is best illustrated by the use of an E_H, pH diagram (Fig. 11.2). At the conditions prevalent in seawater (E_H +0.4 V, pH 8), the stable form of Mn is seen to be the aqueous species, Mn^{2+}, and not any of the solid phases of Mn. The fact that Mn oxides are abundant on the seafloor can be explained on the basis that the Mn oxyhydroxides initially formed in seawater (β-manganite) are not pure mineral phases but have significant concentrations of transition elements and are fine grained, both of which help to stabilize them (Glasby 1974). In fact, 10 Å manganate and δMnO_2 are the principal manganese oxide minerals found in deep-sea manganese nodules (see section 11.4.8) but the free energies of formation of these fine-grained minerals have not been determined. However, the fact that the aqueous species of Mn appear more stable than any of the solid phases of Mn under deep-sea conditions probably explains the slow rate of oxidation of Mn in sea-water.

The kinetics of oxidation of Mn^{2+} in seawater have been discussed by Murray and Brewer (1977) and the following reaction sequence has been proposed.

$$Mn(II) + O_2 \rightarrow MnO_{2\,s} \qquad \textit{slow}$$

$$Mn(II) + MnO_{2\,s} \rightarrow (Mn(II).MnO_2)_s \qquad \textit{fast}$$

$$(Mn(II).MnO_2)_s + O_2 \rightarrow 2MnO_{2\,s} \qquad \textit{slow}$$

$$-d(Mn(II))/\,dt \rightarrow k_o(Mn(II)) + k_1(Mn(II))(MnO_{2\,s})(P_{O2})(OH^-)^2$$

This rate law demonstrates that the oxidation of Mn (II) in seawater is autocatalytic. From this equation, it was calculated that it would take about 1,000 years to oxidize 90% of the Mn present in seawater. Surface catalysis on MnO_2 or FeOOH or bacterial oxidation is therefore required to increase the rate of deposition of Mn^{2+} from solution (Cowen and Bruland 1985; Mandernack et al. 1985; Ehrlich 1996; Hastings and Emerson 1986; Tebo et al. 1997, 2004). Giovanoli and Arrhenius (1988) also proposed that the surface catalyzed oxidation of Mn^{2+} by FeOOH is a rate-controlling step in the formation of marine manganese

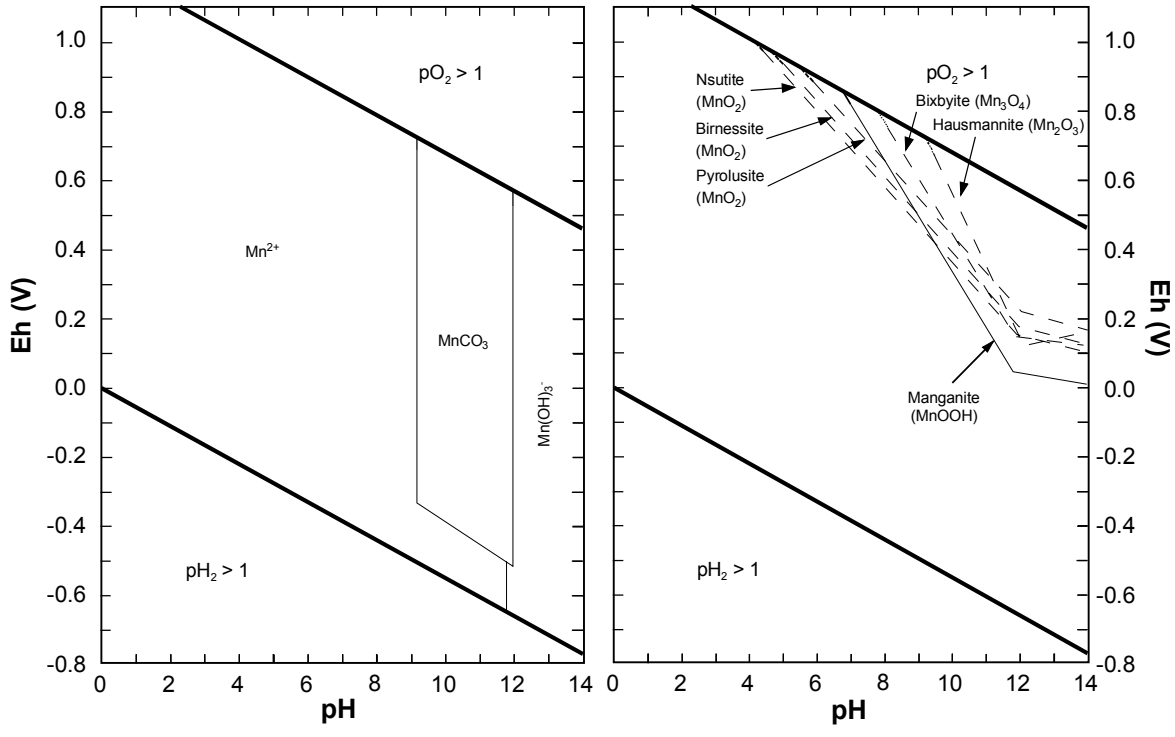

Fig. 11.2 E_H, pH diagram for Mn calculated for the chemical conditions prevailing in the deep sea (after Glasby and Schulz 1999). Note that, under seawater conditions and at an E_H, of +0.4 V and a pH of 8, the stable form of Mn is the aqueous species, Mn^{2+}, and not any of the solid phases of Mn.

deposits. Rate equations and rate constants for the oxidation of manganese in seawater based on field data have been determined by Yeats and Strain (1990), von Langen et al. (1997) and Morgan (2005).

By contrast, the form and concentration of iron in seawater remain poorly known because of the pronounced tendency of Fe(III) species to hydrolyze in aqueous solution (Bruland 1983) (see Chap. 7). Iron occurs in seawater mainly in the hydrolyzed forms $Fe(OH)_3°$ and $Fe(OH)_2^+$ and as $FeCl^+$. The concentration range of Fe in seawater is 0.1-2.5 nmol kg^{-1} giving a Mn/Fe ratio of about unity which is much greater than that in the Earth's crust.

Figure 11.3 shows the vertical distribution of Fe in seawater at the VERTEX-IV site (Bruland et al. 1994). Dissolved Fe shows a maximum concentration in the surface mixed layer (0.35 nmol kg^{-1}) but this declines to a minimum in the subsurface stratified layer (70-100 m) (0.02 nmol kg^{-1}). The high concentration of Fe in the surface waters reflects the strong eolian input into this region. The Fe in the surface layer is rapidly consumed by plankton but is recycled within days. Below 100 m, dissolved Fe displays a nutrient-type distribution. In deep water, the dissolved Fe concentration reaches a value of 0.38 nmol kg^{-1} Fe. Iron is a limiting nutrient in open-ocean surface waters characterized by high nitrate and low chlorophyll contents. Proposals have been made to seed the oceans with Fe in order to stimulate phyto-plankton growth which would hopefully reduce the levels of atmospheric CO_2 (de Baar et al. 1995; Fitzwater et al. 1996). Johnson et al. (1997) have recently presented a model describing the factors controlling the dissolved Fe content in seawater.

Particulate Fe does not show an eolian influence in the surface layer and its distribution is more constant with depth. 48% of Fe in the surface water (0-100 m) is in the dissolved form and 55% in deep water (500 -4,000 m). Most of the particulate Fe in the intermediate and deep water is in the form of refractory alumino-silicate minerals of eolian origin. The higher concentration of particulate Fe in North Atlantic deep water (1.2 nmol kg^{-1}) than in central North Pacific deep water (0.3 nmol kg^{-1}) again reflects the higher input of eolian material into the Atlantic compared to the Pacific Ocean.

Fe behaves in seawater in part as a scavenged-type element and in part as a nutrient-type element as shown by the strong correlation of dissolved Fe with nitrate and phosphate at depths below 100 m.

The stability field of Fe in seawater is best illustrated by the use of an E_H, pH diagram (Fig. 11.4). Solid $Fe(OH)_3$ is shown as the metastable form of iron at the conditions prevalent in sea-water (E_H +0.4 V, pH 8). Actually, akagenéite (β-FeOOH) is the more stable form found in deep-sea manganese nodules (see Sect. 11.4.8) but its free energy of formation has not been determined.

Of the trace elements that are of most interest in the formation of manganese nodules, Co is present in deep ocean water at concentrations of <0.1 nmol kg^{-1}, mainly as Co^{2+}, $CoCO_3°$ and $CoCl^+$ (Bruland 1983; Burton and Statham 1988; Nozaki 1997). Its extremely low concentration suggests that it is rapidly removed from seawater, probably scavenged by manganese oxides. Ni is present in deep ocean water at concentrations of about 10 nmol kg^{-1}, mainly as Ni^{2+} , $NiCO_3°$

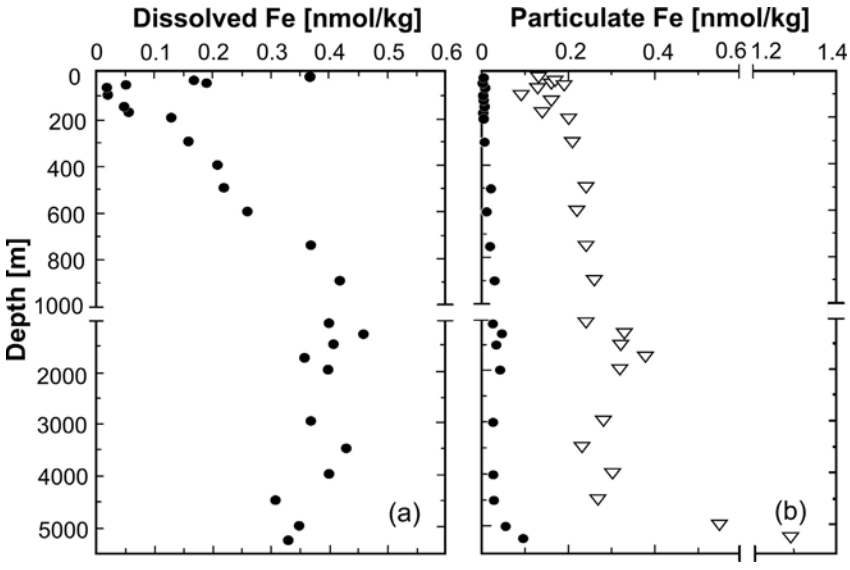

Fig. 11.3 Vertical profiles of (a) dissolved iron (nmol kg^{-1}) and (b) particulate iron (nmol kg^{-1}) at the VERTEX-IV site (after Bruland et al. 1994). For particulate iron, filled circles represent the acetic acid leachable fraction and open triangles represent refractory iron.

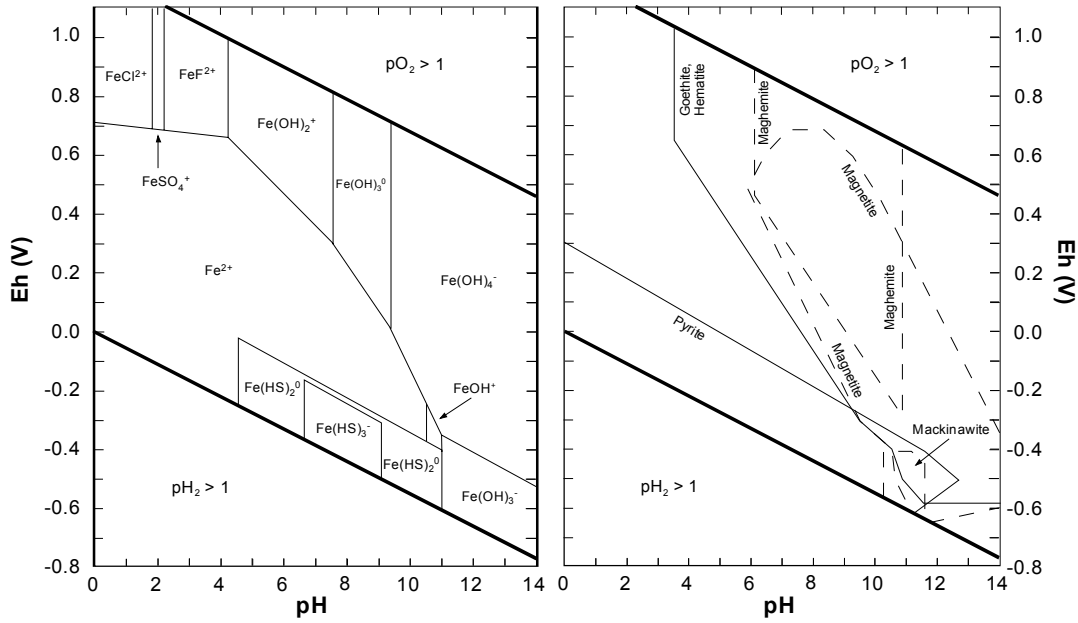

Fig. 11.4 E_H, pH diagram for Fe calculated for the chemical conditions prevailing in the deep sea (after Glasby and Schulz 1999). Note that, under seawater conditions and at an E_H, of +0.4 V and a pH of 8, the metastable form of Fe is $Fe(OH)_3$ and the stable forms magnetite ((Fe, Mg) Fe_2O_4) and maghemite (Fe_2O_3).

and $NiCl^+$, and displays a nutrient-type behavior in seawater. Cu is present in deep ocean water at concentrations of about 6 nmol kg^{-1}, mainly as $CuCO_3°$, $CuOH^+$ and Cu^{2+}, and has a distribution intermediate between that of nutrient-type elements and Mn. Zn is present in deep ocean water at concentrations of about 8 nmol kg^{-1}, mainly as Zn^{2+}, $ZnOH^+$, $ZnCO_3°$, and $ZnCl^{2+}$, and displays a nutrient-type behavior in seawater.

Trace metals in seawater can be characterized as scavenged-type or nutrient-type elements (Bruland et al. 1994; Bruland and Lohan, 2004). On this basis, Co is mainly a scavenged-type element, Ni and Zn are nutrient-type elements, Fe displays an intermediate behavior and Mn is a scavenged-type element strongly influenced by redox processes. Nutrient-type elements have much longer deep-sea residence times than scavenged-type elements. For Zn, this has been estimated to be 22,000 - 45,000 years, for Fe 70 - 140 years and for Mn 20 - 40 years. The residence times for Fe and Mn are short compared to the general oceanic turnover time of about 1,500 years (Bender et al. 1977). The rapid removal of Mn from seawater accounts for its significant fractionation between oceanic basins as well as the widespread occurrence of manganese deposits on the deep-sea floor.

11.3 Sediments

11.3.1 Manganese, Iron and Trace Elements in Deep-Sea Sediments

The distribution of elements in deep-sea sediments has been discussed by Bischoff et al. (1979), Stoffers et al. (1981, 1985), Meylan et al. (1982), Aplin and Cronan (1985), Baturin (1988), Chester (1990), Glasby (1991) and Miller and Cronan (1994).

Deep-sea sediments cover more than 50% of the earth's surface and consist of carbonates, red clay and siliceous ooze (cf. Chap. 1). On average, red clay covers about 31% of the world's ocean basins but its abundance is much higher in the Pacific (49%) than in the Atlantic (26%) and Indian (25%) Oceans (Glasby 1991). Carbonates act as a diluent for the transition elements in deep-sea sediments because of the low contents of these elements in them and the composition of deep-sea sediments is therefore often presented on a carbonate-free basis.

Red clays are mainly allogenic in origin (Glasby 1991). In the Pacific, this allogenic component is dominantly eolian dust. The high input of dust from

the deserts of central Asia explains the higher sedimentation rates of the noncarbonate fraction of sediments from the North Pacific (0.5-6 mm ka^{-1}) than those of sediments from the South Pacific (0.4 mm ka^{-1}). Because of its composite origin, red clay has a similar composition to that of average shale. However, a number of elements are enriched in red clay relative to average shale. These include the transition elements (Mn, Co, Ni, Cu) and Ba (Table 11.1). The transition elements constitute the authigenic fraction of the sediments whereas Ba is biogenically introduced into the sediments as barite. The Fe contents of red clay and average shale, on the other hand, are similar. Red clays are enriched in Mn relative to average shale by a factor of 7, in Co by a factor of 4, in Ni by a factor of 3, in Cu by a factor of 5 and in Fe by a factor of 1.4. By contrast, mildly reducing or seasonally oxidizing nearshore sediments do not incorporate an authigenic fraction and the composition of these sediments is similar to that of average shale. Nonetheless, elevated concentrations of manganese in surficial coastal sediments are well documented (Overnell et al. 1996; Overnell 2002).

The occurrence of an authigenic fraction in red clays reflects the fact that Mn occurs in two valencies and can migrate to regions where more oxidizing conditions prevail. Within red clays, Mn is dominantly in the tetravalent state with an average O:Mn ratio of 1.89 ± 0.05 (Murray et al. 1984). The presence of Mn oxides in the sediments leads to scavenging of transition elements such as Co, Ni and Cu.

The hemipelagic/pelagic transition is important in defining the nature of red clays. This boundary is a redox transition zone. Red clays form in regions of low sedimentation rate where the rate of organic matter deposition is very low. In these sediments, diffusion of oxygen into the sediments exceeds its rate of consumption in oxidizing organic matter. The sediments therefore remain brown throughout their length and Mn, Co, Ni and Cu are enriched in the authigenic fraction of the sediments. Oxic sediments are characterized by sedimentation rates of <40 mm ka^{-1} in regions of moderate productivity. In these sediments, iron is present dominantly in the trivalent state and reduction of nitrate in the pore waters by organic carbon does not occur.

An inverse relationship has been observed between the transition metal contents (Mn, Co, Ni and Cu) of red clays and the sedimentation rate (Krishnaswamy 1976). This relationship suggests that these sediments are characterized by a uniform rate of deposition of the authigenic elements superimposed on a variable deposition rate of detrital elements. This model explains the high concentration of authigenic elements in Pacific pelagic clays where sedimentation rates are low. The higher Mn content of red clays from the South Pacific compared to those from the North Pacific reflects the lower rates of sedimentation there. Chemical leaching techniques have been used to identify the forms of elements in red clays. About 90% Mn, 80% Co and Ni and 50% Cu are considered to be of authigenic origin whereas >90% of Fe is thought to be of detrital origin. Fe therefore occurs dominantly in the allogenic phase of these sediments. Table 11.2 suggests that most of the transition elements are delivered to the sediment/water interface associated with large organic aggregates.

Chemical analyses of red clays taken on a series of transects across the Southwestern Pacific Basin have shown that there is a systematic change in the composition of the red clays across the basin. On a transect from the base of the New Zealand continental slope to Rarotonga, Mn was shown to increase from 0.3-1.4%, Fe from 3-8 %, Co from 25-250 ppm, Ni from 50-250 ppm and Cu from 75-325 ppm (Meylan et al. 1982). However, relative to each other, the elements show an enrichment sequence along the transect of Co>Ni>Mn ≈ Cu>Fe. Mössbauer studies also showed a marked increase in the Fe^{3+}:Fe^{2+} ratio in the sediments with increasing distance from New Zealand which was attributed to the incorporation of Fe oxyhydroxides, probably ferrihydrite, into the sediments (Johnston and Glasby 1982). By contrast, Fe^{2+} is thought to occur in the sediments mainly in montmorillonite and chlorite. A decrease in sedimentation rate from 32 to 2 mm ka^{-1} was also observed along this transect (Schmitz et al. 1986). The sediments on this transect therefore show a decrease in grain size, an increased darkening of the sediments from pale yellowish brown to dusky

Table 11.1 Comparison of the transition metal and Ba contents of Pacific Pelagic Clay and average shale. Mn and Fe in per cent; Co, Ni, Cu and Ba in ppm (after Glasby 1991).

	Pacific Pelagic Clay	Average shale
Mn	0.43	0.05
Fe	5.4	5.2
Co	113	8
Ni	210	29
Cu	230	45
Ba	3900	250

Table 11.2 Rates of deposition (μg cm^{-2} $10^3 yr^{-1}$) of transition elements from eolian dust and organic aggregates and into red clays (after Glasby 1991).

	Dust	Organic aggregates	Red clay
Mn	20-70	1565	1020-1230
Fe	3000-5800	16175	1560-3500
Co	2.7-4	12	4-14
Ni	14-20	15	20
Cu	20-30	490	28-34

brown, increasing transition metal contents, increasing oxidation state of iron, decreasing sedimentation rate and increased abundance of deep-sea manganese nodules with increasing distance from New Zealand. The dusky brown sediments are rich in phillipsite and manganese micronodules (Glasby et al. 1980). Several of the changes along the transect were thought to reflect an increase in the degree of oxidation of the sediments with decreasing sediment accumulation rate caused by a longer contact time of the sediment surface with well-oxygenated ocean bottom water. On a transect from the crest of the East Pacific Rise to New Zealand at 42°S, Stoffers et al. (1985) found similar increases in the contents of Mn, Fe, Co, Ni and Cu in sediments with increasing distance from New Zealand.

In a detailed comparison of sediments from the equatorial North Pacific high productivity zone (Area C) and the low productivity SW Pacific subtropical anticyclonic gyre (Area K), Stoffers et al. (1981) showed that the siliceous oozes from the equatorial North Pacific have much higher contents of Mn, Ni, Cu and Ba but lower contents of Fe and Co than the red clays from the SW Pacific (Table 11.3). Sedimentation rates on a carbonate-free basis for the two areas are of the same order (1-3 mm ka^{-1} for the equatorial North Pacific and 0.5-1 mm ka^{-1} for the SW Pacific). Differences in the transition metal contents of these sediments were therefore considered to be controlled by sediment type rather than sedimentation rate. Calculations based on the equations of Bischoff et al. (1979) confirmed that the hydrogenous (authigenic) component was much higher in Area C (7.9%) than in Area K (3.2%) sediments.

In addition to the authigenic component, there may also be a hydrothermal component in deep-sea sediments. During DSDP cruise 92, the variation in composition of sediments from three drill cores and several piston cores taken on a transect away from the crest of the East Pacific Rise was determined (Lyle et al. 1986; Marchig and Erzinger 1986). It was shown that the Mn accumulation rate in sediments falls off rapidly with increasing distance becoming relatively small 1,000 km from the ridge crest. At 19-20°S, for example, the Mn accumulation rate in the surface sediments declined from 36 mg cm^{-2} ka^{-1} at the ridge crest to 0.2 mg cm^{-2} ka^{-1} 1,130 km away. The corresponding decrease for Fe was from 120 mg cm^{-2} ka^{-1} to 0.68 mg cm^{-2} ka^{-1}. In a similar study at 42°S, the hydrothermal component was shown to decline from about 75% at the ridge crest to zero about 1,000 km away (Stoffers et al. 1985) (Fig. 11.5).

11.3.2 Diagenetic Processes in Deep-sea Sediments

The nature of the diagenetic changes occurring in pelagic sediments depends on the influx of decomposable organic matter to the sediment and the metabolic rate of oxidation (Müller et al. 1988). Three types of diagenetic processes can be distinguished: oxic diagenesis, suboxic diagenesis and anoxic diagenesis. Oxic diagenesis takes place when oxygen remains in the pore waters as in red clays. Mn concentrations in the pore waters remain extremely low (of the order of 2 μg l^{-1}) compared to a concentration of about 0.2 μg l^{-1} in ocean bottom water. Suboxic diagenesis takes place when nitrate reduction occurs in the core and the oxygen content in the pore waters becomes very low. Dissolved Mn concentrations in the pore water can then increase by several orders of magnitude (>1,000 μg l^{-1}) compared to ocean bottom water. Anoxic diagenesis takes place in stratified anoxic basins

Table 11.3 Comparison of the transition metal and Ba contents of sediments (on a carbonate-free basis) from Areas C and K. Mn and Fe in per cent; Co, Ni, Cu and Ba in ppm (after Stoffers et al. 1981).

	Area C	Area K
Mn	1.97	0.8
Fe	4.8	8.39
Co	129	155
Ni	677	235
Cu	1044	275
Ba	3921	730

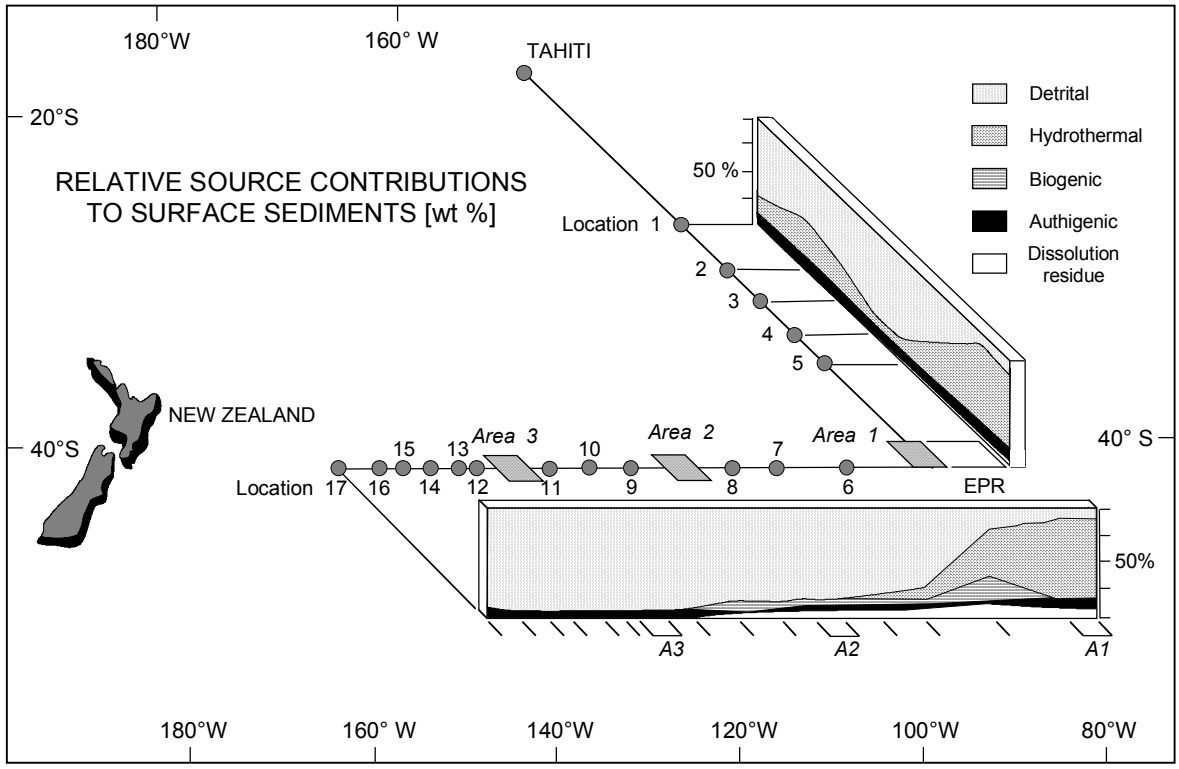

Fig. 11.5 Distribution of the normative sediment components; weight percent of the five individual components present in the sediments along the Tahiti - EPR - New Zealand transect (after Stoffers et al. 1985)

characterized by a well-developed halocline which prevents mixing of the anoxic basinal waters with the overlying sea-water as well as in the deeper layers of sediments from well-oxygenated coastal and upwelling environments. This leads to extensive diffusion of Mn and Fe into the water column from the underlying sediments. As an example, the dissolved Mn and Fe contents attain concentrations of <700 and 120 µg l^{-1} respectively in the anoxic waters of the Gotland Deep, Baltic Sea (Glasby et al. 1997). The diagenetic pathway taken depends principally on the rate of organic carbon accumulation in the sediment.

Within red clays, the diffusive flux of Mn is small (23 µg cm^{-2} ka^{-1}) and corresponds to about 7% of the total sedimentation flux of Mn (Glasby 1991). Mn is therefore largely immobilized in red clays. By contrast, 96% of the Cu in red clays is regenerated from the sediment into the bottom water as a result of the diagenetic flux across the sediment/water interface. Red clays therefore provide a relatively low flux of Mn and transition elements to the sediment surface and this is not an important source of metals for manganese nodule formation in red clay areas.

Müller et al. (1988) have distinguished between 'deep diagenesis' and 'surficial diagenesis'. In Pacific red clays, deep diagenesis results in no significant net upward flux of Mn, Fe, Ni or Cu. Surficial diagenesis is more significant. In siliceous ooze sediments, the regeneration rate of Mn in the surface sediments is of the same order as the accretion rate of Mn in the associated Mn nodules. Surficial diagenesis is therefore a significant source of metals to manganese nodules in siliceous ooze areas. 96% of the metals in the associated manganese nodules come from this source.

In general, the thickness of the oxidized layer in the sediment increases from near-shore and hemipelagic to pelagic environments. This is illustrated in Figure 11.6 which shows the trends for the eastern equatorial Pacific. This diagram confirms the inverse relationship between the thickness of the oxidized layer in the sediment and the biological productivity in the overlying surface waters. In general, there is a transition from tan to green within these sediments resulting from the *in-situ* reduction of Fe (III) to Fe (II) in smectites at the iron redox transition-zone (Lyle 1983; Köning et al. 1997).

In a comparison of pore water profiles of red clays and hemipelagic sediments, Sawlan and Murray (1983) showed that Mn and Fe are below the detection limit in the pore waters of red clays, Ni is present in the same concentation as in ocean bottom water and Cu shows a pronounced maximum at the sediment-water interface. In hemipelagic clays, denitrification becomes important and remobilization of Mn and Fe takes place. Ni correlates with Mn in the pore waters suggesting that it is associated with the Mn oxides in the solid phase. Cu is regenerated very rapidly at the sediment-water interface. The diffusive flux of Mn in hemipelagic sediments was determined to be in the range 2,200-33,000 $\mu g\ cm^{-2}\ ka^{-1}$. More detailed studies of pore water profiles in five different areas of the Californian Borderland confirmed the importance of Mn recycling in the surface sediments when the oxygen content of the bottom waters exceeds 0.1 $ml\ l^{-1}$ (Shaw et al. 1990). Co and Ni appeared to be scavenged by Mn oxides and trapped in the surface sediments whereas the accumulation of Cu appeared to be more closely related to the flux of biogenic material to the sediment.

Based on a detailed study of pore water profiles in sediment cores from the eastern equatorial Atlantic, Froelich et al. (1979) were able to show that oxidants are consumed in the order of decreasing energy production per mole of organic carbon oxidized (O_2 > Mn oxides ≈ nitrate > Fe oxides > sulfate). A schematic representation of the profiles is shown in Figure 11.7. From this diagram, it is seen that the reduction and remobilization of Mn takes place in zone 4. This is followed by the upward diffusion and reoxidation of Mn in zone 3. This process enables Mn to be stripped from the sediments as they accumulate and to be redeposited as a discrete layer within the sediment column. An example of this process is given in Figure 3.8. Of course, the depth at which these processes take place is controlled by the influx of organic matter to the sediments which governs the nature of the diagenetic process occurring there. In regions of extremely high productivity characterized by organic-rich hemi-pelagic sediments (such as found in the Panama Basin), burrowing by macrofauna can markedly increase the rate of recycling of Mn in the bioturbated zone of these sediments (Aller 1990). In this situation, Mn-oxide rich sediments and organic matter are mixed into the anoxic layers of the sediment by bioturbation, thereby permitting remobilization of Mn^{2+} in the sediment column (Thamdrup and Canfield 1996). However, reduction of Mn oxides was shown to play only a minor role in the oxidation of organic carbon in continental margin sediments taken off Chile (Thamdrup and Canfield 1996) (see Chapter 7). The maintenance of high Mn oxide reduction rates therefore depends on the continuous mixing of Mn oxides and fresh organic matter into the sediments through bioturbation or other mixing processes.

In addition to the above examples of steady state diagenesis, non-steady state diagenesis may occur in deep-sea sediments when turbidites are deposited in abyssal plains (Thomson et al. 1987). A color difference is often seen in the upper layers of the turbidite. This is a consequence of the 'oxidation front' in which oxygen from the overlying pelagic sediment, often carbonate ooze, diffuses down into the underlying turbidite sequence and oxidizes organic carbon there. As a result, oxygen and nitrate are reduced to almost zero below the front but Mn and Fe are mobilized in the sediment. Mn migrate upwards and is immobilized at the oxidation front. Ultimately, it may be fixed in the sediment as a manganese carbonate. Within a long sediment core, a number of turbidite sequences, and therefore fossil oxidation fronts, may be seen. Other examples of the non-steady state deposition of Mn in deep-sea sediments have been recorded at the glacial/interglacial boundary (Wallace et al. 1988; Gingele and Kasten 1994).

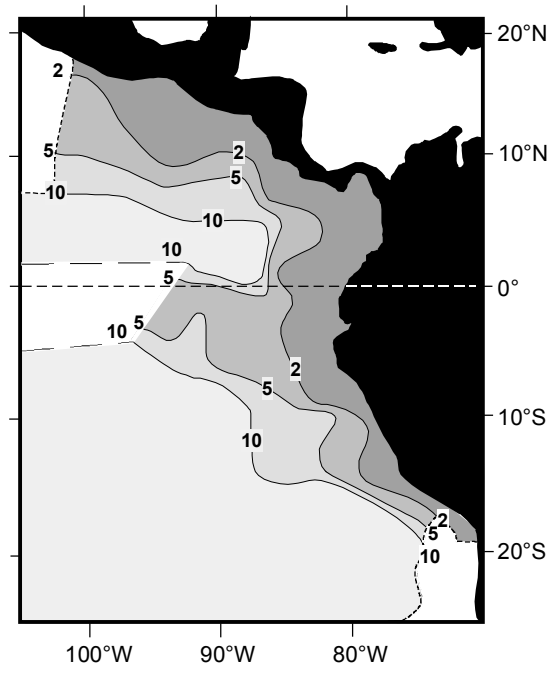

Fig. 11.6 Variation of the thickness (in cm) of the oxidized surface layer of sediments from the eastern equatorial Pacific (after Lyle 1993). In conjunction with the regional distribution of the biological productivity of the surface waters (Fig. 11.12), this pattern indicates that early diagenesis in the sediments is controlled on a regional scale by the input of biological detritus into the sediments.

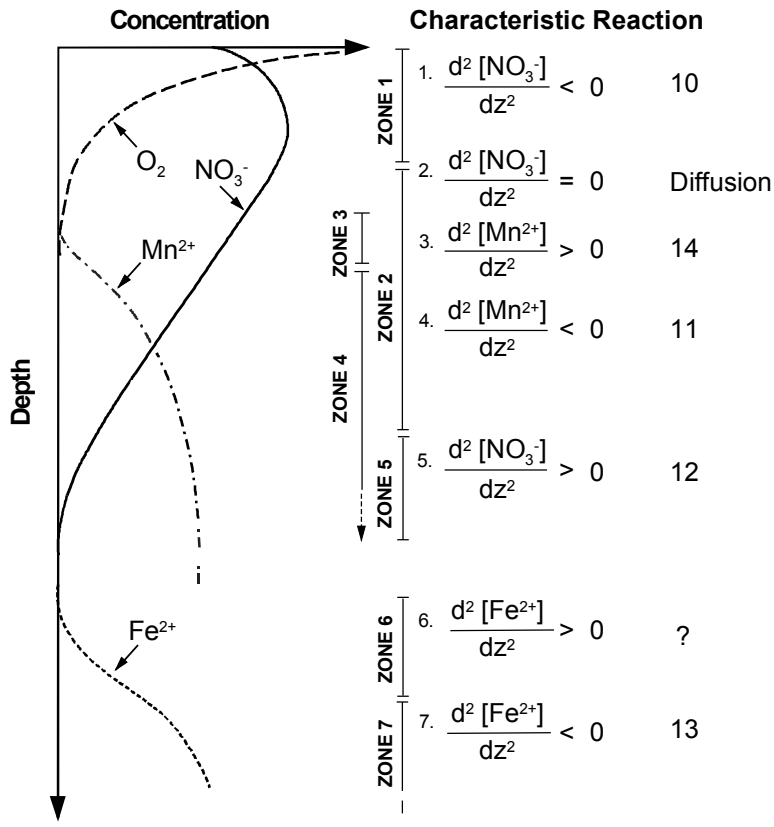

Fig. 11.7 Schematic representation of trends in pore water profiles for the principal oxidants in marine sediments. Depths and concentrations in arbitrary units (after Froelich et al. 1979). This pattern reflects the sequence of reduction of the principal oxidants in the sediment column (O_2>Mn oxides=nitrate>Fe oxides>sulfate).

11.4 Manganese Nodules and Crusts

There are three principal types of manganese deposits in the marine environment. *Manganese nodules* generally accumulate in deep water (>4,000 m) in oceanic basins where the sedimentation rates are low. They usually grow concentrically around a discrete nucleus. Growth occurs mainly at sediment-water interface. *Manganese crusts* accumulate on submarine seamounts and plateaux at depths >1,000 m where bottom currents prevent sediment accumulation. They generally form on submarine outcrops. *Ferromanganese concretions* occur in shallow marine environments (e.g. the Baltic and Black Seas) and in temperate-zone lakes. They grow much faster than deep-sea nodules and are quite different in shape, mineralogy and composition from them.

There are also three principal modes of formation of these deposits. *Hydrogenous deposits* form directly from seawater in an oxidizing environment. They are characterized by slow growth (about 2 mm Ma^{-1}). Manganese nodules tend to form on red clays and Co-rich manganese crusts on rock substrates. The high Mn/Fe ratio in deep sea water compared to the earth's crust is mainly responsible for the formation of hydrogenous manganese deposits with Mn/Fe ratios of about unity. *Diagenetic deposits* result from diagenetic processes within the underlying sediments leading to upward supply of elements from the sediment column. These deposits are characterized by faster growth rates (10-100 mm Ma^{-1}) and are often found on siliceous oozes. *Hydrothermal deposits* precipitate directly from hydrothermal solutions in areas with high heat flow such as mid-ocean ridges, back-arc basins and hot spot volcanoes. They are characterized by high to extremely high growth rates (>1,000 mm Ma^{-1}) and low to very low trace element contents. They tend to be associated with hydrothermal sulfide deposits and iron oxyhydroxide crusts.

11.4.1 Deep-Sea Manganese Nodules

Deep-sea manganese nodules occur mainly in deep-ocean basins characterized by low sedimentation rates (i.e. <5 mm ka^{-1}) where inputs of calcareous ooze,

turbidity flows and volcanic ash are low. They therefore occur in highest abundances on red clay and siliceous ooze far from land. They occur worldwide and are found in most major oceanic basins. Their distribution is also related to the patterns of oceanic bottom water flow and, to a lesser extent, to the availability of potential nuclei on which they grow such as weathered volcanic rock, pumice, whales' ear-bones, sharks' teeth, fragments of older nodules and indurated sediment. Antarctic Bottom Water (AABW) is the major oceanic bottom current in the Pacific. Its influence is seen in the lowered sedimentation rates, and therefore increased nodule abundance, along its flow path. A huge literature on deep-sea nodules has developed over the last 30 years, including a number of standard texts on the subject (Mero 1965; Horn 1972; Glasby 1977; Anon 1979; Bischoff and Piper 1979; Sorem and Fewkes 1979; Cronan 1980; Varentsov and Grasselly 1980; Roy 1981; Teleki et al. 1987; Baturin 1988; Halbach et al. 1988; Nicholson et al. 1997; Cronan 2000).

In the Pacific Ocean, the distribution of manganese nodules has been mapped as part of the Circum-Pacific Map Project using data from 2,500 bottom camera stations and from sediment cores (Piper et al. 1987) (Fig. 11.8). Although considerable variability in nodule abundance within individual stations was observed, high coverage of nodules was recorded in five main regions: between the Clarion and Clipperton Fracture Zones (C-C F.Z.) in the equatorial North Pacific and extending westwards into the northern sector of the Central Pacific Basin, in the abyssal plain area around the Musicians Seamounts in the Northeast Pacific Basin, in the central sector of the Southwestern Pacific Basin, in an E-W trending belt in the Southern Ocean coincident with the Antarctic Convergence, and in the northern sector of the Peru Basin. Andreev and Gramberg (2004) have recently published a more detailed map of the mineral resources of the world ocean including manganese nodules.

In discussing the composition of deep-sea manganese nodules, it should be born in mind that the composition of nodules varies within individual nodules as seen in the discrete micro-banding in the nodules, locally (on the scale of hundreds of meters) and regionally (over thousands of km) (e.g von Stackelberg and Marchig 1987). In spite of this, regional patterns in the composition of nodules are commonly observed such that we can reasonably compare and contrast the characteristics of nodules from different physiographic provinces of the world ocean as attempted here (cf. Cronan 1977; Piper and Williamson 1977; Sorem and Fewkes 1979).

In the following section, the distribution, mineralogy and composition of manganese nodules from three of these regions is considered in order to illustrate the different modes of formation of nodules in different settings. A detailed comparison of the characteristics of the nodules from these three regions has already been presented by Glasby et al. (1983).

Southwestern Pacific Basin

The Southwestern Pacific Basin has an area of $10 \cdot 10^6$ km^2. It is bounded by New Zealand-Tonga-Kermadec Arc, the East Pacific Rise and the Polynesian island chain and has a maximum depth 5,800 m. It lies beneath subtropical anticyclonic gyre which is a low productivity area. Two cruises of R.V. Tangaroa were undertaken in 1974 and 1976 to study the distribution and mode of formation of nodules in the Southwestern Pacific and Samoan Basins (Glasby et al. 1980). On a transect from New Zealand to Rarotonga in the Cook Islands, it was shown that the maximum abundance of nodules (>20 kg m^{-2}) occurs on the dusky brown clays in the region 220-745 km S.W. of Rarotonga. The western sector of the basin, particularly N.E. of New Zealand, was largely devoid of nodules. This was attributed to the influx of terrigenous sediments from the New Zealand landmass which raised the sedimentation rate above the threshold for nodule formation. The morphology of the nodules in the Southwestern Pacific Basin is somewhat variable but those taken S.W. of Rarotonga are 40% s[S]m, 17% m[S]m and 16% s[E]m (see box for explanation). 72% of these nodules are small (<30 mm), 26% medium (30-60 mm) and 2% large (>60 mm). The nodules are dominantly spheroidal with smooth surface texture when small but become more ellipsoidal and develop equatorial rims with increasing size. The larger nodules also tend to exhibit differences in the surface texture between the upper and lower surfaces. This reflects the fact that the larger nodules have been static at the seafloor for longer than is necessary to form the external layer of the nodule (i.e. their rate of rolling is slower than the rate of growth). Mineralogically, the nodules consist of δMnO_2, quartz and feldspar. Table 11.4 lists the average composition of nodules from S.W. Pacific Basin and the adjacent Samoan Basin. The average Ni+Cu+Co content of the nodules on the transect from New Zealand to Rarotonga is 1.00%. This is well below the level considered necessary for economic exploitation even though the Southwestern Pacific Basin is thought to contain $10 \cdot 10^9$ t of nodules. A subsequent E-W transect across the Southwestern Pacific Basin at 42°S undertaken during cruise SO-14 of R.V. Sonne showed

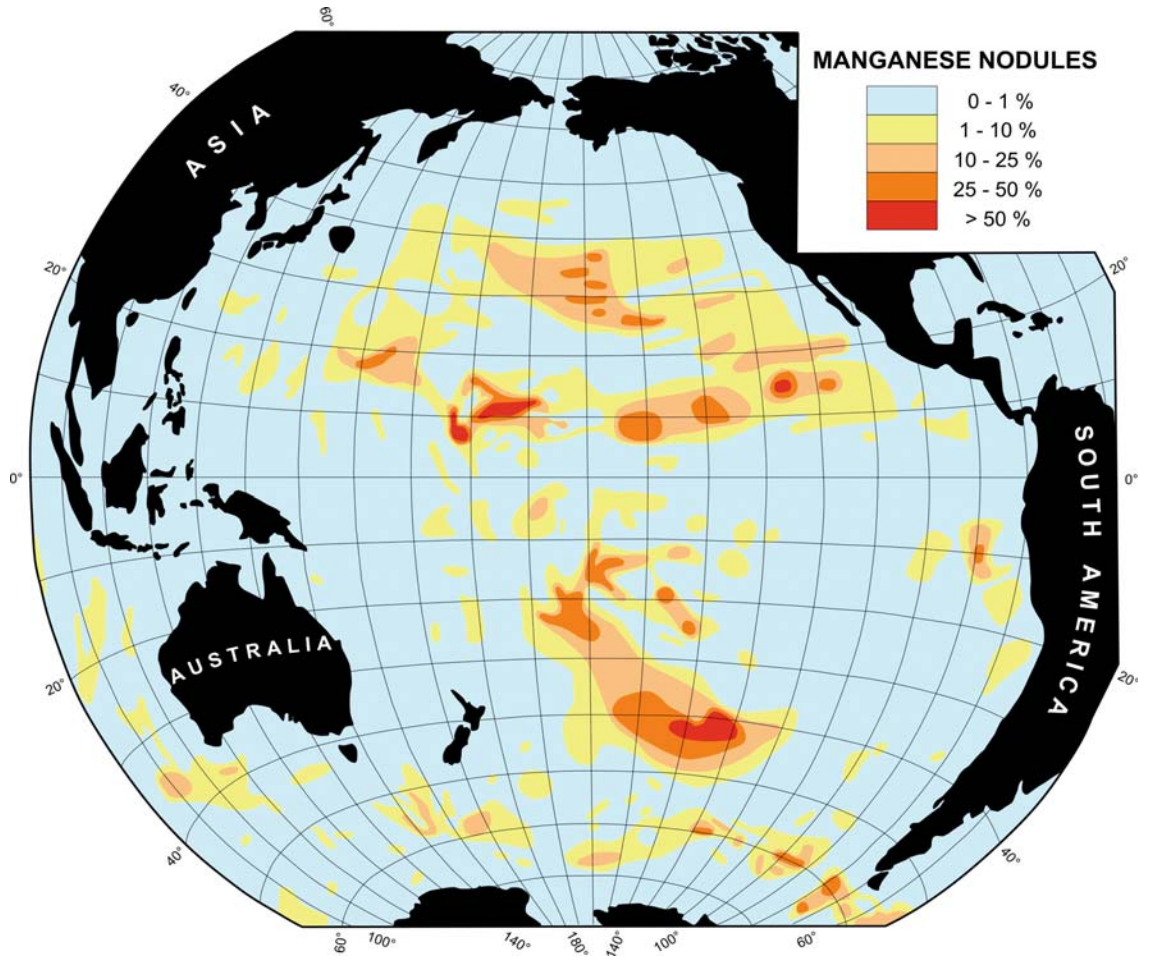

Fig. 11.8 Schematic map showing the distribution of manganese nodules in the Pacific Ocean compiled as part of the Circum-Pacific Map Project (Piper et al. 1985). The contours represent the percentage cover of the ocean floor by manganese nodules. Diagram prepared with the permission of D.Z. Piper, USGS.

that the highest abundances of nodules occur in the far eastern sector of the basin furthest from land (Plüger et al. 1985).

Descriptive classification of manganese nodule types (after Glasby et al. 1980).

Prefix: (Nodule size based on maximum diameter)

- s = small (<30 mm)
- m = medium (30-60 mm)
- l = large (>60 mm)

Bracketed: (Primary nodule shape)

- S = speroidal
- E = ellipsoidal
- D = discoidal
- P = polynucleate
- T = tabular
- F = faceted (polygonal)
- V = scoriaceous (volcanic)
- B = biological (shape determined by shark's tooth)

Suffix: (Nodule surface texture)

- s = smooth
- m = microbotryoidal
- b = botryoidal
- r = rough

Examples:

- m[S]m = medium-sized spheroidal nodule with microbotryoidal surface texture.
- $l[D]^{b}_{r}$ = large discoidal nodule with botryoidal upper surface texture and rough lower surface texture.
- s[S-F]s = small spheroidal nodule with significant facing, smooth surface texture.

Southwestern Pacific Basin nodules are considered to be hydrogenous in origin based on their average Mn/Fe ratio of about unity, Ni+Cu contents of <1%, δMnO_2 as the principal Mn oxide phase and growth rates of 1-2 mm Ma^{-1} (Dymond et al. 1984).

Clarion-Clipperton Fracture Zone Belt

The C-C F.Z. belt is the area bounded by the Clarion F.Z. to north and the Clipperton F.Z. to the south. The water depth varies from 5,300 m in the west to 4,300 m in the east (Andreev and Gramberg 1998). The C-C F.Z. is a high productivity area characterized by the occurrence of siliceous sediments. The sedimentation is controlled largely by bottom current activity. The area is dominated by an abyssal hill topography. There is a great variability in nodule distribution and type which depends on the sediment type and accumulation rate, bottom current activity, benthic biological activity (bioturbation), bottom topography, availability of potential nodule nuclei and productivity of the surface waters (Friedrich et al. 1983; Halbach et al. 1988; von Stackelberg and Beiersdorf 1991; Skornyakova and Murdmaa 1992; Jeong et al. 1994, 1996; Knoop et al. 1998; Morgan 2000).

Within the C-C F.Z., there appear to be two discrete nodule types; larger 'mature' nodules and smaller 'immature' nodules. The larger 'mature' nodules make up 26% of the nodules by number but 92% by weight. The larger nodules are dominantly m-l$[E,D]_b^s$, the so-called hamburger-shaped nodules which have an equatorial rim corresponding to the sediment-water interface. The nodules become flatter with increasing size and have a maximum diameter of 140 mm. These nodules are characterized by hydrogenous growth on the upper surface and diagenetic growth on the lower surface. Figures 11.9 and 11.10 show the principal features of these hamburger nodules. By contrast, the morphology of the nodules from the slopes of seamounts is s-m[S,P]s-m. These nodules form at the sediment surface and are characterized by hydrogenous growth. The principal minerals present are todorokite and δMnO_2. Table 11.4 lists the average composition of nodules from the Clarion-Clipperton F.Z. belt. There is an inverse relation between nodule grade and abundance which vary from 3.4% Ni+Cu and 3 kg m^{-2} to 0.3% Ni+Cu and 16 kg m^{-2}. The high Ni+Cu nodules are dominantly diagenetic in origin and the low Ni+Cu nodules dominantly hydrogenous in origin. The high contents of Ni+Cu in the diagenetic

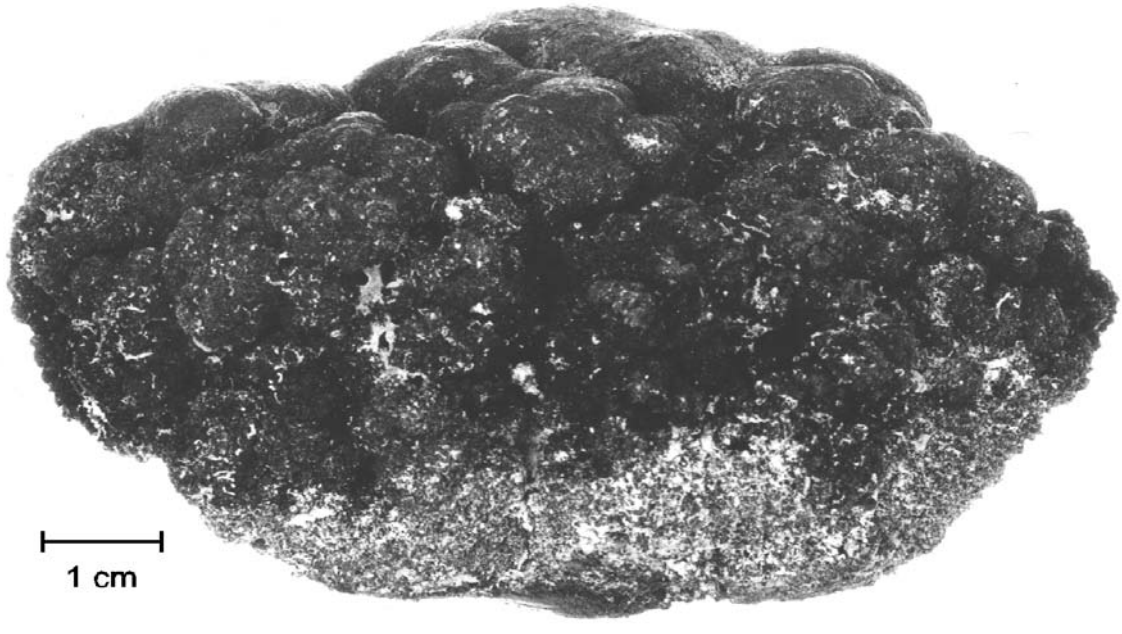

Fig. 11.9 Hamburger-shaped nodule from the Clarion-Clipperton F.Z. region displaying a smooth surface texture on the upper surface and a rough surface texture on the underside (l [D] ^s_r). Sample collected at Stn 321 GBH, R.V Sonne cruise SO-25 (7°57.30'N, 143°28.92'W, 5153 m). Photograph courtesy of U. von Stackelberg, BGR.

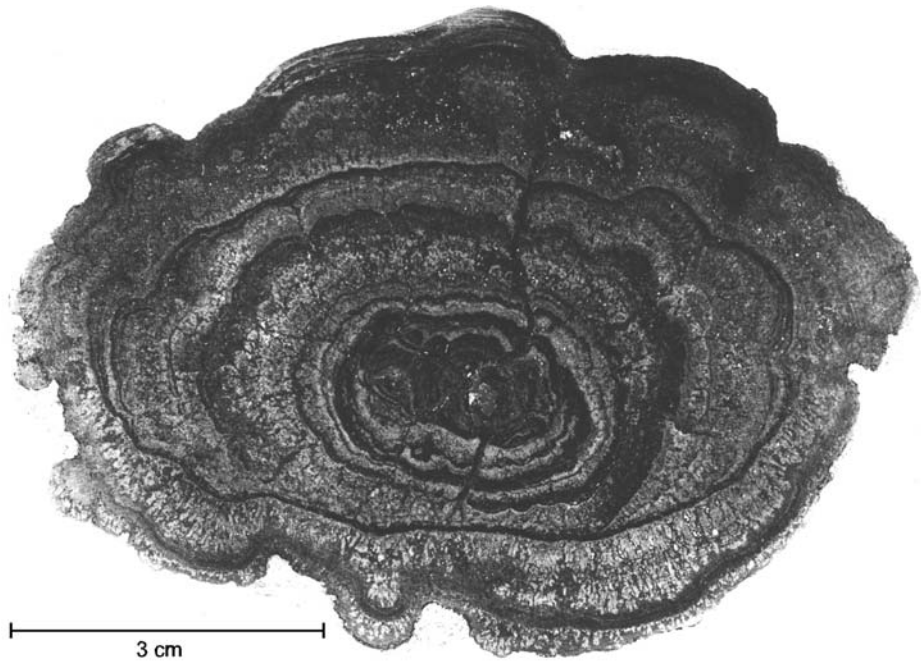

Fig. 11.10 Vertical section of a hamburger-shaped nodule from the Clarion-Clipperton F.Z. region displaying a layered growth structure (l D $^{s}_{r}$). The nodule nucleus is a nodule fragment. Sample collected at Stn 178 GBH, R.V Valdivia cruise VA 13/2 (9°22.5'N, 145°53.1'W, 5231 m). Photograph courtesy of U. von Stackelberg, BGR.

nodules from this area ensure that the C-C F.Z. is the prime target area for the economic exploitation of manganese nodules (cf. Morgan 2000).

C-C F.Z. nodules may be considered to be diagenetic in origin based on their average Mn/Fe ratio of about 2.5, Ni+Cu contents of <2.5%, 10 Å manganate as the principal Mn oxide phase and growth rates of 10-50 mm Ma^{-1} (Dymond et al. 1984). The influence of oxic diagenesis on nodule formation is the result of low sedimentation rates and low inputs of organic carbon to sediments. The sediments are oxidizing with an E_H of +0.4 V at 8m depth in the sediment column (Müller et al. 1988). Ni and Cu on the undersides of the nodules are ultimately derived from the dissolution of siliceous tests in the sediment (Glasby and Thijssen 1982). Dissolved silicate concentrations in the sediment pore waters may attain values of up to 900 µM. Ni^{2+} and Cu^{2+} substitute in the interlayer spacings of 10 Å manganate on the undersides of the nodules resulting in differences in the compositions of the upper and lower surfaces of the nodules (Dymond et al. 1984). In general, the tops of these nodules are enriched in Fe, Co and Pb and the bottoms in Mn, Cu, Zn and Mo (Raab and Meylan 1977).

Table 11. 4 Comparison of the average compositions of Mn nodules from S.W. Pacific Basin and Samoan Basin (after Glasby et al. 1980), the Clarion-Clipperton Fracture Zone region (after Friedrich et al. 1983) and the Peru Basin (after Thijssen et al. 1985).

	S.W. Pacific Basin	Samoan Basin	C-C F.Z.	Peru Basin
Mn (%)	16.6	17.3	29.1	33.1
Fe (%)	22.8	19.6	5.4	7.1
Co (%)	0.44	0.23	0.23	0.09
Ni (%)	0.35	0.23	1.29	1.4
Cu (%)	0.21	0.17	1.19	0.69
Mn/Fe	0.73	0.88	5.4	4.7

Peru Basin

The Peru Basin is a relatively shallow oceanic basin with depths typically in the range 3,900-4,300 m which is close to the depth of the Carbonate Compensation Depth (CCD) (4,250 m) and lies in a region of high biological productivity. Manganese nodules were initially recovered during cruises SO-04 and SO-11 of R.V. Sonne and investigated in part because of their economic potential (Thijssen et al. 1985; von Stackelberg 1997, 2000). Subsequently, the nodule field was investigated during cruises SO-61, SO-79 and SO-106 as part of the DISCOL program, a long-term, large-scale disturbance-recolonization experiment to assess the potential environmental impact of nodule mining (von Stackelberg 1997; Thiel 2001).

Peru Basin nodules are quite different from those in other regions of the ocean floor. They tend to be large and mamillated with an average Mn/Fe ratio of 4.7 and an average Ni+Cu content of about 2.1% (Thijssen et al. 1985). Table 11.4 lists the average composition of nodules from the Peru Basin. The nodules are friable and contain fragments of fish bones or broken nodules as nodule nuclei. Nodule density averages >10 kg m^{-2} but achieves a maximum value of 53 kg m^{-2}. The highest abundance of nodules is found

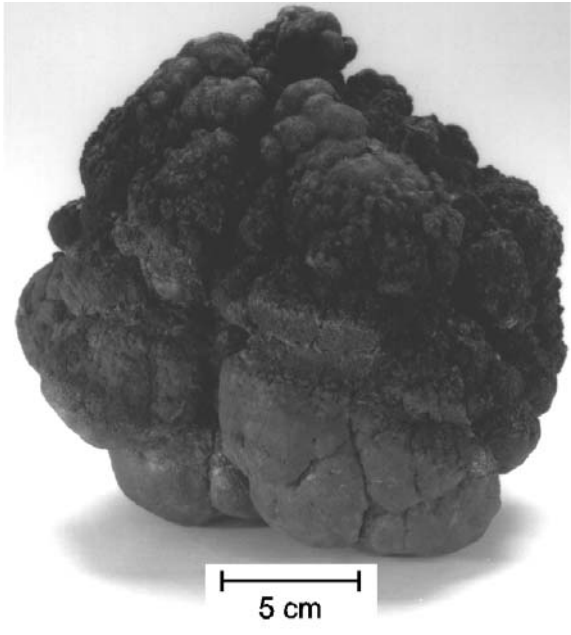

Figs 11.11 Sperical nodule with a cauliflower-shaped surface from the Peru Basin displaying a rough surface texture on the upper surface and a smooth surface texture on the underside (l [S] $^{r}_{s}$). Sample collected at Stn 25 KG, R.V Sonne cruise SO-79 (6°51.99'N, 90°26.52'W, 4170 m). Photograph courtesy of U. von Stackelberg, BGR.

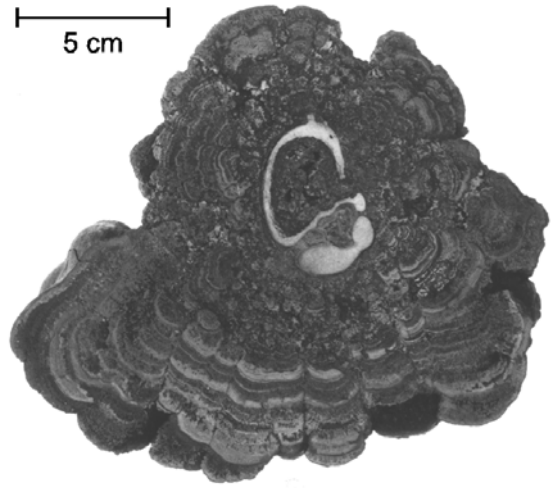

Figs 11.12 Vertical section of an asymmetric nodule from the Peru Basin with a cetacean earbone nucleus (l [S] $^{r}_{s}$). Sample collected at Stn 63 KG, R.V Sonne cruise SO-79 (6°45.58'N, 90°41.48'W, 4257 m). Photograph courtesy of U. von Stackelberg, BGR.

near the CCD. Although only 3.8% of the nodules by number are in the >80 mm size class, these nodules make up 56% of the total weight of the nodules. The largest nodule recovered was 190 mm in diameter. The morphology of the nodules is a function of the size class. Nodules <20 mm in diameter are dominantly fragments of larger nodules and less commonly discrete ellipsoidal nodules with botryoidal surface texture. Nodules in the 20-60 mm size classes are dominantly ellipsoidal to discoidal with the position of the sediment-water interface clearly defined. The upper surface of these nodules is mamillated with micro-botryoidal surface texture whereas the lower surface is less mamillated and smoother. Nodules in the >60 mm size class are dominantly highly mamillated and spheroidal with botryoidal surface texture on the upper surface and smooth to micro-botryoidal on the lower surface. Figures. 11.11 and 11.12 show the principal features of these large nodules. For every nodule encountered at the sediment surface, 1.25 nodules occur to a depth of 2.5 m in the sediment column. Buried nodules have the same morphology as surface nodules but different surface texture indicating that material has been removed from the surface of the nodule by dissolution after burial. von Stackelberg (1997) has shown that the redox boundary separating soft oxic surface sediments from stiffer suboxic sediments occurs at a depth of about 100 mm in the sediment column. Highest growth rates occur on the underside of large nodules immediately above the

redox boundary. Strong bioturbation occurs throughout the region and helps maintain the nodules at the sediment surface.

Peru Basin nodules are considered to be diagenetic in origin with maximum Mn/Fe ratios of >50, corresponding to Ni+Cu in these samples of <1.4%. 10 Å manganate as the principal Mn oxide phase and growth rates of 100-200 mm Ma^{-1} (Dymond et al. 1984). Nodule compositional data for this assessment are taken from Halbach et al. (1980) and Thijssen et al. (1985) and nodule growth rates from Reyss et al. (1985) and Bollhöffer et al. (1996, 1999). The influence of suboxic diagenesis on nodule growth is the result of higher sedimentation rates and higher inputs of organic carbon into the sediments. Mn is strongly remobilized by dissolution of Mn micronodules within the sediment column. This leads to the high Mn/Fe ratios and low Ni+Cu contents in the nodules. The nodules are characterized by increasing substitution of Mn^{2+} in the interlayer spacings of 10 Å manganate.

11.4.2 Influence of Diagenesis on Nodule Growth

Perhaps the most comprehensive explanation of the role of hydrogenetic and diagenetic processes on manganese nodule accretion has been presented by Dymond et al (1984). On their classification, *hydrogenous deposition* involves the direct precipitation or accumulation of colloidal metals oxides from seawater. Strictly, this involves deposition of manganese oxides on surfaces in contact with seawater such as involved in the formation of manganese crusts. In practice, manganese nodules formed on red clays have characteristics very similar to those of manganese crusts and are therefore considered to be hydrogenous in origin. However, Aplin and Cronan (1985) have argued that no nodules resting on or in marine sediments can be considered entirely free of diagenetic influences.

Oxic diagenesis refers to processes occurring within oxic sediments. Decomposition and oxidation of labile organic matter and the dissolution of labile biogenic components such as siliceous tests may release biologically-bound metals into the sediment pore waters which may ultimately be incorporated into the nodules. Dissolution of siliceous tests may also introduce silica into the sediment pore waters which may react with amorphous ferromanganese oxides to form nontronite (Dymond and Eklund 1978). This process fixes silica and Fe in the sediment column and releases transition elements such as Mn, Co, Ni, Cu and Zn into the sediment pore waters for incorporation into the nodules. Jung and Lee (1999) have suggested that formation of manganese nodules may be episodic under the influence of oxic diagenesis. Under these conditions, manganese and associated transition metals would be remobilised in oxygen-depleted environments which develop as a result of the decomposition of organic matter in burrows and supplied episodically to nodule surfaces during periods of intermittent bottom water flow strong enough to stir up the bioturbated sediment.

Suboxic diagenesis involves the reduction of Mn (IV) to Mn (II) within the sediment column and then reoxidation of Mn (II) to Mn (IV) during the formation of the nodules. These diagenetic processes are controlled by redox processes within the sediment column and are therefore dependent on depth in the

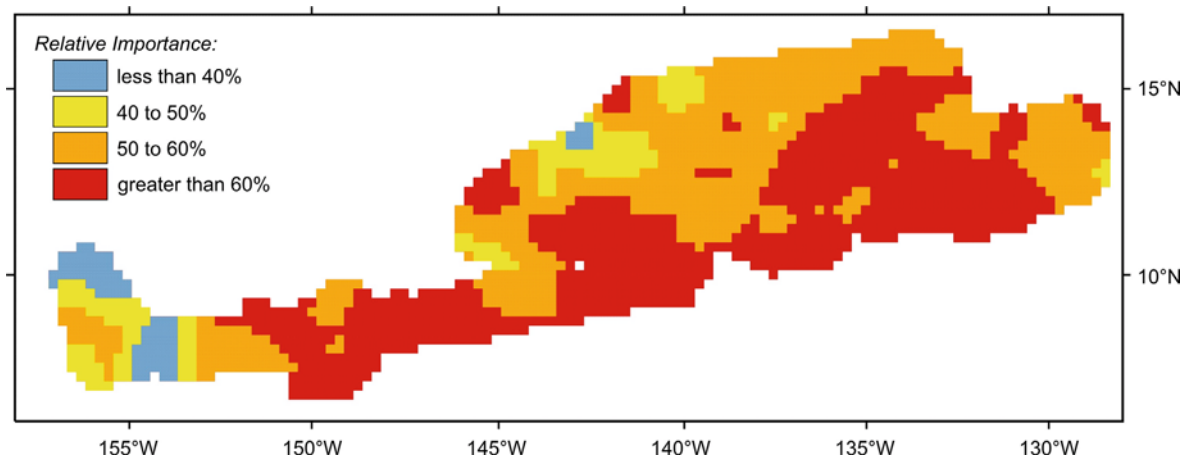

Fig. 11.13 Contour plot of the diagenetic accretion compositional end member of manganese nodules which shows that this end member increases in relative proportion as the equatorial zone of high productivity is approached as a consequence of the increase in both the primary productivity and sedimentation rate (after Knoop et al. 1998).

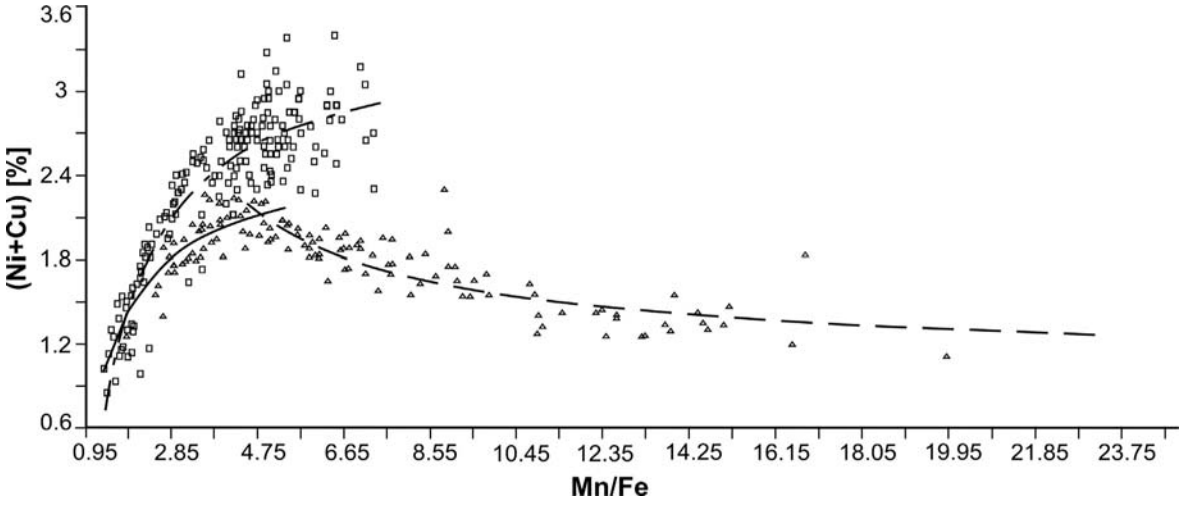

Fig. 11.14 Hyperbolic regression curves of Ni+Cu against Mn/Fe for nodules from the Clarion-Clipperton F.Z. region (upper curve) and Peru Basin (lower curve) (after Halbach et al. 1981).

sediment column. In most cases (as in the Peru Basin), these nodules are formed in oxic sediments overlying reducing sediments. The diagenetic supply of metals to the nodules normally takes place at or near the sediment surface. Because the metals are released within the sediment column and migrate upwards, they tend to be incorporated on the underside of nodules. This frequently results in differences in composition between the upper and lower surfaces of diagenetic nodules. Manganese micronodules may play a key role in retaining transition elements in the sediment column until they are released on further burial of the micronodules.

Diagenetic processes may therefore involve recycling of elements within the sediment column prior to their incorporation in nodules. The characteristics of each of these nodule types have been given in the previous sections. In addition to influencing the mineralogy and composition of the nodules, diagenetic processes also influence their surface texture; hydrogenous nodules tend to have smooth surface texture and diagenetic nodules botryoidal to rough surface texture.

From the above comments, it will be seen that the principal factor driving the diagenetic milieu in the sediments is the biological productivity of the oceanic surface waters. A map of biological productivity of Pacific ocean surface waters shows that the productivity of the northern sector of the Southwestern Pacific Basin is 50-100 gC m^{-2} yr^{-1}, in the C-C F.Z. is in the range 100-150 gC m^{-2} yr^{-1} and in the Peru Basin is 100-150 gC m^{-2} yr^{-1} (Fig. 12.5) (cf. Cronan 1987, 1997; Müller et al. 1988). The importance of the productivity of the surface waters to the diagenetic component of manganese nodules in the C-C F.Z. is well illustrated in Figure 11.13 which shows that the diagenetic component of the nodules increases from west to east as the equatorial zone of high productivity is approached (cf. Skornyakova and Murdmaa 1992; Morgan 2000).

The influence of biological productivity on nodule composition is perhaps best illustrated by the hyperbolic regression curve of Cu and Ni against Mn/Fe for nodules from C-C F.Z. and Peru Basin (Fig. 11.14). This diagram can be divided into three parts. Hydrogenous nodules deposited entirely from seawater have Mn/Fe ratios of about unity and low Ni+Cu contents. Nodules influenced by oxic diagenesis have Mn/Fe ratios of up to 5 (but more typically about 2.5) with correspondingly high Ni+Cu contents. Nodules influenced by suboxic diagenesis have Mn/Fe ratios of up to 50 but lower Ni+Cu contents. The maximum Ni+Cu contents of nodules correspond to a Mn/Fe ratio of about 5 and is found at the so-called point of reversal.

For this purpose, we may therefore consider hydrogenous deep-sea nodules to be a baseline. When oxic diagenesis takes place, Mn, Ni and Cu are released into the sediment pore waters and are ultimately incorporated into the nodules. Ni^{2+} and Cu^{2+} substitute in the phyllomanganate lattice (see below). This explains the high Mn/Fe ratios and Ni+Cu contents of oxic nodules. When sub-oxic diagenesis takes place, Mn^{2+} is remobilized into the reducing sediments and

migrates upwards towards the sediment surface where it is either oxidized to Mn (IV) at the nodule surface or substitutes in the phyllomanganate lattice as Mn^{2+}. This behavior explains both the very high Mn/Fe ratios of suboxic nodules and their correspondingly low Ni+Cu contents. The boundary between oxic and suboxic diagenesis is marked by a Mn/Fe ratio in the nodules of about 5. The nature of the diagenetic processes occurring in the sediments depends directly on the input of organic carbon and therefore on the productivity of the overlying surface waters.

Based on a study of manganese nodules taken on the Aitutaki-Jarvis Transect in the S.W. Pacific, Cronan and Hodkinson (1994) also demonstrated the influence of the CCD on nodule composition. Above the CCD, accumulation of carbonate tests was thought to dilute the organic carbon in the sediments, thus inhibiting diagenesis, whereas, below the CCD, the decay of organic material in the water column was thought to reduce its effectiveness in driving diagenetic reactions. Cronan and Hodkinson (1994) indeed found that Mn, Ni, Cu and Zn were most concentrated in nodules taken near the CCD at the north of the transect in an region of high productivity and least concentrated in nodules taken away the CCD at the south of the transect in a region of low productivity. They therefore inferred that diagenetic cycling of Mn, Ni, Cu and Zn to the nodules is enhanced as a result of the decay of organic material near the CCD.

On a more local scale, the influence of diagenetic processes on nodule morphology and composition has been related to variations in sedimentation rate in areas of hilly topography within the C-C F.Z. (von Stackelberg and Marchig 1987; von Stackelberg and Beiersdorf 1991). On the flanks of hills and in parts of basins, sedimentation rates are lower and dominantly diagenetic nodules are formed whereas, in areas of sediment drift, sedimentation rates are higher and dominantly hydrogenous nodules are formed. These processes are related to the degree of decomposition of organic matter within the sediment column. Where sedimentation rates are low, organic matter is rapidly consumed within the sediment releasing Mn^{2+} into the pore water and resulting in the formation of dominantly diagenetic nodules. In areas of sediment drift, on the other hand, the organic carbon is buried within the sediment stimulating bioturbation and the resultant biogenic lifting of the nodules to the sediment surface.

Bioturbation is an essential requirement for benthic lifting of manganese nodules and maintaining the nodules at the sediment surface. In both the C-C F.Z. and the Peru Basin, the biological productivity of the oceanic surface waters is high enough that the amount of organic matter reaching the sea floor is sufficient to stimulate the activity of sediment-feeding organisms. As a result, bioturbation appears to be the dominant factor in maintaining nodules at the sediment surface in the C-C F.Z. (von Stackelberg and Beiersdorf 1991; Skornyakova and Murdmaa 1992) and the Peru Basin (von Stackelberg 1997, 2000). Several mechanisms have been proposed by which nodules could be maintained at the sediment surface by bioturbation. These include biological pumping, burrowing by crack propagation as well as bioturbation by benthic fauna and megafauna (Sanderson 1985; McCave 1988; Banerjee 2000 and Dogan et al. 2005). The biological productivity of the surface waters in the Southwestern Pacific Basin, on the other hand, is much lower than that in the C-C F.Z. and the Peru Basin and the abundance of benthic fauna on the sea floor is therefore much reduced. This may account for the greater influence of ocean bottom currents in maintaining nodules at the sediment surface there as proposed by Glasby et al. (1983). The biological productivity of the oceanic surface waters may therefore also influence the way in which nodules are maintained at the sediment surface.

In addition to the above, Calvert and Piper (1984) have proposed a diagenetic source of metals derived from sediments far away for nodules occurring in an erosional area with thin sediment cover in the C-C F.Z. The metals were thought to be transported to the site of deposition by oceanic bottom water, probably AABW. Although this process is well known in shallow-water continental margin areas such as the Baltic Sea, only limited evidence to support this hypothesis has been presented for the deep-sea environment.

11.4.3 Rare Earth Elements (REE) as Redox Indicators

A key parameter in understanding nodules formation is the redox milieu of the environment at the time of deposition. This can influence the mineralogy and therefore composition of the nodules (see below). In this regard, Glasby (1973) used the Ce/La ratio of nodules as a redox indicator. He showed that deep-sea nodules from the NW Indian Ocean had much higher Ce/La ratios (4.4) and ΣREE contents (490 ppm) than those from shallow-water continental margin environments such as Loch Fyne, Scotland (1.9 and 29 ppm, respectively). The higher REE contents of the deep-sea nodules were taken to reflect the more oxidizing conditions in the deep sea which facilitated the oxidation of the trivalent Ce^{3+} in seawater to CeO_2 on the surface of the nodules. The lower ΣREE

contents of the shallow-water continental margin concretions was taken to reflect the remobilization of Mn in the sediment column which resulted in the fractionation of Mn from Fe, Co, Ni, Cu and REE in the concretions. It was suggested that the REE were adsorbed from seawater onto colloidal FeOOH in the nodules. The high rate of manganese remobilization in the shallow-water continental margin sediments also resulted in growth rates of the associated concretions two orders of magnitude higher than those of the deep-sea nodules (Ku and Glasby 1972).

Based on these ideas, Glasby et al. (1987) attempted to use the Ce/La ratios of deep-sea manganese nodules as a means of tracing the flow path of the AABW in the S.W. and Central Pacific Ocean. On this basis, the Ce/La ratios in the deep-sea nodules should decrease along the flowpath of the AABW as the oxygen in the bottom waters is consumed. The data confirmed that the ΣREE contents of the nodules are strongly correlated with Fe resulting in higher REE contents in nodules from the Southwestern Pacific Basin compared to those from the C-C F.Z (La 169 v 93 ppm). They also showed a systematic decrease in the Ce/La ratios of the nodules from the Southwestern Pacific Basin to the C-C F.Z. and on to the Peru Basin as follows: Area III (9.6) > Area K (8.0) > Area C (3.7) > Peru Basin (2.0) > Area G (1.5) > Area F (1.4). The Peru Basin and Areas G and F are situated in the equatorial South Pacific in regions which do not lie directly under the flow path of the AABW and which are characterized by sluggish bottom water flow (Nemoto and Kroenke 1981; Davies 1985). This factor explains the low Ce/La ratios of these samples. The sequence of these ratios confirms that the Ce/La ratio of deep-sea manganese nodules can be used to trace the flow path of the AABW and therefore that the Ce/La ratios of manganese nodules can be used as a redox indicator in the deep-sea environment. Subsequent work on the REE contents of manganese nodules taken on an E-W transect across the Southwestern Pacific Basin at 42°S showed that the highest Ce/La ratios and ΣREE contents of the nodules occur in the central part of the basin which is exposed to the strongest flow of AABW (and therefore the most oxygenated conditions) (Kunzendorf et al. 1993).

More recently, Kasten et al. (1998) have determined the REE contents of a suite of manganese nodules from the South Atlantic to see if a similar relationship between the Ce/La ratios of the nodules and AABW flow could be observed there. In fact, the Ce/La ratios of the nodules decrease in the sequence Lazarev Sea, Weddell Sea (10.4 and 9.7) > East Georgia Basin (6.5-7.1) > Argentine Basin (5.0) but then increase in the Brazil Basin (6.2) and Angola Basin (9.8 and 15.1). A further decrease was observed in the Cape Basin (7.6). In addition, an extremely high Ce/La ratio of 24.4 had already been determined for nodules sampled north of the Nares Abyssal Plain in the North Atlantic. These data reflect the more complicated pattern of bottom water flow in the Atlantic compared to the Pacific Ocean. It is believed that the penetration of more oxygenated North Atlantic Deep Water (NADW) into the South Atlantic accounts for the higher Ce/La ratios in the nodules from the Angola and Brazil Basins. The influence of AABW could therefore be traced only as far north as the Argentine Basin. These data confirm the potential importance of REE studies in deep-sea manganese nodules in tracing oceanic bottom water flow.

Of particular interest in this regard is the study of REE patterns of different types of nodules from DOMES Site A in the C-C F.Z. by Calvert et al. (1987) on nodules which had previously been investigated by Piper and Blueford (1982) and Calvert and Piper (1984) (see sections 11.4.2 and 11.4.10.2). These authors demonstrated that there were three end-member types of nodules at this site, granular nodules from the valley which formed on thin (<20 cm) Quaternary sedimentary sections and displayed the highest Mn/Fe, Cu/Ni, todorokite/δMnO_2 ratios and the lowest Ce/La ratios, smooth nodules from the uplands which formed on thick (>36 cm) Quaternary sections and displayed the lowest Mn/Fe, Cu/Ni, todorokite/δMnO_2 ratios and highest Ce/La ratios and an intermediate type of nodules. The authors interpreted these differences in Ce/La ratios of the nodules in terms of variations in the composition of seawater from which the nodules formed, either from geochemically more evolved AABW in the valley or from more local sources of seawater in the highlands. However, other authors have interpreted such local variations in nodule type in other areas of rugged bottom topography in the C-C F.Z. in terms of the formation of three genetic types of nodules, hydrogenous, diagenetic, and mixed hydrogenous/diagenetic (Heye 1978; Glasby et al. 1982; Skornyakova and Murdmaa 1992). At DOMES Site A, the extreme hydrogenous endmember is characterized by a Mn/Fe ratio of 1.1, Ni + Cu of 1.0% and a Ce/La ratio of 2.7 and the extreme diagenetic endmember by a Mn/Fe ratio of 5.2, Ni + Cu of 2.9% and a Ce/La ratio of 2.5. Although the Ce/La ratios for these two nodules are quite similar, the highest Ce/La ratio for the hydrogenous nodules was 3.7 and the lowest ratio for the diagenetic nodules 1.6 (see Glasby et al. 1987; Kunzendorf et al. 1993). This suggests that variations in the REE patterns of nodules at DOMES

Site A may be better interpreted in terms of variations in nodule type within the area rather than local variations in seawater chemistry as proposed by Calvert et al. (1987).

In addition, De Carlo and McMurtry (1992) have analyzed 32 samples of Co-rich Mn crusts from the Hawaiian Archipelago for REE (see section 11.4.4). These samples contained on average 287 ppm La and 1,277 ppm Ce giving an average Ce/La ratio of 4.5. This is intermediate between the ratios in nodules from the Aitutaki Passage (Area K) and the C.C. FZ (Area C) and is compatible with a hydrogenous origin for these crusts.

11.4.4 Co-Rich Mn Crusts

Co-rich Mn crusts may be defined as hydrogenous manganese crusts having Co contents >1% (Manheim 1986; Mangini et al. 1987; Hein et al. 2000). These crusts are typically 5-100 mm thick and occur on older seamounts (100-60 Ma) in many of the seamount chains in the equatorial Pacific such as the Mid-Pacific Mountains and Line Islands. The crusts are commonly found on exposed rock on seamount slopes or on the summits of oceanic plateaux at water depths of 3,000-1,100 m. Principal substrates include basalts, hyaloclastites, indurated phosphorite and claystone. A vertical section of a Co-rich Mn crust is shown in Fig. 11.15. On plateaux and flat terraces where fragments of rock or manganese crusts have accumulated, manganese nodules may be seen lying on the surface of calcareous ooze. Ripple marks indicating the presence of strong bottom currents are sometimes observed on this ooze. The average composition of crusts from the 1,500-1,100 m depth zone in the Mid-Pacific Mountains has been reported as Mn 28.4%, Fe 14.3%, Co 1.18%, Ni 0.50%, Cu 0.03%, Pt 0.5 ppm, Mn/Fe 2.0. δMnO_2 is the principal manganese mineral present and they have a growth rate of 1-2 mm Ma^{-1}. The crusts have attracted economic interest as a potential source of Co and, to a lesser extent, Pt. The areas in which these crusts generally form lie well above the CCD. Crusts therefore tend to form in regions of strong bottom current activity which can prevent the deposition of calcareous ooze by erosion.

The variation in the composition of manganese crusts from the Mid-Pacific Mountains with water depth is presented in Table 11.5. These data show that these crusts are hydrogenous in origin (based on their Mn/Fe ratios) but they tend to have much higher Co and lower Cu contents than deep-sea nodules from the same region. The Mn/Fe ratios, Co and Ni contents are highest but the Cu contents lowest in crusts in the depth range 1,900-1,100 m. The positive correlation of Mn, Co and Ni reflects that association of these elements in δMnO_2. Overall, the Pt content of the crusts is very high, in the range 0.2-1.2 ppm with an average of 0.5 ppm.

Halbach and Puteanus (1984) showed that the dissolution of calcareous tests in the water column plays a key role in the incorporation of Fe into these crusts. The calcareous tests contain about 500 ppm Fe. The flux of Fe to the surface of the crusts derived from the release of colloidal Fe oxyhydroxide particles on dissolution of the calcareous tests was estimated to be about 15 $\mu g\ cm^{-2}\ a^{-1}$ which is almost equivalent to the flux of Fe in the concretions of 22.4 - 44.8 $\mu g\ cm^{-2}\ a^{-1}$. The rate of incorporation of Fe into the crusts is therefore related to the position of the lysocline. Based on such considerations, these authors concluded that the metal supply from the water column to the crusts

Table 11.5 Variation of the composition of manganese crusts from the Mid-Pacific Mountains with water depth (after Mangini et al. 1987). Analyses expressed as wt. % of dried material.

water depth (m)	Mn	Fe	Co	Ni	Cu	Mn/Fe
1100 - 1500	28.4	14.3	1.18	0.50	0.03	1.99
1500 - 1900	24.7	15.3	0.90	0.42	0.06	1.61
1900 - 2400	25.5	16.1	0.88	0.41	0.07	1.58
2400 - 3000	20.5	19.5	0.69	0.18	0.09	1.05
3000 - 4000	20.5	18.0	0.63	0.35	0.13	1.41
4000 - 4400	19.7	16.7	0.67	0.24	0.10	1.17

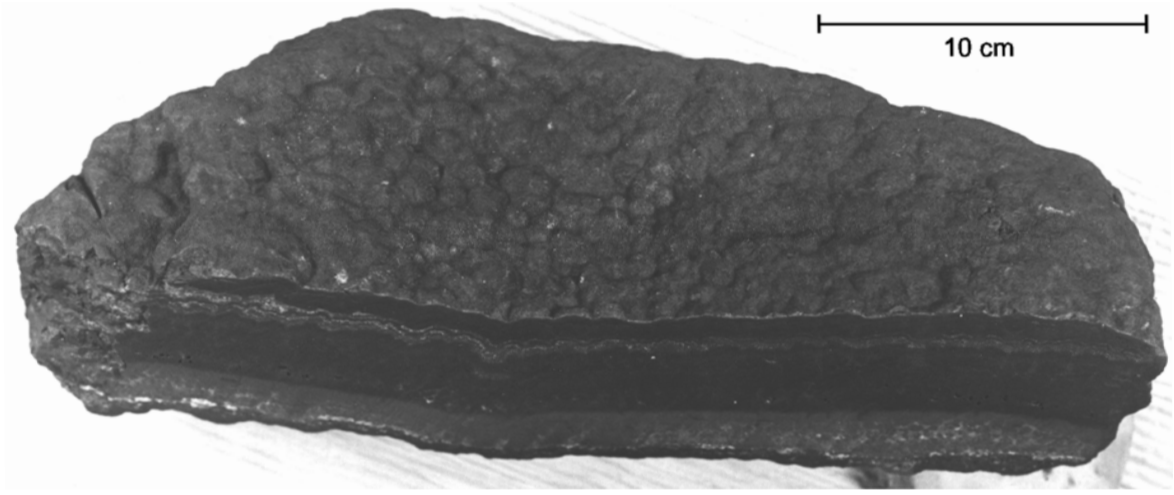

Fig. 11.15 Vertical section of a Co-rich Mn crust from the flanks of a guyot on the Ogasawara Plateau; N.W. Pacific (25°18.9'N, 143°54.8'E; 1515 m) collected by dredge during a cruise of the GSJ with R.V. Hakurei-maru in 1986. The substrate (not clearly seen) is phosphatized limestone. The crust is more than 20 cm across, about 10 cm thick and has a knobby surface texture. Element contents are: Mn 21.7%, Fe 18.9%, Co 0.81%, Ni 0.31%, Cu 0.04%, Pb 0.26% and Pt 0.29 ppm. The upper layer of the crust displays the highest Co content and the bottom layer the highest Pt (0.78 ppm). δMnO_2 is the principal mineral present with minor quartz and plagioclase. Photograph courtesy of A. Usui, GSJ.

is controlled by a number of factors such as changes in oceanic productivity, depth of the lysocline, rate of $CaCO_3$ dissolution and strength of AABW flow.

The highest Co contents are found in crusts occurring in the depth range 1,900-1,100 m which corresponds to the depth of the oxygen minimum zone. In samples taken from summits and the upper parts of slopes at depths less than 1,500 m, the Co contents of the crusts sometimes exceed 2%. At this depth, Mn tends to remain in solution because the deposition of MnO_2 is not favored at these low oxygen contents. The deposition rate of MnO_2 is therefore at a minimum and the Mn content in seawater at a maximum of about 2 nmol kg^{-1}. The flux of Co to the surface of the crusts remains constant with water depth at about 2.9 μg cm^{-2} ka^{-1}. The Co content of crusts is therefore a maximum just below the oxygen minimum zone and no special source of Co is required to explain their formation (Puteanus and Halbach 1988).

Pt is also significantly enriched in Co-rich crusts (Hein et al. 1988, 1997; Halbach et al. 1989). However, the mechanism of enrichment in the crusts is not well understood. Hodge et al. (1985) argued that Pt is oxidized from the $PtCl_4^{2-}$ state in seawater to the tetravalent state in manganese nodules. This process was thought to be responsible for the anomalously high Pt/Pd ratios in nodules (50-1,000) compared to seawater (4.5). However, Halbach et al. (1989) considered that this process would not be possible because the first formed tetravalent species, $PtCl_6^{2-}$, would be very stable in oxygenated seawater. Instead, they proposed that the $PtCl_4^{2-}$ would be reduced to Pt metal in the crusts with some minor amounts of Pt being introduced from cosmic spherules. Mn^{2+} was assumed to be the reducing agent for the reduction of the $PtCl_4^{2-}$.

However, Stüben et al. (1999) subsequently plotted stability field diagrams for Pt and Pd and showed that Pt is present in seawater dominantly as $Pt(OH)_2°$ and is close to saturation under seawater conditions. From this, it was argued that Pt is enriched in Co-rich crusts mainly as a result of the preferential adsorption of $Pt(OH)_2°$ onto the surface of Mn and Fe oxyhydroxide minerals. Pd, on the other hand, lies at the boundary of the stability fields of $PdCl_4^{2-}$ and $Pd(OH)_2°$ and is probably undersaturated in seawater. Since $PdCl_4^{2-}$ can not be adsorbed on Mn oxyhydroxides which have a negative surface charge, this would explain the so-called negative Pd anomaly in marine manganese deposits.

For Cu, the EH-pH diagram shows that the boundary between Cu^{2+} and $CuCl_3^{2-}$ as the dominant species in seawater lies slightly above the normal range of redox conditions in seawater (E_H of +0.48 V) (Fig. 11.16). At an E_H of +0.4 V, the concentration of Cu^{2+} in seawater would still be sufficient for it to be incorporated into manganese nodules by sorption on the surface of negatively charged MnO_2 (Glasby 1974;

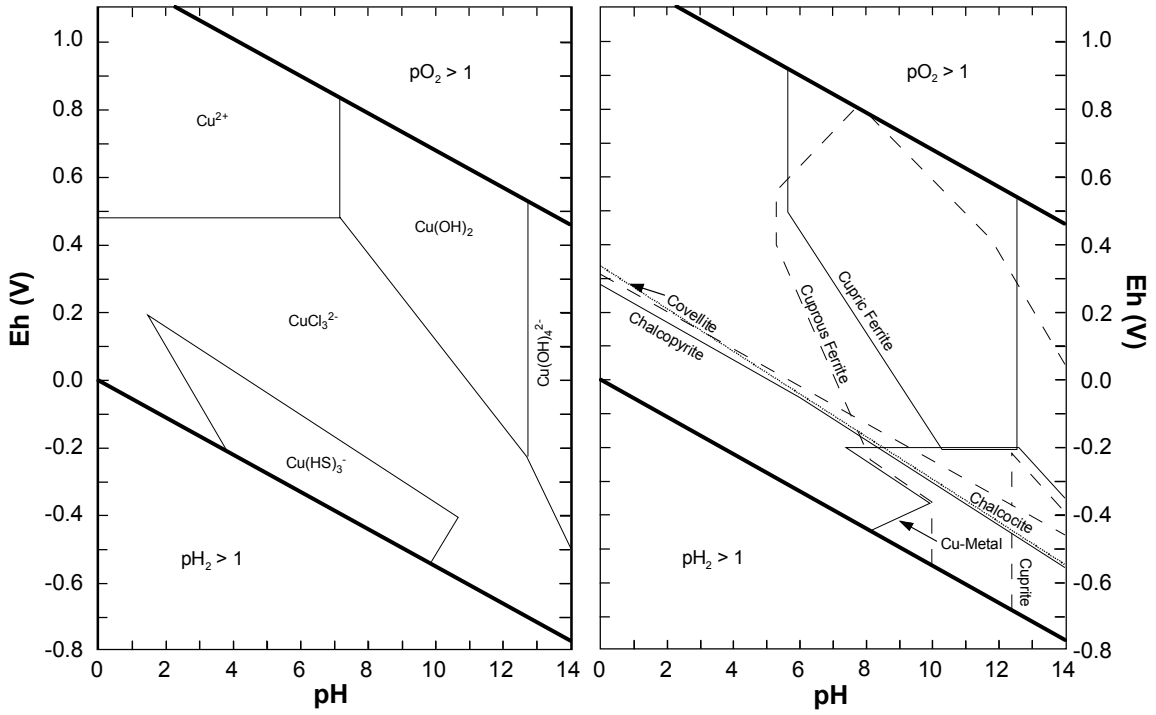

Fig. 11.16 E_H, pH diagram for Cu calculated for the chemical conditions prevailing in the deep sea (after Glasby and Schulz 1999). Note that, at pH 8, the metastable form of Cu is $Cu(OH)_2$ at an E_H, > +0.48 V. However, if the E_H, drops to +0.4 V corresponding to the E_H of seawater, the anionic species, $CuCl_3^{2-}$, becomes the more stable species. It is believed that the dominance of $CuCl_3^{2-}$ in seawater in the oxygen minimum zone accounts for the low Cu contents in Co-rich Mn crusts.

Glasby and Thijssen 1982). At somewhat lower E_H values, however, the concentration of Cu^{2+} in seawater would decline drastically and the anionic species $CuCl_3^{2-}$ would become the dominant species. Its sorption on MnO_2 would then be inhibited by charge considerations. This may well explain the high Ni/Cu ratios observed in cobalt-rich manganese crusts (max. 15) formed adjacent to the oxygen minimum zone where less oxidizing conditions prevail (Mangini et al. 1987; Meylan et al. 1990).

In many crusts, two generations of crustal growth can be observed, an older crust (18-12 Ma) and a younger crust (<12 Ma) which are separated by a thin phosphorite horizon (e.g. Halbach and Puteanus 1984; Mangini et al. 1987; Puteanus and Halbach 1988). However, McMurtry et al. (1994) and Jeong et al. (2000) subsequently obtained quite different ages for this boundary which are difficult to explain. For example, McMurtry et al. (1994) considered this boundary to have a minimum Oligocene age (28-33 Ma) and possibly a Late Paleocene age (55 Ma) based on dating of francolite in the Schumann Seamount crust. Jeong et al. (2000) also dated the age of this boundary in two crusts from seamounts in the Marshall Islands and Micronesia at 25 Ma. Pulyaeva (1997), on the other hand, tentatively accepted the boundary age for the younger crust generation proposed by Halbach and Puteanus (1984) for custs from the Magellan Seamount chain.

However, these age differences may be a case of mistaken identity (see section 11.4.10.1). Hein et al. (1993) have reported that two major phosphogenic episodes took place in the oceans during the period of formation of older crust layers centred on the Eocene-Oligocene (~34 Ma) and Oligocene-Miocene (~24 Ma) boundaries with a minor event in the Middle Miocene (~15 Ma). It is therefore possible that older ages for phosphogenesis reported by both McMurtry et al. (1994) and Jeong et al. (2000) correspond to one of the older episodes of phosphogenesis described by Hein et al. (1993, 2000). This view is supported by the observation of Jeong et al. (2000) that phosphatization on the seamounts of the Marshall Islands lasted until the peak of the second major epoch of phosphogenesis (25 Ma) reported by Hein et al. (1993) and was much earlier than the middle Miocene phosphatization (18-12 Ma) which is generally believed to be the time of crust phosphatization in the Pacific.

Koschinsky et al. (1997) have also related differences in composition between the older and younger layers of Co-rich crusts to the expansion of the oxygen minimium zone during periods of phosphatization of the older crust layers which led to the diagenetic remobilization of certain elements within this layer of the crust.

In order to be of potential economic interest, crusts should have Co contents >0.8%, average crustal thicknesses >40 mm and be situated in an area of subdued small-scale topography. Based on their extensive experience of studying Co-rich Mn crusts, Hein et al. (1987) listed a number of other criteria for locating interesting crusts. The crusts should be situated on large volcanic edifices shallower than 1,500-1,000 m and older than 20 Ma occurring in areas of strong oceanic bottom currents. The volcanic structures should not be capped by large modern atolls or reefs and the seamount slopes should be stable. The area should not be influenced by the input of abundant fluvial or eolian debris and there should be no local active volcanism. Most importantly, the area should be characterized by a shallow and stable oxygen minimum zone. In particular, the importance of mass wasting of coral debris from atolls and guyots in tropical environments is stressed. In a detailed sampling programme around islands and seamounts in the area of the Manihiki Plateau in the equatorial South Pacific, Meylan et al. (1990) recovered only thin Mn crusts with a maximum thickness of 20 mm because of the extensive mass wasting of limestone debris in the region which gave insufficient time for thick crusts to develop.

11.4.5 Shallow-Marine Ferromanganese Concretions

Shallow-water continental margin ferromanganese concretions have been reported in a number of areas such as the Baltic Sea, Black Sea, Kara Sea, Loch Fyne, Scotland, and Jervis Inlet, British Columbia (Calvert and Price 1977). In fact, these were the first type of marine Mn deposits to be discovered, during the 1868 Sofia expedition to the Kara Sea led by A.E. Nordenskiøld (Earney 1990).

Ferromanganese concretions from the Baltic Sea have been described in detail by Glasby et al. (1997a). Three main types of concretions occur there (spheroidal, discoidal and crusts). The concretions frequently, although not always, form around a glacial erratic seed or nucleus and display alternate banding of Fe- and Mn-rich layers tens to hundreds of μm thick. Mineralogically, the concretions consist of 10 Å manganate with abundant quartz and lesser amounts of feldspar and montmorillonite. The composition of the concretions is highly variable reflecting, in part, the variable amount of erratic material in the concretion. The composition is controlled by the redox characteristics of the environment. In particular, the higher Mn/Fe ratios of concretions from Kiel Bay compared to those from other areas of the Baltic reflects the diagenetic remobilization of Mn from the adjacent muds into the concretions during the summer anoxia (Table 11.6). This may be considered to be an example of the role of *anoxic diagenesis* in the formation of shallow-marine ferromanganese concretions (Glasby et al. 1997a). Cu, Zn and Pb may be trapped as sulfides in the associated sediments and this may explain their low contents in

Table 11.6 Average composition of ferromanganese concretions from various basins of the Baltic Sea. Mn and Fe in per cent; Co, Ni, Cu and Zn in ppm (after Glasby et al. 1997a).

	Gulf of Bothnia	Gulf of Finland	Gulf of Riga	Gotland Region	Gdansk Bay	Kiel Bay
Mn	14.6	13.3	9.7	14	8.7	29.3
Fe	16.6	19.7	22.8	22.5	18.5	10.1
Co	140	96	64	160	91	77
Ni	260	35	47	750	148	97
Cu	80	9	17	48	42	21
Zn	200	113	135	80	137	340
Mn/Fe	0.88	0.68	0.43	0.62	0.47	2.9

the concretions compared to deep-sea nodules. The growth rates of the concretions have been estimated to be 3-4 orders of magnitude higher than those of deep-sea nodules. A 20 mm diameter concretion is therefore about 500-800 years old (Glasby et al. 1996). This means that these concretions are transient features on the sea floor. In active areas of the sea floor, concretions may be buried by sediment during storms and new concretions then begin to form on erratic material exposed at the sediment surface. Certain anthropogenic elements, notably Zn, are enriched in the outer layers of the concretions as a result of the pollution of Baltic seawater over the last 160 years or so. Zn profiles in the outer layers of these concretions can therefore be used to monitor heavy-metal pollution in Baltic (Hlawatsch 1999; Hlawatsch et al. 2002). This technique will be useful if the planned clean up of the Baltic Sea is to be achieved during the present century.

Baltic Sea concretions can be classified into three main types based on their abundance, morphology, composition and mode of formation: those from the Gulfs of Bothnia, Finland and Riga, from the Baltic Proper and from the western Belt Sea.

Concretions from the Gulf of Bothnia are most abundant in Bothnian Bay where the abundance reaches 15-40 kg m^{-2} in an area of about 200 km^2. This is equivalent to about 3 million tons of concretions and has led to these deposits being evaluated as a possible economic source of Mn. These concretions are mainly spheroidal up to 25-30 mm in diameter and are formed in the uppermost water-rich sediment layers at well-oxidized sites. They are most abundant where sedimentation rates are <0.4 mm a^{-1}.

Concretions from the Baltic Proper are found mainly around the margins of the deep basins in a depth range 48-103 m. The concretions are mainly discoidal 20-150 mm in diameter and crusts. Their abundance is mainly sporadic and more rarely common to abundant. Locally, abundances of 10-16 kg m^{-2} are attained. Their formation is the result of the build up of Mn and Fe in the anoxic waters of the deep basins of the Baltic Proper. During major inflows of North Sea water (>100 km^3) into the Baltic which occur on average once every 11 years, the anoxic waters are flushed out of the basins. Mn and Fe precipitate out as an unstable gel but are ultimately incorporated into the concretions as

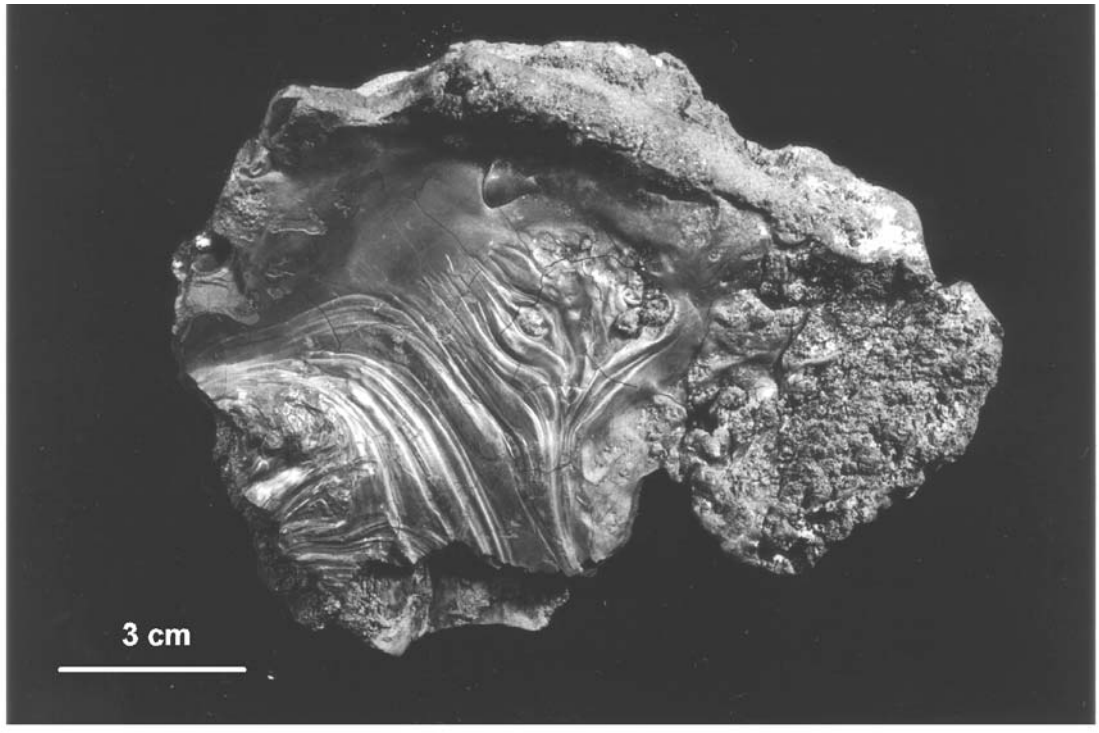

Fig. 11.17 A photograph showing the upper surface of a hydrothermal Mn crust from the Tyrrhenian Sea (39°31.40'N, 14°43.67'E, 996 m). Part of the surface displays the characteristic black metallic sheen of hydrothermal crusts (after Eckardt et al. 1997).

oxyhydroxides. These concretions occur mainly on lag deposits in the vicinity of the halocline where strong bottom currents occur.

Concretions from Kiel Bay in the western Belt Sea occur in a narrow depth range of 20-28 m at the boundary between sands and mud in zones of active bottom currents. They occur as coatings on molluscs and as spheroidal and discoidal concretions. The formation of the concretions is influenced by the development of summer anoxia which leads to the diagenetic remobilization and lateral transport of Mn. This accounts for the high Mn/Fe ratios of these concretions.

Marcus et al. (2004) have studied the speciation of Mn, Fe, Zn and As in one of the Baltic Sea concretions described by Hlawatsch et al. (2002) by means of micro X-ray fluorescence, micro X-ray diffraction and micro X-ray spectroscopy. The concretion was shown to consist of thin, alternating Fe- and Mn-rich layers. The Fe-rich layers consisted of two-line ferrihydrite in which As was mostly pentavalent and the Mn-rich layers consisted of birnessite in which Zn is tetrahedrally coordinated and sorbed in the interlayers of birnessite. The occurrence of ~15% of As(III) in Fe-rich layers and of ~15% Mn^{3+} in Mn-rich layers was thought to reflect the stagnation of the bottom waters at the time of the deposition of the Fe- and Mn-rich layers.

11.4.6 Hydrothermal Manganese Crusts

At mid-ocean ridges, three types of submarine hydrothermal minerals are found, sulfide minerals associated with silicates and oxides, sharply fractionated oxides and silicates of localized extent and widely dispersed ferromanganese oxides. The ferromanganese oxides are generally considered to have precipitated last in this sequence and are thought to represent a late-stage, low-temperature hydrothermal phase with temperatures of deposition estimated to be in the range 20-5°C (Burgath and von Stackelberg 1995). The hydrothermal Mn deposits are characterized by high Mn/Fe ratios and low contents of Cu, Ni, Zn, Co, Pb and detrital silicate minerals. They have growth rates exceeding 1,000 mm Ma^{-1} in some cases, more than three orders of magnitude faster than that of hydrogenous deep-sea nodules and crusts.

Compared to hydrogenous Mn nodules and crusts, hydrothermal Mn crusts are relatively restricted in the marine environment and make up less than 1% of the total Mn deposits in the world ocean. These crusts occur in all types of active oceanic environments such as at active mid-ocean spreading centers in the depth range 250-5,440 m, in back-arc basins in the depth range 50-3,900 m, in island arcs in the depth range 200-2,800 m (Eckhardt et al. 1997), in mid-plate submarine rift zones in the depth range 1,500-2,200 m (Hein et al. 1996) and at hot spot volcanoes in the depth range 638-1,260 m (Eckhardt et al. 1997). Fossil submarine hydrothermal manganese deposits have also been recovered from sediment cores in the Izu-Bonin Arc (Usui 1992) and the Central Pacific Basin (Usui et al. 1997).

Submarine hydrothermal Mn crusts have been reported from Enareta and Palinuro seamounts in the Tyrrhenian Sea (Eckhardt et al. 1977), along the Izu-Bonin-Mariana Arc (Usui et al. 1986, 1989; Usui and Nishimura 1992; Usui and Terashima 1997; Usui and Glasby 1998) and at the Pitcairn hotspot (Glasby et al. 1997b; Scholten et al. 2004). The Tyrrhenian Sea crusts consist of porous, black, layered Mn oxides up to 45 mm thick. In some cases, the surface has a black metallic sheen. The crusts overlie substrates such as calcareous sediment, siltstone and oyster shells. A photograph of a hydrothermal Mn crust from the Tyrrhenian Sea is shown in Figure 11.17. The crusts consist dominantly of 10Å manganate and 7Å manganate with minor quartz, illite, montmorillonite, plagioclase and goethite. The sample having the highest Mn content contained 54.2% Mn, 0.07% Fe, 33 ppm Ni, 200 ppm Cu, 20 ppm Zn, 11 ppm Pb and 910 ppm Ba with a Mn/Fe ratio of 774. It also had a low REE abundance and a negative Ce anomaly.

Submarine hydrothermal Mn crusts are also relatively common along the Izu-Bonin-Mariana Arc. Recent hydrothermal manganese crusts associated with active hydrothermal systems tend to occur on seamounts or rifts located about 5-40 km behind the volcanic front on the Shichito-Iwojima Ridge. Fossil hydrothermal Mn crusts associated with inactive hydrothermal systems occur on seamounts located on older ridges running parallel to the volcanic front in both forearc and backarc settings. Fossil hydrothermal Mn crusts are generally overlain by hydrogenetic Mn oxides. The thickness of the overlying hydrogenetic Mn crust depends on the length of time since hydrothermal activity ceased. Figure 11.18 shows the distribution of recent and fossil submarine hydrothermal Mn crusts across the Izu-Bonin Arc. Mineralogically, the hydrothermal Mn deposits consist of 10 Å manganate and/or 7 Å manganate. The Mn/Fe ratios of these deposits range from 10 to 4,670 and the contents of Cu, Ni, Zn, Co and Pb from 20 to 1,000, 1 to 1,403, 1 to 1,233, 6 to 209 and 0 to 93 ppm, respectively.

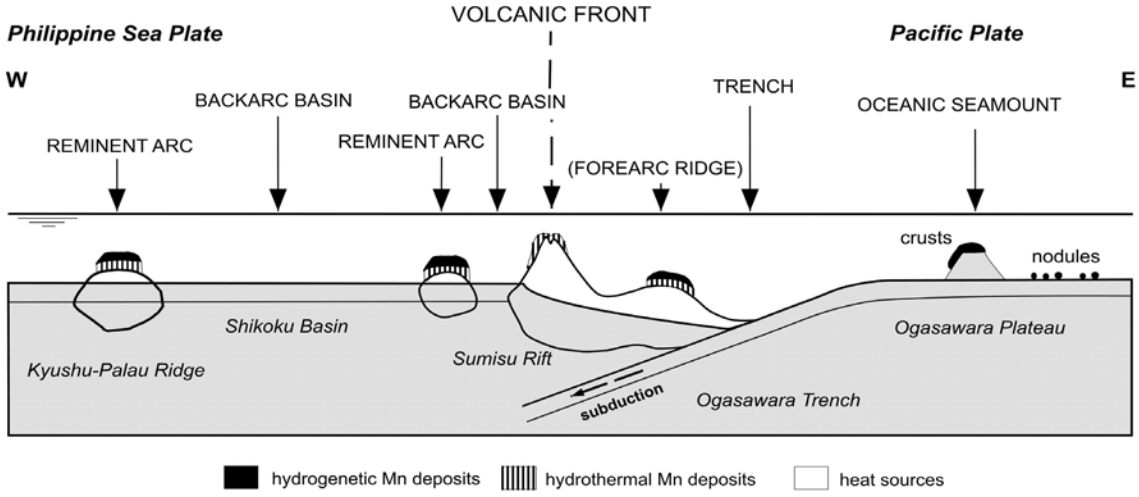

Fig. 11.18 A schematic diagram showing the distribution of hydrogenous and hydrothermal Mn deposits across an E-W section of the northwest Pacific island arc, south of Japan (after Usui and Terashima 1997). Four types of deposit are observed: i. hydrogenous Mn crusts and nodules occurring on Pacific seamounts and in deep-sea basins, ii. hydrogenous crusts on marginal seamounts of the remnant arcs, iii. modern hydrothermal Mn deposits associated with submarine volcanoes and backarc rifts in the active volcanic ridge, and iv. fossil hydrothermal Mn deposits usually overlain by younger hydrogenous Mn crusts from seamounts of the remnant arc. Each type of deposit has its own characteristic mineralogy, composition and growth rate. The growth of these deposits is closely related the evolution of the island arc system.

At the Pitcairn hotspot, massive hydrothermal Mn crusts display the highest Mn/Fe ratios (2,440), the lowest contents of Ni (18ppm) and Zn (21ppm) as well as the lowest aluminosilicate fraction (<1%) in individual horizons (sample 69-3 DS at a depth of 7-8 mm). This type of crust may therefore be considered to represent the most extreme hydrothermal endmember. The other types of hydrothermal Mn crust are probably formed as a result of the interpenetration and replacement of volcanoclastic sands or biogenic carbonates by hydrothermal Mn oxides. The low contents of Fe, Ni and Zn in the massive crusts were thought to reflect the rapid incorporation of these elements into sulphide minerals within the interior of the hotspot volcano such that only a small proportion of these elements are available for incorporation in the crusts. The small positive Eu anomaly in the crusts on a NASC-normalized basis indicated lower temperatures of the hydrothermal fluids within the hotspot volcano (<250ºC) compared to those at mid-ocean ridges (c.350ºC). A laser-ablation ICP-MS profile in one of the crusts revealed varying REE concentrations and patterns in the different layers of the crust. These data showed that the hydrothermal component was variable during the formation of the crust and was almost 100% in the upper layers of this crust but about 80% in the lower layers.

In addition to submarine hydrothermal manganese crusts formed near submarine hydrothermal vents, submarine hydrothermal plumes can transport detectable amounts of manganese up to 1,000 km from the crests of mid-ocean ridges (Burton and Statham 1988) (see section 11.2). Under favourable circumstances, part of this manganese can then settle out over manganese nodule fields and contribute to nodule growth. As an example, Chen and Owen (1989) identified a hydrothermal component in deep-sea manganese nodules from the southeast Pacific based on Q-mode factor analysis of compositional data for 76 nodules. The hydrothermal component was shown to have a Mn/Fe ratio of 0.31 which is typical of metalliferous sediments and to be distributed in two areas, one west of the East Pacific Rise between 3 and 25°S and the other east of the East Pacific Rise south of 25°S. These observations are supported by the subsequent identification of hydrothermal helium plumes in the South Pacific by Lupton (1998) in which a pair of intense hydrothermal plumes was observed to extend westwards from the East Pacific Rise at 10°S and 15°S at a water depth of 2,500 m and a plume of lesser intensity to extend eastwards into the Chile Basin at 30°S. The study of Chen and Owen (1989) therefore showed that a hydrothermal component can be incorporated into deep-sea manganese nodules forming within 1,000 km or so of an active mid-ocean ridge and not just into metalliferous sediments as is commonly assumed (Kunzendorf et al. 1993; Marchig 2000; Dekov et al. 2003; van de Fliert et al. 2003a).

11.4.7 Micronodules

Manganese micronodules are an important reservoir for Mn and associated transition elements in oxic deep-sea sediments (Stoffers et al. 1984). They are generally <1 mm in diameter. By contrast, macronodules are generally >3-6 mm. There is therefore a size gap in which no Mn deposits are found. This is a consequence of the fact that macronodules require a discrete nucleus several mm in diameter on which to form (Heath 1981). The abundance of micronodules appears to be inversely related to the sedimentation rate with highest abundances occurring in dark brown clays where sedimentation rates are low. The shape and internal structure of the micronodules is dependent on the nature of the seed material around which they form, of which calcareous tests, siliceous tests and volcaniclastic material are the most important. Micronodules tend to predominate in the coarse fraction of the sediment. The mineralogy and composition of the micronodules tend to be similar to that of the associated nodules, although differences do exist. Micronodules tend to have higher Mn/Fe ratios than nodules from the same sediment core. These differences are related to the depth of occurrence of the micronodules within the sediment column and reflect the importance of diagenetic processes in remobilizing elements within the sediment. In this sense, micronodules may be considered a transient feature which serves as a medium for recycling elements within the sediment and ultimately into manganese nodules. The study of micronodules has received relatively little attention because of the difficulty of hand picking them from the sediment.

In a detailed study of micronodules from various areas of the Pacific, Stoffers et al. (1984) showed that micronodules are characterized by regional variations in shape, texture, mineralogy and composition. Micronodules from the Southwestern Pacific Basin are most abundant in the dark brown clays of the central part of the basin. Mineralogically, these micronodules consist of 10 Å manganate and δMnO_2 with traces of quartz, phillipsite, quartz and feldspar. They have Mn/Fe ratios of 2.4 and Ni+Cu contents of 1.3%. These Mn/Fe ratios are somewhat higher than for the associated nodules but the Ni+Cu contents somewhat lower. The micronodules are botryoidal with smooth surface texture. Under the SEM, the surfaces of the micronodules display a honeycomb texture.

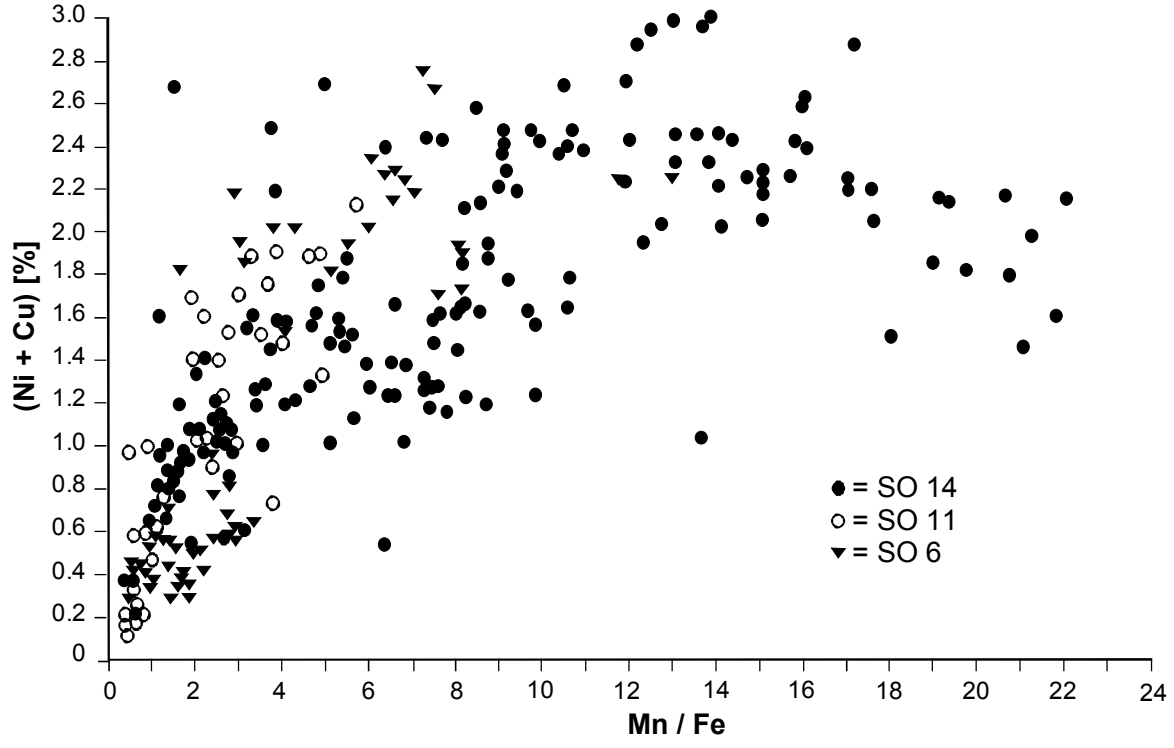

Fig. 11.19 A plot of Ni+Cu against Mn/Fe for micronodules from various areas in the Pacific (after Stoffers et al. 1984). SO-06 samples taken from the Clarion-Clipperton F.Z. region, SO-11 from the Peru Basin and SO-14 from the Southwestern Pacific Basin.

Micronodules from the C-C F.Z. occur mainly within siliceous ooze. They consist of 10 Å manganate with traces of quartz and sometimes phillipsite. They have Mn/Fe ratios of 4.7 and Ni+Cu contents of 1.7%. Again, the Mn/Fe ratios are somewhat higher than for the associated nodules but the Ni+Cu contents somewhat lower. The micronodules are dominantly spheroidal or have rod-like structures. Under the SEM, the surfaces of the micronodules consist of plates.

Micronodules from the Peru Basin occur in three stratigraphic horizons. The upper 50-100 mm of the core consists of a homogeneous brown calcareous-siliceous mud containing a high abundance of micronodules. The micronodules are larger (125-500 mm) than those taken deeper in the core (40-125mm) and have a mamillated botryoidal surface texture similar to that of the associated macronodules. They consist of 10 Å manganate with traces of quartz and feldspar. They have Mn/Fe ratios of 8.7 and Ni+Cu contents of 2.1%. These sediments are underlain by a highly bioturbated light yellowish brown mud containing varying amounts of calcareous and siliceous organisms. These micronodules have a smooth surface texture. The replacement of radiolaria and foraminifera can be clearly seen under the SEM. The micronodules are coarsely crystalline with well-defined rod-like structures. They consist of 10 Å manganate with traces of quartz and feldspar and have Mn/Fe ratios of 1.9 and Ni+Cu contents of 0.9%. The sharp drop in the Mn/Fe ratios of these micronodules compared with those from the sediment surface suggests that remobilization of Mn and associated transition elements has taken place within this sediment horizon. At the base lies a dark overconsolidated clay with a low content of siliceous tests but containing volcanic glass and fish teeth. These micronodules have Mn/Fe ratios of 5.0 and Ni+Cu contents of 1.3%. The high Mn/Fe ratios of these micronodules suggest a well-oxidized sedimentary environment from which no diagenetic remobilization has taken place. The importance of element remobilization in the yellowish brown muds is confirmed by the fact that micronodule abundance is high in the surface sediments, low in the yellowish brown muds and high again in the dark brown clays.

A plot of Ni+Cu against Mn/Fe for micro-nodules from various areas in the Pacific is presented in Figure 11.19. It is seen that, although Mn/Fe ratios in micronodules >20 can occur, particularly in the Peru Basin, there is no well-defined point of reversal such as observed for Mn nodules (Fig. 11.14), although there is a flattening of the curve at a Mn/Fe ratio of about 10. This is a consequence of the fact that the micronodules occur within the sediment column where conditions are less oxidizing than at the sediment surface. Pore waters are not as enriched in Mn, Ni and Cu within the sediment as at the sediment surface and the Mn/Fe ratios and Ni+Cu contents of micronodules are never as high as in the associated macronodules. Diagenetic fractionation of elements in micronodules is therefore not as pronounced as in the associated macronodules.

11.4.8 Mineralogy

There are three principal phases in manganese nodules, Mn oxides which tend to incorporate cationic transition metal species such as Ni^{2+}, Cu^{2+} and Zn^{2+}, Fe oxyhydroxides which tend to incorporate anionic species such as HPO_4^{2-}, $HAsO_4^{2-}$, HVO_4^{2-}, MoO_4^{2-} and WO_4^{2-} as well as the REE and Co^{3+} and detrital aluminosilicates which consist of elements such as SiO_2, Al_2O_3, TiO_2 and Cr_2O_3. In addition, carbonate fluorapatite (francolite) also occurs in older generations of Co-rich manganese crusts and as a discrete layer between the older and younger crust generations. Concentrations of individual elements in deep-sea Mn nodules and crusts therefore tend to covary with the relative amounts of these four phases (cf. Koschinsky and Halbach 1995; Koschinsky and Hein, 2003).

Three principal Mn oxide minerals are found in Mn nodules and crusts. Their principal X-ray diffraction peaks are given below together with their alternative mineral names (in parenthesis):

10 Å manganate 9.7 Å 4.8 Å 2.4 Å 1.4Å
(todorokite, buserite, 10 Å manganite)

7 Å manganate 7.3 Å 3.6 Å 2.4 Å 1.4Å
(birnessite, 7 Å manganite)

δMnO_2 2.4 Å 1.4Å
(vernadite)

Mn oxide minerals are characterized by fine grain size in the range 100-1,000 Å. These minerals are poorly crystalline and give diffuse X-ray diffraction patterns. FeOOH minerals also tend to be fine grained with sizes of the order of 100 Å and are generally X-ray amorphous (Johnson and Glasby 1969). In chloride-bearing solutions such as seawater, akagenéite (β-FeOOH) has been identified as the principal iron oxyhydroxide mineral present by Mössbauer spectroscopy (Johnston and Glasby 1978). However, there are no independent Fe-bearing minerals in Mn nodules.

Rather, δMnO_2 may be considered to be a randomly stacked Fe-Mn mineral. Some authors have suggested that there is usually an intimate association of δMnO_2 and $FeOOH \cdot xH_2O$ in deep-sea hydrogenous nodules due to the transport of minerals as colloidal particles and subsequent coagulation of these particles (Halbach et al. 1981). Detrital minerals such as quartz and feldspar normally give much stronger X-ray diffraction peaks than the Mn and Fe oxides. Within various types of nodules and crusts, the following Mn and Fe oxide minerals tend to be found.

Shallow-water concretions (Baltic Sea, Loch Fyne, Scotland)	10 Å manganate
Hydrothermal Mn crusts	10 Å manganate + 7 Å manganate
Deep-sea hydrogenous Mn nodules and crusts	δMnO_2

Deep-sea diagenetic Mn nodules 10 Å manganate

Within the Mn oxide minerals, there is a well-known dehydration sequence, 10 Å manganate → 7 Å manganate → δMnO_2 (Glasby 1972; Dymond et al. 1984). Samples collected on board ship must therefore be preserved moist in seawater to prevent mineralogical change on drying (Glasby et al. 1997a). A similar redox sequence 10 Å manganate → 7 Å manganate → δMnO2 is also observed in nodules. This means that nodules formed in less-oxidizing environments tend to contain 10 Å manganate whereas those formed in more-oxidizing environments tend to contain δMnO_2 (Glasby 1972). This trend is confirmed by the O/Mn ratios in nodules which vary from 1.60 in shallow-water concretions to 1.95 in deep-sea nodules. 98% of the Mn in deep-sea nodules is therefore in the Mn (IV) form (Murray et al. 1984; Piper et al. 1984).

Modern ideas on the structure of Mn oxides are based largely on the work of R. Giovanoli of the University of Berne. Much of this work was carried out on synthetic 10 Å (Na^+)-manganate prepared by the rapid oxidation of $Mn(OH)_2$ with O_2 for 5 hrs. Two types of 10 Å manganate may be considered. Todorokite is a large tunnel-structure mineral based on MnO_6 octahedra which can not expand or contract on heating to 100°C (or even 400°C) (Burns and Burns 1977, 1980; Turner and Buseck 1981; Waychunas 1991; Mellin and Lei 1993; Lei 1996; Post 1999). Buserite, on the other hand, is a phyllomanganate mineral with an expandable or contractible sheet-like structure (Giovanoli and Bürki 1975; Giovanoli 1980, 1985; Giovanoli and Arrhenius 1988; Waychunas 1991; Kuma et al. 1994; Usui and Mita 1995; Post 1999). It contains exchangeable interlayer cations (Ca^{2+}, Mg^{2+}, Cu^{2+}, Ni^{2+}, Co^{2+}, $2Na^+$) which occupy specific lattice sites. The ratio of these metals to Mn is 1:6 or 1:7. The uptake sequence of these metals into the buserite structure is $Cu^{2+} > Co^{2+} > Ni^{2+} > Zn^{2+} > Mn^{2+} > Ca^{2+} > Mg^{2+} > Na^+$. Fe can not enter the buserite lattice because any Fe^{2+} would be oxidized to insoluble FeOOH by Mn^{4+}. Instead, any excess FeOOH in the sediments reacts with the dissolving siliceous tests to form nontronite and therefore fix Fe in siliceous sediments. This explains the high Mn/Fe ratios in diagenetic nodules from oxic environments. Buserite may be considered to be an expandable or contractible sheet which can accommodate hydrated stabilizing interlayer cations. It can therefore be distinguished from todorokite by expanding the interlayer spacing to 25 Å on treatment with dodecylammonium hydrochloride or contracting it to 7 Å on heating in air to 100°C. Usui et al. (1989) had previously described the influence of divalent cations in stabilizing the structures of todorokite-like and buserite-like manganese oxide minerals in seawater, in air and dried in air at 110°C (cf. Usui 1979).

Mellin and Lei (1993) have explained the mineralogy of the principal marine Mn deposits in the following terms. Low-temperature hydrothermal 10 Å manganate has a less stable todorokite-like structure with tunnel walls composed of $Mn^{2+}O_{2x}^{2-}(OH)_{6-2x}$ octahedra. High-temperature hydrothermal 10 Å manganate has a more stable todorokite-like structure as a result of the oxidation of interlayer Mn^{2+}. In both cases, divalent cations such as Cu^{2+}, Ni^{2+} and Zn^{2+} are deposited as sulfides prior to the deposition of Mn minerals which explains the low contents of these metals in these deposits. Diagenetic 10 Å manganate, on the other hand, has an unstable buserite-like structure. Divalent cations such as Ni^{2+}, Cu^{2+}, Zn^{2+}, Mg^{2+} and Ca^{2+} can substitute for $2Na^+$ in the interlayer spacing. Diagenetic deep-sea nodules formed in oxic environments have high Cu^{2+} and Ni^{2+} contents (up to 2%) as a result of the release of these elements from siliceous tests. The resulting high contents of Ni+Cu in these nodules explain their commercial interest. Diagenetic shallow-water concretions have low Cu^{2+} and Ni^{2+} contents (<0.1%) as a result of trapping these elements in the sediment column as sulfides. The composition of marine manganese deposits therefore reflects both the mineralogy of the sample and the availability of the transition metal ions for nodule formation (Glasby and Thijssen 1982).

The mineralogical data reported above were obtained from X-ray diffraction analysis. However, this technique has distinct limitations when applied to the

study of marine manganese nodules and crusts where the minerals making up these deposits are fine grained and the powder diffraction patterns for many of these minerals are similar (Post 1999). This makes the unambiguous identification of these minerals difficult (Manceau et al. 1992a). For this reason, other techniques have been used to study the mineralogy of these deposits at the micron (μm) level such as electron diffraction (Varentsov et al. 1991) and X-ray absorption spectroscopy (XAS). XAS includes both X-ray absorption near-edge structure (XANES) and extended X-ray absorption fine structure (EXAFS) (Manceau et al. 1992a,b, 2002; Drits et al. 1997; Silvester et al. 1997). Studies using these techniques were initiated by F.V. Chukhrov, Director of the Institute of Geology of Ore Deposits of the Russian Academy of Sciences in Moscow, in the 1980s (e.g. Chukhrov et al. 1989) and achieved world recognition following joint Franco-Russian work on this topic.

Using these methods, it was established that the 10 Å phase in manganese nodules actually belongs to one of at least seven minerals each with different structural characteristics: asbolane (a Co-Ni-bearing manganese oxide mineral), buserite-I, buserite-II, todorokite, mixed-layered phases: asbolane-buserite-I, buserite-I-buserite-II and buserite-I-"defective lithiophorite" (Manceau et al. 1987, 1992b; Drits et al. 1997). In the case of the manganese crust from Krylov Seamount located in the eastern North Atlantic on the Cape Verde plate, Varentsov et al. (1991a) showed that the lower layers of the crust consisted dominantly of Fe-vernadite (δMnO_2) and goethite with admixtures of mixed layered asbolane-buserite whereas the upper layers consisted of Fe-vernadite and feroxyhite ($\delta FeOOH$) with subordinate amounts of birnessite, mixed-layered asbolane-buserite and goethite (cf. Varentsov et al. 1991b). This sequence was thought to reflect a significant hydrothermal input into the crust when it first formed near the crest of the Mid-Atlantic Ridge which was followed by a dominantly hydrogenous origin. In addition, asbolane has been shown to occur as flakes and microflakes in manganese crusts and nodules from the Atlantis Fracture Zone and Krylov Seamount in the Atlantic Ocean, the Kurchatov Fracture Zone and the Chile Plate in the Pacific Ocean and in manganese micronodules in nannofossil ooze from the Indian Ocean (Chukhrov et al. 1982, 1983).

An important question is the anomalous position of Co in the geochemistry of manganese nodules. Glasby and Thijssen (1982) have interpreted this in terms of the crystal field characteristics of Co. On this basis, Co^{3+} (d^6) is stable in nodules in the low spin state with octahedral coordination and has an ionic radius of 0.53 Å which is almost identical to that of Fe^{3+} and Mn^{4+}. As such, Co may substitute in either MnO_2 or FeOOH as the trivalent ion but not in the interlayer spacing of 10 Å manganate as the divalent ion as is the case for Ni^{2+}, Cu^{2+}, Zn^{2+} and Mn^{2+}. The ability of Co to substitute in both Mn and Fe oxyhydroxides leads to its correlation with either Mn or Fe in nodules or crusts depending on the environment of formation (Burns and Burns 1977, 1980; Halbach et al. 1983; Giovanoli and Arrhenius 1988). Experimental evidence has confirmed that Co^{3+} is the dominant form of Co in Mn nodules (Dillard et al. 1984; Hem et al. 1985; Manceau et al. 1997).

11.4.9 Dating

Deep-sea Mn nodules and crusts are amongst the slowest growing minerals on Earth (Manheim 1986). They have a minimum growth rate of 0.8 mm Ma^{-1} (Puteanus and Halbach 1988) which is equivalent to the formation of about one unit cell every year. Shallow-water concretions grow about 10^4 times faster. Several methods have been used to date deep-sea manganese nodules and crusts (Ku 1977; Mangini 1988).

One of the earliest methods used to date nodules involved K-Ar dating of the volcanic nucleus of the nodule. This method is of limited value because submarine weathering of the core often invalidates the results. In addition, the method makes no allowance for any time gap between the formation of the nucleus and subsequent Mn accretion or for hiatuses in growth of the Mn deposit. Only a minimum average growth rate is therefore obtained. Although this method was used by early workers (e.g. Barnes and Dymond 1967), it is too crude to be of much value now.

In addition, Moore and Clague (2004) have recently demonstrated the progressive thickening of ferromanganese crusts along the Hawaiian Ridge with increasing distance from the Hawaiian hotspot (Loihi Seamount). From a comparision of the maximum thicknesses of the submarine crusts along the ridge with radiometric ages of adjacent subaerial features, these authors estimated the growth rates of the crusts to be about 2.5 mm Ma^{-1}. This growth rate was then used to deduce the ages of landslide deposits and volcanic fields occurring away from the axis of the ridge from the estimated ages of associated crusts. This may be considered to be an example of indirect dating of ferromanganese crusts.

Several attempts have been made to date Mn nodules and crusts by paleontological methods. Initial

studies by Harada and Nishida (1976, 1978) established slow growth rates for the outer layers of some deep-sea nodules (1.0-6.7 mm Ma^{-1}) but higher rates for the inner layers of some nodules (39 mm Ma^{-1}) based on biostratigraphic analysis of calcareous microfossils. Cowen et al. (1993) subsequently determined the ages of different layers of a Mn crust (KK84-RD50 S1B) from Schumann Seamount in the North Pacific based on the identification of coccolith imprints at various depths in the crust (see section 11.4.10.1). In a detailed study, Pulyaeva (1997) also identified three main periods of growth of Co-rich Mn crusts from the Magellan Seamounts in the western Pacific based on a study of calcareous microfossils. On this basis, it was established that the crusts began forming intermittently in the Late Cretaceous in the presence of phosphatized nannoforaminifera. The crusts attained a composition similar to that of today in the Eocene but the Miocene-Pliocene was shown to be the most favourable period for growth of the crusts. Numerous interruptions in the growth of the crusts were observed with major regional hiatuses being recorded at the Cretaceous-Paleocene and Eocene-Oligocene boundaries (see section 11.4.10.1). More recently, Shilov (2004) has reported on a major programme of dating manganese nodules from the C-C F.Z. based on age determinations of radiolaria in the nodules. From this, he was able to demonstrate that active growth of the manganese nodule fields started between the Late Oligocene and Early Miocene at about 23.7 Ma and that the principal layers which make up 50-80% of the total nodule volume in individual nodules were formed in the Middle Eocene (16.6-11.2 Ma) and Late Miocene-Pleistocene (11.2-1.8 Ma). He also established that the highest growth rates of the nodules (2.5-3.7 mm Ma^{-1}) occurred during the Pleistocene-Holocene (1.8-0 Ma). These ages are in agreement with the findings of Glasby (1978) who recorded the presence of buried manganese nodules in D.S.D.P. cores associated with sediments of Oligocene age and older (cf. Usui and Ito 1994; Ito et al. 1998) and by von Stackelberg and Beiersdorf (1991) who showed that most of the nodules in the C-C F.Z. southeast of Hawaii began their growth at Tertiary hiatuses. These ages are much older than the middle Miocene age (~12-15 Ma) obtained by Kadko and Burckle (1980) for two nodules from the C-C F.Z. based on the age of fossil diatoms in the nodules.

Nonetheless, most modern methods of dating Mn nodules and crusts rely on radiometric determinations. There are three principal methods available based on the following isotope ratios $^{230}Th/^{232}Th$, $^{231}Pa/^{230}Th$ and ^{10}Be. The half lives of ^{230}Th, ^{231}Pa and ^{10}Be are 75,200 a, 32,000 a and 1.5 Ma, respectively (Turekian and Bacon 2004). The $^{230}Th/^{232}Th$ and $^{231}Pa/^{230}Th$ methods can therefore only date samples to ages of 300,000 and 125,000 a (corresponding to 4 half lives of the isotopes), respectively, which is equivalent to the outer 1-2 mm of a deep-sea nodule or crust. The ^{10}Be method, on the other hand, permits dating back to ~10 Ma which is equivalent to a depth of a few cm in some samples (Turekian and Bacon 2004). Hein et al. (2000) have compiled a list of all isotopically-determined growth rates of hydrogenous Mn crusts to that date.

The ^{238}U and ^{235}U decay-series methods are based on the fact that ^{230}Th and ^{231}Pa are generated in seawater by the decay of U isotopes. The isotopes are then carried to the sea floor on particles and incorporated into the nodules and crusts. The residence times for Th and Pa in seawater are short (less than 40 and 160 years respectively). The distribution of ^{230}Th and ^{231}Pa with depth in nodules or crusts can be measured by counting a particles after separation from the nodule material and plating on a planchet or more rapidly by α-track counting on nuclear emulsion plates. The growth rate of the nodule or crust can then be calculated from the formula

$$dC/dt = S\,dC/dx - \lambda C$$

$$\text{or} \quad C_{(x)} = C_0 \exp(-x\lambda/S)$$

where $C_{(x)}$ is the concentration at depth x, ë is the decay constant of the nucleus ($=\ln 2/\tau_{1/2}$), $\tau_{1/2}$ the half life of the nuclide and S the nodule growth rate.

The $^{230}Th/^{232}Th$ and $^{231}Pa/^{230}Th$ methods were the first radiometric methods to be used for dating of manganese nodules but their application was limited because of the short half lives of ^{230}Th and ^{231}Pa. In spite of the limitation of working with samples from the uppermost 1-2 mm of the sample, high resolution studies of nodules have been achieved using this method. For example, Eisenhauer et al. (1992) analyzed 69 samples to a depth of 1.4 mm with a resolution of 0.02 mm in the VA 13/2 Mn crust sample (see section 11.4.10.1). The samples were analyzed by alpha counting after chromatographic separation of thorium from uranium and electroplating the elements on stainless steel holders. However, the development of the thermal-ionization mass spectrometric (TIMS) method for determining U and Th isotopes increased the precision of the measurements and extended the possibilities of this method (Chabaux et al. 1995, 1997).

In particular, Böllhofer et al. (1996, 1999) used this method to investigate the growth rates of diagenetic

manganese nodules from the Peru Basin. These nodules were shown to have high growth rates of ~110 mm Ma^{-1} but with frequent oscillations in growth rate which were attributed to transitions in the glacial/interglacial cycle. These climatic variations were assumed to control the depth of the suboxic/oxic boundary in the sediment leading to changing growth rates and the development of distinct laminations within the nodules. However, von Stackelberg (1997, 2000) subsequently observed that the highest growth rates in these nodules occur on the underside of large nodules which repeatedly sink to a level immediately above the redox boundary where diagenetic recycling of Mn is at a maximum. These authors therefore suggested that layering of these nodules was the result of the lifting of these nodules by benthic organisms within the oxic surface sediments from a diagenetic to a hydrogenous environment rather than the result of climatic change as proposed by Böllhofer et al. (1996, 1999).

Han et al. (2003) also established that there are four orders of basic cyclic growth patterns in a deep-sea manganese nodule from the C-C F.Z. based on analysis of samples taken at intervals of 0.1 mm in the outer 1.3 mm of the nodule using the $^{230}Th_{excess}/^{232}Th$ method. These growth patterns were named laminae bonds, laminae zones, laminae groups and laminae pairs and had thicknesses of 402-454, 185-206, 58-67 and 15-18 μm, respectively. This rhythmic growth was considered to be related to Milankovitch cycles with the growth cycles of the laminae, bands and zones corresponding to the periods of eccentricity, obliquity and precession of the Earth's orbit, respectively. From the thicknesses of these laminae, it was was then possible to establish a net growth rate of the outer layers of the nodule of 4.5 mm Ma^{-1} based on the Earth's orbital cycle in close agreement with the rate of 4.6 mm Ma^{-1} determined by $^{230}Th_{excess}/^{232}Th$ dating of the nodule. This is an excellent example of the high resolution that can now be attained using $^{230}Th/^{232}Th$ dating.

^{10}Be dating involves a measurement of the depth profile of ^{10}Be in a deep-sea nodule or crust. The half life of ^{10}Be is 1.5 Ma which normally permits dating back to ~10 Ma, although earlier authors dated crusts back to ~14 Ma by analyzing larger amounts of material for the older samples (Segl et al. 1989). ^{10}Be is a cosmogenic nuclide which is deposited at the sea surface before being mixed into the oceans. Its residence time in the ocean is about 1,000 yrs. Because of its greater half life, ^{10}Be can be measured to much greater depths within the nodule or crust (> 40 mm) than the U decay-series isotopes (1-2 mm). Post-depositional diffusion of ^{10}Be is not considered a problem in determining the growth rates of the nodule or crust (cf. Kusakabe and Ku 1984). The development of accelerator mass spectrometry (AMS) led to a reduction in sample sizes and counting times by several orders of magnitude compared to measurements based on radioactive decay. Much better resolution can therefore be obtained and dating to 15 Ma is now possible. This predates the age of the lower Miocene Antarctic glaciation. Discontinuities in the growth rates of nodules and crusts can also be determined from breaks in the ^{10}Be depth profile. As an example, Koschinsky et al. (1996) determined the growth rates of the surface layers of two NE Atlantic manganese crusts to be 3 and 4.5 mm Ma^{-1} using this method. Mangini et al. (1990) and Usui et al. (1993) also determined the growth rates of S.W. Pacific nodules to be in the range 1.1-6.0 mm Ma^{-1}.

A particularly interesting application of the ^{10}Be method involved the dating of entrapped manganese nodules in an ODP sediment core taken in the Campbell Nodule Field located at the foot of the Campbell Plateau in the Southwestern Pacific Basin (Graham et al. 2004). From the ages of the rims of the buried nodules, it was concluded that bottom water circulation was more intense, and therefore sedimentation rates were lower, during the periods 10-5.5 Ma and 1.5-0 Ma which facilitated the maintenance of the nodules at the sediment surface. However, a major limitation of the ^{10}Be method is that it does not permit the direct determination of the ages of the earliest sections of Co-rich Mn crusts. ^{10}Be dating must therefore be used in conjunction with other methods for this purpose.

Sr isotope stratigraphy has also been developed as a high resolution stratigraphic method for determining the growth rates of hydrogenous and hydrothermal Mn crusts based on a comparison of the Sr isotope ratios of individual layers in the crust with Sr isotope curves for seawater (Futa et al. 1988). In principal, this method can be used to identify hiatuses in the growth of the crusts to ages in excess of 20 Ma. However, von der Haar et al. (1995) subsequently demonstrated that Sr in the crusts is extracted from both the phosphatic and detrital phases of the crust during leaching and that the Sr in the Mn oxide phase exchanges with seawater throughout the history of the crust. The method therefore appears to be of little value in dating Mn crusts.

In addition, indirect methods of dating Mn crusts have been developed such as the one based on the inverse relationship between the Co content of the crusts and their rate of accumulation (Manheim and Lane-Bostwick 1988; Puteanus and Halbach 1988).

Based on the analysis of 520 samples of ferromanganese crusts from ~250 locations, it was established that the flux of Co into ferromanganese crusts is constant over the entire period of growth of the crusts whereas the flux of Mn into the crusts is variable. As a consequence, the content of Co in crusts is inversely proportional to the rate of formation of the crust. It therefore became possible to derive an empirical equation relating the growth rate of each layer in a crust to the Co content in that layer by fitting data derived from the ^{10}Be dating of 20 ferromanganese crusts. This led to the formulation of the equation G (mm Ma^{-1}) = 1.28/[Co(%) – 0.24] where G is the growth rate of the layer of the crust under consideration from which the growth rate and therefore the age of the crust can be derived. However, modification of this equation is required in cases where phosphatization of the crust has occurred. The great advantage of this method is that it requires no further radiometric age determinations to date a crust of unknown age. It is therefore much easier to calculate the growth rates of manganese crusts using this method than by the other methods. Frank et al. (1999a) have confirmed the validity of the Co geochronometer and shown that it provides detailed information on the growth history of ferromanganese crusts prior to 10-12 Ma where the ^{10}Be method can not be applied.

Growth rates of shallow-water ferromanganese concretions from Mecklenburg Bay in the Baltic Sea have also been determined by ^{210}Pb dating (half life of ^{210}Pb is 22.3 years) and by comparison of the distribution of the Zn concentration (on a mm scale) in the outer layers of selected concretions with the distribution of Zn in dated sediment cores from the same area (Hlawatsch 1999). These data gave growth rates for the concretions in the range 0.018 - 0.21 mm a^{-1} which are 4 to 5 orders of magnitude higher than for the deep-sea manganese deposits. Liebetrau et al. (2002) also determined the growth rates of concretions from this area from the distribution of $^{226}Ra_{excess}$/Ba ratios with depth in selected concretions (half life of ^{226}Ra is 1622 years) and obtained somewhat lower growth rates in the range 0.0075 - 0.021 mm a^{-1}. From these data, the maximum age of these concretions was calculated to be 4,300 ± 300 years which is close to the period when sea level stabilized at its present level in the Baltic about 5,500 to 4,500 years ago. By contrast, very little information is available on the growth rates of submarine hydrothermal manganese crusts at present (Lalou et al. 1983; Usui and Nishimura 1992; Usui and Terashima 1997).

11.4.10 Mn Crusts as Paleoceanographic Indicators

11.4.10.1 Recording Hiatuses in Mn Crusts

Mn crusts may be considered to be condensed stratigraphic sections that record variations in paleoceanographic conditions with time. High resolution dating of Mn crusts can therefore be used to record the occurrence of major paleoceanographic events. A number of such studies has been undertaken (Segl et al. 1989; McMurtry et al. 1994; Koschinsky et al. 1996; Frank et al. 1999a). In this section, the results of two detailed studies of dating deep-sea manganese crusts using various methods of radiometric dating are presented. In addition, the distribution of the long-lived radiogenic isotopes of Nd, Pb, Be, Hf and Os in Co-rich Mn crusts has been extensively used to study the patterns of deep ocean circulation and the provinciality of these crusts over the past 10-15 years. This topic has been excellently reviewed by Frank (2002).

One of the most thoroughly studied Mn crusts was collected on top of an abyssal seamount at 4,830 m water depth in the equatorial N. Pacific in 1976 during cruise VA 13/2 of R.V. Valdivia (sample 237 KD) (Friedrich and Schmitz-Wiechowski 1980). It is a large hemispherical Fe-Mn crust 500 mm in diameter and up to 250 mm thick partly covering a basalt substrate. It is quite different in character from the Co-rich Mn crusts described in section 11.4.4. The volcanic seamount on which it occurs was formed about 65 Ma near crest of the East Pacific Rise. Submarine weathering of glass on the surface of the submarine basalt led to formation of an 8 mm thick nontronite layer. The seamount migrated north across the equatorial high productivity belt during which time it was above the Carbonate Compensation Depth (CCD).

The mode of formation of this crust has been outlined by von Stackelberg et al. (1984). Below a depth of 40 mm, the crust was characterized by higher Fe contents which could be attributed to the dissolution of calcareous tests resulting in an increased supply of iron to the crust. Goethite was the main mineral formed and could be seen as yellowish-brown flecks. Calcareous tests were also observed within the crust. At 40 mm, there is an abrupt change in composition of the crust with higher Mn/Fe (1.6) and Ce/La (3.5) ratios and higher contents of Ni (0.45%) and Cu (0.25%) above that boundary. These changes were associated with the development of a strong AABW at 12 Ma. From 10-0 mm, the chemical compo-

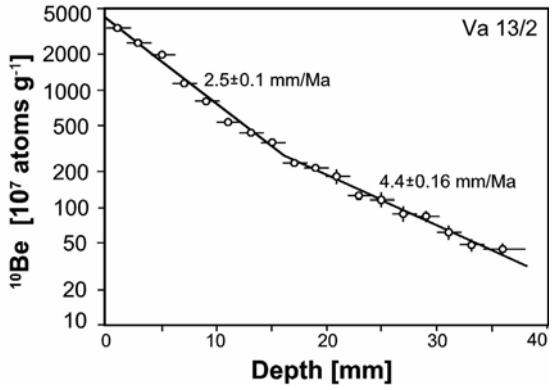

Fig. 11.20 Profile of ^{10}Be with depth in the Mn crust VA 13/2 from the Clarion-Clipperton F.Z. region showing the change in a growth rate in the crust at a depth of 16 mm (after Segl et al. 1989). Other time markers in the crust were marked by changes in the structure of the crust.

sition was again similar to that below 40 mm reflecting the weak influence of AABW at present.

^{10}Be dating of the crust was undertaken by Segl (1984, 1989). Figure 11.20 shows the variation in growth rates within the crust. An age of 12-13 Ma was determined at a depth of 36 mm in the crust. This was taken to correspond to the build up of East Antarctic ice sheet, the onset of high AABW velocities, increased ventilation of the deep ocean and a major erosional event in Pacific. At 6.2-6.7 Ma at a depth of 16 mm in the crust, there was a change of growth rate and a visible change in crustal structure. This was taken to correspond to a decrease in global $\delta^{13}C$, a lowering of sea level, isolation and drying of Mediterranean, shoaling of the Panama Isthmus and an increase in bottom water circulation rates and oceanic fertility. At 3 Ma at a depth of 8 mm in the crust, there was a visible change in crustal structure. This was taken to correspond to closure of the Panama Isthmus and the onset of northern hemisphere glaciation. These events are recorded in many manganese crusts in the World Ocean. Subsequent determination of the distribution of Nd isotopes within this crust showed a decrease in the ε_{Nd} values from 3-5 Ma to the present (see later). These data suggest that the closure of the Panama Isthmus about 3-4 Ma may have played a role in reducing the inflow of Atlantic-derived Nd into the Pacific Ocean (Burton et al. 1997; Ling et al. 1997).

High resolution ^{230}Th profiles were also obtained by Eisenhauer et al. (1992) for this crust as part of a detailed study of growth rates in crusts during last 300 ka. 69 samples were taken in the upper 1.4 mm of crust at intervals of 0.02 mm. Fig. 11.21 shows the high resolution growth rates for the crust. From 0 - 0.88 mm, the growth rate was determined to be 6.6 ± 1.1 mm Ma^{-1}, from 0.9 - 1.28 mm 6.1 ± 1.7 mm Ma^{-1} and from 1.3-1.4 mm 5.8 ± 1.4 mm Ma^{-1}. Two breaks in the growth rate were observed. These correspond to standstills in growth at 284-244 ka and 138-128 ka which are equivalent to glacial stages 8 and 6. The growth rates of the crust were seen to be higher during interglacial (stages 1 and 5) and lower during glacial stages. These data imply a correlation between the growth rate of nodules and crusts and climate in the late Quaternary as previously proposed by Mangini et al. 1990a).

Most recently, supernova debris has been identified within the VA 13/2 crust based on a study of the distribution of ^{60}Fe in a well-resolved time profile within this crust (Knie et al. 2004). 28 samples between 1-2 mm thick representing a total period of about 13 Ma were dated by means of the ^{10}Be method. A ^{60}Fe anomaly was detected at a depth corresponding to an age of 2.8 Ma (the half life of ^{60}Fe is 1.49 Ma). The ^{60}Fe measured at this time horizon corresponds to an influx

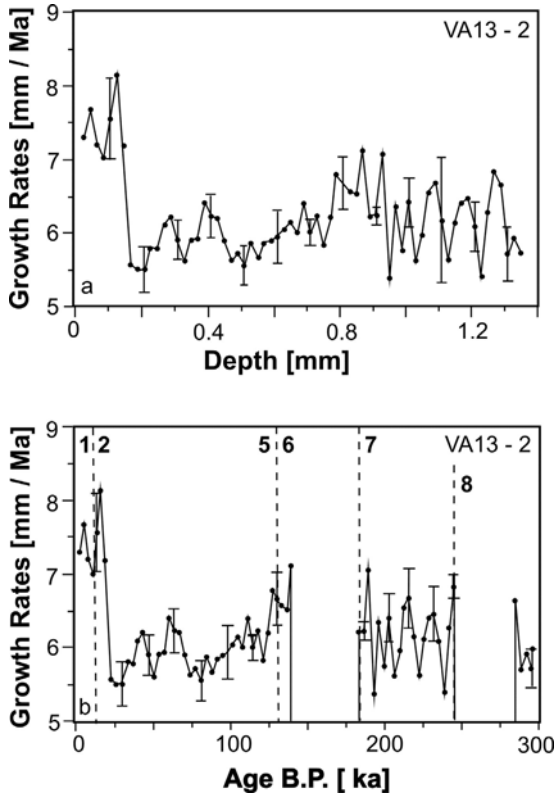

Fig. 11.21 High resolution growth rates for Mn crust VA 13/2 plotted as a function of depth in the crust (a) and of time (b) (after Eisenhauer et al. 1992). The major climatic changes are marked by dotted lines. High growth rates are mainly associated with interglacial stages (especially during the Holocene and stage 5) whereas low growth rates are associated with glacial stages. Periods of growth standstills are associated with glacial stages 6 and 8.

of about 2.9 x 10^6 atoms of ^{60}Fe cm^{-2} to the Earth's surface. This amount is compatible with the ^{60}Fe being derived from an exploding supernova located about 10 light years from Earth. This event began at ~3.0 Ma and lasted ~300 ka and therefore coincides with the onset of N. Hemisphere glaciation at 2.8 Ma. The explosion released as much energy as the sun will do in its entire lifetime. The authors speculated that the interstellar particles may have acted as nuclei for the condensation of water and therefore cloud formation in the atmosphere. This offers the possibility that the Northern Hemisphere glaciation may have been controlled by interstellar events and not by changes in CO_2 levels in atmosphere as is more commonly assumed. A weak ^{244}Pu signal from this explosion was also detected in the crust (Wallner et al. 2003).

The VA 13/2 crust has also been used for paleoceanographic studies by a number of authors (Abouchami et al. 1997; Ling et al. 1997; David et al. 2001; Frank et al. 1999b; van de Fliert et al. 2004a).

Detailed studies have also been carried out on the Co-rich Mn crust (KK84-RD50 S1-B), a 95 mm thick crust, which was sampled at a depth of 2,250-2,600 m from near the summit of Schumann Seamount, one of the Musicians Seamounts, located 700 km north of Kaui, Hawaii. The initial study was based on identification of coccolith imprints in the crust from which the ages of different layers of ages of the individual layers could be determined (Cowen et al. 1993). These ages were not well constrained and varied from 1-4 Ma to >10 Ma. However, the minimum age for the upper 27 mm of the crust was shown to be Eocene giving an average growth rate for the crust of about 0.5 mm Ma^{-1}. Extrapolating this growth rate through the entire 95 mm of the crust gave a very much older age for the crust than was accepted for Co-rich crusts at that time.

Subsequently, McMurtry et al. (1994) carried out a very detailed study of this crust using a variety of techniques including ^{10}Be profiling of the crust, determination of $^{87}Sr/^{86}Sr$ and $\delta^{18}O$ isotopic ratios of included phosphatized limestone debris and vein infillings and Co chronometry of the ferromanganese layers. Using the ^{10}Be method, it was possible to date only the upper 12 mm of this crust with the lower 82 mm of the crust lying beyond the limits of this method. However, by combining the ^{10}Be data with results obtained from microfossil dating (Cowen et al. 1993) and Co chronometry, it was possible to establish that formation of the crust began at least in the Eocene and possibly as far back as the Cretaceous. Within the crust, eight major disconformities were identified of which three of the upper disconformities in the crust were placed at the Plio-Pliocene, the Middle Miocene and, tentatively, the Paleocene-Eocene boundaries. As previously described, McMurtry et al. (1994) considered the boundary between the older and younger crust layers had a minimum Oligocene age (28-33 Ma) but was possibly of Late Paleocene age (55 Ma) but this may reflect the fact that these boundaries correspond to different episodes of phosphogenesis from that described by Halbach and Puteanus (1984) (see section 11.4.4).

In order to assess the validity of the $^{87}Sr/^{86}Sr$ method of dating manganese crusts, von der Haar et al. (1995) carried out a series of leaching experiments on the Schumann Seamount crust in which it was established that Sr was leached from both phosphatic material and aluminosilicate detritus within the crust. It was also shown that Sr within the oxides exchanges with seawater strontium throughout the history of the deposit. These results cast severe doubt on the validity of the Sr isotopic method for determining the ages of these crusts (see section 11.4.9). In addition, De Carlo (1991) analyzed 11 samples at various depths in the Schumann Seamount crust for REE in an attempt to reconstruct its growth history (see section 11.4.3). The results are somewhat surprising in that they show a steady increase in the Ce/La ratio of the deposit from the base of the crust (4.5 at a depth of 78-95 mm) to a maximum of 7.0 at 63-68 mm and then a steady decline to 3.0 at a depth of 0-5 mm. It is not easy to understand why the most oxidizing conditions in the water column should prevail at a depth of 63-68 mm in the crust corresponding to a Paleocene age (McMurtry et al. 1994).

In addition, ^{10}Be dating of seven manganese nodules from the Southwestern Pacific Basin was carried out by Mangini et al. (1990b). In one nodule (143GB), extrapolation of the nodule growth rates indicated that the nodule began forming at about 14.5 Ma. At 6 Ma, there was a major change in structure of the nodule. Within the outer layer of the nodule, concentric layers filled with detritus corresponding to ages of 3.2 and 1.3 Ma. However, there was no corresponding change in growth rate at any of the intervals, the growth rate remaining constant with time. This study confirmed that these ages are important time markers which had previously been recorded in many Pacific pelagic sediments and manganese crusts and nodules.

The dates of the hiatuses reported above are consistent with the ages listed by Frank (2002) for major paleogeographic changes in the Pacific resulting from the opening and closing gateways which are thought to have been responsible for large-scale reorganizations of global ocean circulation and are linked to changes in global climate. In the Pacific, these include

the rifting and northward drift of Australia from Antarctica which began at about 55 Ma (and is associated with an abrupt negative ~3 ppt global carbon isotope excursion which has been attributed to the dissociation of 2,000 - 6,000 Gt of methane hydrates; Norris and Röhling 1999; Zachos et al. 2001; Dickens 2004), the development of the deep-water passage through the Tasman Strait at about 36 Ma (Ling et al. 1997), the opening of the Drake Passage at about 23 Ma which is thought to have initiated ocean bottom water flow through the Samoan Passage (Lonsdale 1981), the development of Antarctic glaciation about 14 Ma ago, an increase in ocean bottom circulation rates at 6.2 Ma and closing of the Panama Isthmus about 3.5 Ma ago (see also Segl et al. 1989; Xu 1997). Of these, the most important for the formation of oceanic manganese nodules and crusts was the Middle Miocene climate transition which occurred between 14.3 and 13.8 Ma (Shevenell et al. 2004). This event resulted in a cooling of the surface waters in the southwest Pacific by 6 - 7°C at ~55°S and was responsible for the development of the modern pattern of deep ocean bottom water flow. In addition, there was a general cooling of the global climate since the Eocene climate maximum at about 50 Ma, although this general trend has been punctuated by a series of steps (Zachos et al. 2001). The observations presented above show that Co-rich manganese crusts record these changes in ocean circulation, although perhaps not with the precision that one might hope for.

It is well known that deep circulation of the oceans is much more pronounced during periods of „ice house Earth“ (characterized by Polar ice sheets and a well-developed cryosphere) than during periods of „greenhouse Earth“ (when the cryosphere is absent). The „ice house Earth“ is generally taken to include the Oligocene, Late Miocene, Pliocene and Pleistocene and the „greenhouse Earth“ the Cretaceous, Paleocene and the Eocene (Jenkyns and Wilson 1999; Zachos et al. 2001). Ventilation, and therefore the degree of oxygenation, of the deep ocean, is controlled by the density difference between surface seawater and deep ocean bottom water which induces deep circulation of the oceans and is much more pronounced during periods of „ice house Earth“ than during periods of the „greenhouse Earth“. This trend is illustrated by the dominance of deep-sea manganese nodules in D.S.D.P. cores since the Eocene (Glasby 1978).

Kaiko (1998) has confirmed this trend by demonstrating that the low oxygen events in the oceans during the past 120 Ma have coincided with warm episodes in the oceans based on his benthic foraminiferal dissolved-oxygen index. Pulyaeva (1997) has also shown that the average Co content of Co-rich crusts from the Magellan Seamounts has increased steadily from 0.16% in the Late Cretaceous to 0.57% in the Eocene and 0.72% in the Miocene-Pleistocene whereas P_2O_5 showed the opposite trend declining from 13.5% to 1.3% during this period (von Stackelberg et al. 1984; De Carlo 1991; Frank et al. 1999b; see section 11.4.9). This trend reflects the increased ventilation of the oceans through time and, in particular, the development of a more pronounced oxygen minimum zone in the ocean following the Middle Miocene climate transition.

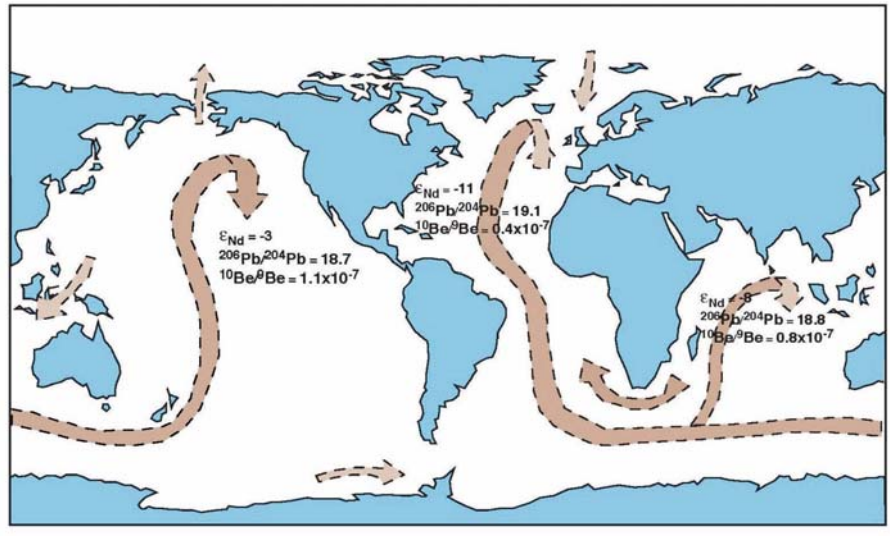

Fig. 11.22 Schematic representation of deep-water flow in the world ocean based on characteristic changes in the isotopic composition of Nd, Pb and Be in ferromanganese crusts with location. The isotopic data are taken from Albarède and Goldstein (1992) and von Blanckenburg (1996a,b) (after Hein et al. 2000, Fig. 9.10).

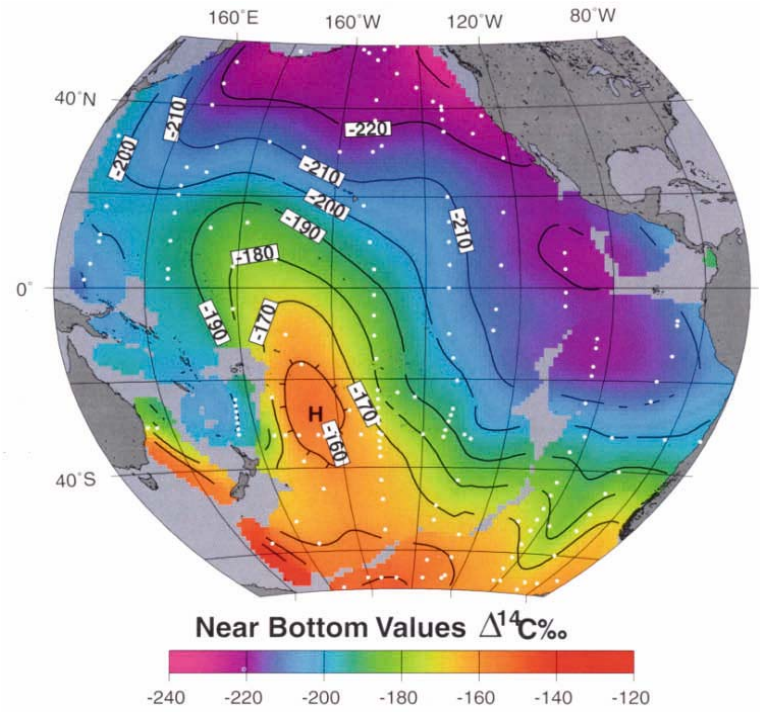

Fig. 11.23 Schematic representation of the distribution of $\delta^{14}C$ in Circum Polar Deep Water at depths >3,500 m. The tongue of high $\delta^{14}C$ shows the present-day path of circum-polar water entering the Pacific. The water flows northwards along the western Pacific island arc system and then clockwise north of the equator. The oldest water is found in the NE sector of the Pacific (after Schlosser et al. 2001, plate 5.8.17).

11.4.10.2 Application of Isotopic Studies of Co-rich Mn Crusts to the Study of Present-day Deep-ocean Circulation

The release of trace metals with different isotopic ratios from the Earth's crust by weathering or hydrothermal activity is the basis for the observed variability of isotopic composition of these metals in the oceans (Frank 2002). Albarède and Goldstein (1992) pioneered the application of isotopic studies of ferromanganese deposits to the study of present-day deep-ocean circulation by mapping the Nd isotopic composition of 270 samples of ferromanganese crusts and nodules from the world ocean. The results showed a marked similarity between regional Nd isotopic variations of the crusts and nodules and the broad pattern of present-day deep-ocean circulation. This was somewhat surprising in view of the short residence time of Nd in seawater (~10 - 10^3 years) compared with the much longer time scale of ferromanganese formation which is measured in millions of years but reflects the stability of deep-sea circulation since the Pliocene integrated over time. Subsequently, von Blanckenburg et al. (1996a) measured Pb isotope ratios ($^{206}Pb/^{204}Pb$ and $^{208}Pb/^{204}Pb$) in ferromanganese crusts from the world ocean and showed that these isotopic ratios are remarkably uniform in the Pacific reflecting the fact that Pb is extremely well mixed as a result of its short residence time in ocean bottom waters (80-100 years).

The Pb isotope ratios also indicated that Pb is more juvenile in the Pacific than in the Atlantic Ocean. From this, it was deduced that the Pb in the Pacific Ocean is derived principally from the subduction of MORB and pelagic sediment at volcanic arcs and from continental margin volcanics whereas in the Atlantic Ocean it is derived principally from riverine particulate matter. Von Blanckenburg et al. (1996b) also measured beryllium isotope ratios ($^{10}Be/^{9}Be$) in ferromanganese crusts from the world ocean and showed that the $^{10}Be/^{9}Be$ ratios in the crusts are in close agreement with seawater values from the same area and that the $^{10}Be/^{9}Be$ ratios of the crusts decrease along the path of ocean bottom water flow and correlate with the $\Delta^{14}C$ age of the deep-ocean bottom water flow. The residence time of Be in the Pacific away from the margins was estimated to be 600 ± 100 years.

These observations enabled Hein et al. (2000) to prepare a schematic map of deep-ocean flow in the world ocean showing the characteristic changes in the Nd, Pb and Be isotopic composition of the ferromanganese crusts along the bottom water flow path (Fig. 11.22). Particular interest in this figure lies in comparing this schematic flow path with the actual flow path of Pacific deep water based on measurements of the $\Delta^{14}C$ age of the deep bottom waters as presented by Schlosser et al. (2001, Plate 5.8.17; Fig. 11.23). These data confirm that the ocean bottom water flow in the Pacific is counter-clockwise with the oldest waters being found in the

northeast Pacific. However, these figures give no indication as to whether these bottom waters are transported eastwards into the equatorial North Pacific. This is important because it determines whether manganese nodules from the C-C F.Z. were formed under the influence of the AABW (see section 11.4.3).

It is generally accepted that the Pacific Ocean bottom waters originate from the northward flow of the Circumpolar Deep Water (CDW) which flows east of the Campbell Plateau and Tonga-Kermadec Ridge and then onwards to the Samoan Passage (Reid and Lonsdale 1974; Taft et al. 1991; Schmitz 1995; Hogg 2001; Schlosser et al. 2001). Although the use of the term CDW to describe the bottom water flow in the western Pacific is correct (Clarke et al., 2001), most of the older literature cited in this chapter refers to this flow as AABW. Based on geostrophic calculations from the results of WOCE Leg 31 in 1994, it was estimated that the northward transport of bottom waters through the Samoan Passage at depths greater than 4,000 m is 7.8 Sv of which 4.8 Sv has a potential temperature below 0.8°C making it the coldest abyssal water in the South Pacific (Roemmich et al. 1996; Rudnick 1997). Previous studies had indicated that ~3 Sv of AABW flow northwards out of the Samoan Passage and that this water mass then bifurcates at a latitude of about 7° 50'S with the minor branch turning to the northeast (Edmond et al. 1971; Macdonald and Hollister 1973). This branch was then thought to flow southeastwards along the western side of the Line Islands Ridge before turning east and crossing the ridge at the Horizon and Clarion Passages (Gordon and Gerard 1970; Edmond et al. 1971; Johnson 1972). However, it should be emphasized that the flow paths of the ocean bottom currents in their approach to these two passages are not well constrained.

Edmond et al. (1971) estimated that the flow of water through the Horizon Passage was approximately 0.4 Sv and presumed that only a minor part of this flow passes through the Clarion Passage and into the C-C F.Z. However, Mantyla (1975) subsequently noted that the Clarion Passage is deeper and wider than the Horizon Passage and estimated the potential temperature of the bottom waters in the Clarion Passage to be 0.87°C confirming the flow of bottom water through the Clarion Passage. However, the magnitude of this flow is unknown and it is clear that the Line Islands Ridge constitutes a formidable barrier to the flow of deep

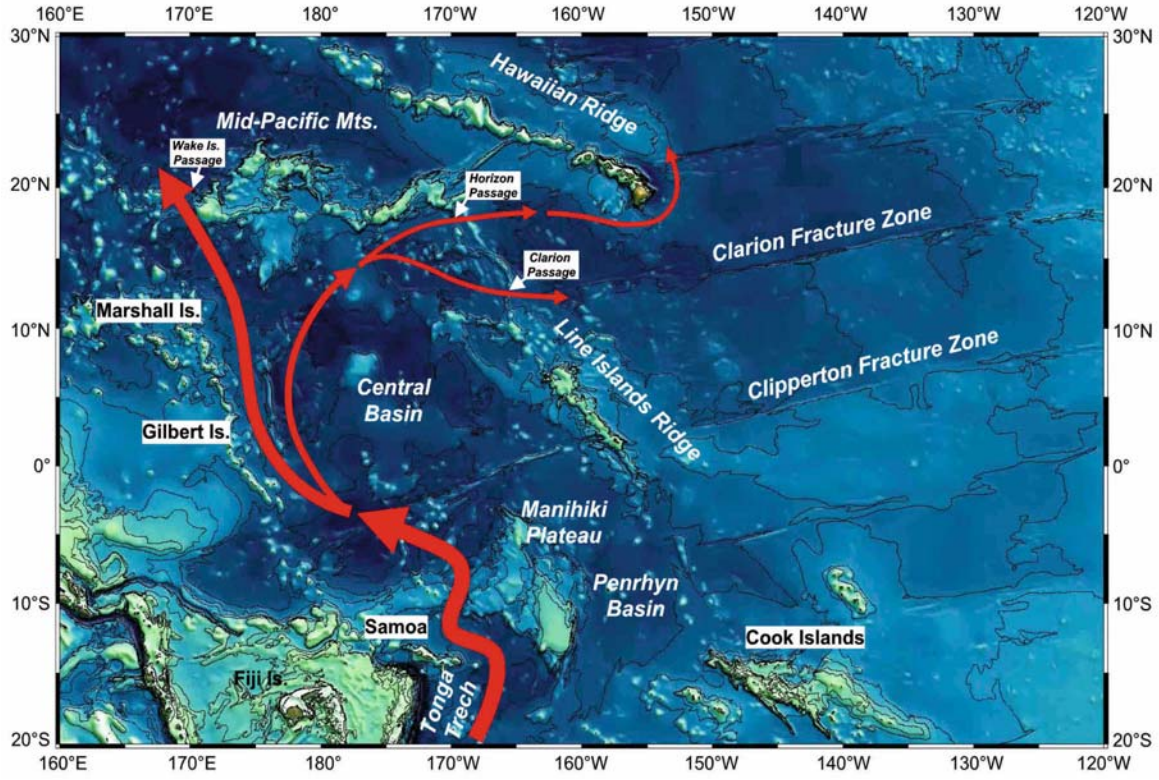

Fig. 11.24 Schematic map showing the inferred paths of oceanic bottom currents in the western Pacific (after Lonsdale 1981). Base map taken from the GEBCO bathymetric map of the Pacific Ocean.

water into the C-C F.Z. Fig. 11.24 illustrates the principal pathways of oceanic bottom water flow mentioned above.

In an early study of oceanic bottom water flow within the C-C F.Z., Johnson (1972) deployed free-fall bottom current meters in an area north of the Clipperton Fracture Zone where substantial sediment erosion was known to occur. The limited data showed that the bottom currents were generally slow (<10 cm sec^{-1}) but fluctuated markedly due to a strong semi-diurnal tidal component. It was also established that the currents flowed mainly to the east with minor variations due to topographic effects. In addition, data from a 14-day record of bottom current measurements taken at 210 m above the sea floor revealed an averge bottom water flow of 2.0 cm sec^{-1} in an ENE direction with peak velocities of up to 16.5 cm sec^{-1} at semidiurnal periods. These data showed that peak velocities of bottom water transport were strong enough to erode and transport sediment in the area (Amos et al. 1977).

More detailed studies in the C-C F.Z. were carried out during the period 1986 to 1989 in which a grid of bottom-moored instruments was deployed (Kontar and Sokov 1994). In general, the bottom currents were shown to be weak with velocities not greater than 4 cm sec^{-1}. However, a benthic storm lasting 10 days was recorded during these observations in which bottom currents with average velocities of 10 -15 cm sec^{-1} were measured. It was thought that these storms were related to periods when the sea surface was elevated by more than 4 cm above the norm which would lead to the excess kinetic energy at the sea surface being transmitted to the seafloor at depths > 3,000 m (Kontar and Sokov 1994). Other measurements of oceanic bottom water flow in the DOMES areas of the C-C F.Z. have been reported by Hayes (1979, 1998).

Within the Samoan Passage, the most rapid drift deposition occurred in the Late Oligocene-Early Miocene and in the Late Miocene-Early Pliocene (Lonsdale 1981). Both these periods were characterized by intensified bottom circulation These times correspond roughly with periods of enhanced sediment erosion in the C-C F.Z. (van Andel et al. 1975) in accordance with the ages of the nodules in the C-C F.Z. as reported by Shilov (2004) (see section 11.4.9).

Mangini et al. (1982) also established that there had been a marked increase in deep circulation in the Pacific at ~70 ka corresponding to the end of interglacial cycle stage 5 based on ^{230}Th and ^{231}Pa dating in 9 out of 13 sediment cores from the C-C F.Z. and in all 4 cores from the Aitutaki Passage. These results supported the idea that the onset of glacial events increased ocean bottom water flow in the C-C F.Z., although this effect may have been masked by bioturbation in the sediment cores in some cases.

In a detailed study of the DOMES Site A in the C-C F.Z., Piper and Blueford (1982) described an apparently anomalous situation in which small, polynucleate nodules with smooth surface texture and δMnO_2 as the principal manganese oxide phase formed in Quaternary sediments with variable thickness >40 cm located on the side of an W-E-trending valley whereas large nodules with granular surface texture and todorokite as the principal manganese oxide phase formed on Tertiary sediments at sites of active erosion on the sea floor. This is contrary to the normal trend where the diagenetic influence on nodules growth is more pronounced in those areas with higher sedimentation rates (see section 11.4.2). However, this area is unusual in that the topographic fabric lies W-E. It was therefore thought that the AABW would be channelled through the valley creating an erosional area on its southern flanks. In other areas of the C-C F.Z., however, the alignment of the topographic fabric may lie normal to the flow path of the AABW.

The data presented above paint a picture of relatively weak bottom currents in the C-C F.Z. resulting from the limited inflow of bottom water through the Clarion Passage. However, physical oceanographic data suggest that there are at least three components to the bottom currents, namely AABW flow, tidal effects and benthic storms. At present, it is not possible to quantify the relative importance of these components, although it is believed that the intensity of bottom water flow has fluctuated through time, for example during glaciations. Nonetheless, there is indirect evidence that the C-C F.Z. has been a dynamic and fluctating environment during the entire period of formation of deep-sea manganese nodules. Of particular interest is the observation of Knoop et al. (1998) that the relative influence of oxic diagenesis declines and that of suboxic diagenesis increases along the flow path of the AABW through the C-C F.Z. This may explain the trend of decreasing Ce/La ratios of deep-sea manganese nodules along the flow path of the AABW in the equatorial North Pacific as noted in section 11.4.3. Skornyakova and Murdmaa (1992) have also suggested that benthic storms play a key role in the formation of diagenetic nodules in the C-C F.Z. because they resuspend the active surface layers of the radiolarian ooze resulting in the burial of the nodules under a thin layer of semi-fluid sediment. This then acts as a source of transition elements such as Mn, Ni, Cu and Zn to the nodules and leads to the development of the rhythmic structure characteristic of these nodules. By contrast, hydrogenous nodules

in the area form under the influence of strong, stable bottom currents which ensure long-term contact of the nodule surface with seawater.

In the Peru Basin, two main flow paths into the basin have been recognized, both northwards from the South East Pacific Basin into the Chile Basin and thence into the Peru Basin (Lonsdale 1976). Inflow of oceanic bottom water into the Peru Basin from the northwest across the East Pacific Rise is blocked by the Galapagos Rise.

11.4.10.3 Application of Isotopic Studies of Co-rich Mn Crusts to the Study of Paleocean Circulation

The application of isotopic studies has also led to considerable advances in understanding the paleoceanographic conditions of formation of ferromanganese deposits in the Pacific Ocean and elsewhere (Frank 2002). Detailed studies on the isotopic composition of various elements have been carried out on a number of ferromanganese crusts throughout the Pacific. These include studies on Nd (Abouchami et al. 1997; Ling et al. 1997; O'Nions et al. 1998; Frank et al. 1999a,b; van de Fliert et al. 2004a,b,c), Pb (Abouchami et al. 1997; Christensen et al. 1997; Ling et al. 1997; O'Nions et al. 1998; Frank et al. 1999a,b; van de Fliert et al. 2003, 2004a,b,c), Hf (David et al. 1999; van de Fliert et al. 2004a,b,c), Os (Burton et al. 1999), Th (Rehkämper et al. 2004) and Fe (Beard et al. 2003; Lavasseur et al. 2004). Frank (2002) has plotted the time slice data for the Nd and Pb isotope distributions in the world ocean at 8 Ma, 6 Ma, 5 Ma, 1.5 Ma and the Present in which only five samples are shown for the entire Pacific Ocean reflecting the extremely sparse database on which to draw any conclusions.

As an example, we may consider the application of Nd isotopes of ferromanganese crusts to the study of paleoceanographic conditions in the Pacific. Nd is removed from the ocean water column by particle scavenging and has a global ocean residence time in deep waters of 600-2,000 years (Frank 2002). Its isotopic distribution in seawater is characteristic of individual water masses and is related to the weathering of Nd from different types continental crust with different ages. In the Pacific, the island arc rocks surrounding the ocean are composed of young mantle-derived material with high (radiogenic) ε_{Nd} values of up to + 20. The isotopic ratios are expressed as ε_{Nd} values because of the very small variations in the $^{143}Nd/^{144}Nd$ ratios in seawater which are mostly in the fourth or fifth decimal place (Frank 2002).

Ling et al. (1997) analyzed the Nd isotopic composition of three ferromanganese crusts taken from different water depths (4,800, 2,300 and 1,800 m) in the central Pacific. The ε_{Nd} pattern of the deepest crust over the past 20 Ma was shown to be similar to that of the two shallower crusts but about 1.0-1.5 units more negative. This was taken to indicate the long-term stratification of the Pacific over this period. O'Nions et al. (1998) subsequently confirmed the provinciality of Pacific Ocean water relative to Atlantic and Indian Ocean water based on an analysis of ε_{Nd} values of crusts from the Indian and Atlantic Oceans over this period. Ling et al. (1997) also demonstrated a steady increase in the ε_{Nd} values of these crusts from 10 to 3 Ma followed by a decrease to the present. This was interpreted to be the result of the progressively restricted access of Atlantic Ocean water to the Pacific via the Panama gateway which finally closed at 5-3 Ma leading to intensification of NADW (North Atlantic Deep Water) and greater production of AABW in the Pacific (Burton et al. 1997). However, this conclusion was disputed by Frank et al. (1999b) who argued that the contribution of Atlantic waters through the Panama gateway in the 3-4 Ma prior to its closure would have been very small. Instead, these authors proposed that this decrease in ε_{Nd} values during the last 3-4 Ma was related to an increased input of aeolian material into the Pacific (Frank 2002).

Van de Fliert et al. (2004b) also used Nd and Pb isotopic profiles in two carefully chosen ferromanganese crusts from the Lord Howe Rise in the S.W. Pacific and the Nova Trough in the equatorial Pacific to identify the relative influence of the equatorial Pacific and southwest Pacific bottom waters on the isotopic compositions of the crusts. The results were then used as a time series to reconstruct Cenozoic circulation patterns for the region. From this, it was possible to establish the influence of the progressive build up of Antarctic Circumpolar Current (ACC) from 38 Ma to 21/17 Ma as a result of the opening of the Tasmanian gateway and the Drake Passage and the development of the East Antarctic Ice Sheet from 17 Ma onwards. A major change in the Nd isotopic composition in the Lord Howe Rise crust from ~10 Ma onwards was also observed which was thought to reflect the increasing influence of equatorial Pacific deep water and was attributed to the closure of the Indonesian Seaway and reorganization of oceanic circulation in the S.W. Pacific. Abouchami et al. (1997) also showed that the Nd isotopic composition of the crusts has been more or less constant during the last glacial stages.

The above observations demonstrate not only the importance of isotopic studies on marine ferromanga-

nese crusts in evaluating paleoceanographic conditions in the world ocean but also the relative paucity of data, especially in the Pacific Ocean.

11.4.11 Economic Prospects

In 1965, J.L. Mero proposed that manganese nodules could serve as an economic resource for Ni, Cu and Co. In his book, he painted a picture of an essentially limitless resource of over one trillion tonnes of manganese nodules on the Pacific deep-sea floor which were growing at a rate faster than could possibly be exploited (Mero 1965). Although he grossly overestimated the economic potential of the nodules, his work was hugely influential and set in train a number of major national programs to explore the resource potential of manganese nodules. In 1972-1982, the U.S. International Decade of Ocean Exploration (IDOE) program was initiated to facilitate scientific research on deep-sea Mn nodules in the equatorial North Pacific as it was then known. Strong German, French and Soviet programmes were also undertaken to evaluate nodules as an economic resource. The period 1972-1982 became the „Golden Age" for manganese nodule research. During this period, there were 30-40 U.S. cruises, 26 German cruises and 42 French cruises to study nodules focussed mainly on this region. In addition, seven consortia were formed to investigate the possible commercial exploitation of the nodules. Mero (1977) subsequently estimated that the North Pacific high-grade area covering an area of about 6 million km^2 contained about 11,000 Mt of Mn, 115 Mt of Co, 650 Mt of Ni and 520 Mt of Cu. He also claimed that „within the next five to ten years, assuming no political and/or legal interference, the nodules should be in full-scale economic production as a valuable source of important industrial metals." More recently, Morgan (2000) has estimated that there are 34,000 Mt of nodules located in an area of 9 million km^2 in the C-C F.Z. and that these nodules contain approximately 7,500 Mt of Mn, 78 Mt of Co, 340 Mt of Ni and 265 Mt of Cu.

Several factors combined to end this optimism (Glasby 2000, 2002). For example, a major factor in this belief was the assumption of world metal prices would continue to rise in real terms based on the prediction of global mineral shortages by the Club of Rome. However, although world metal prices did indeed rise from about 1965 to about 1976, the long-term trend for Ni and Cu from then on was downwards (Fig. 11.25). In addition, the economic feasibility of deep-sea mining based on the assumption of very high capital investment and an enormous throughput of nodules (Medford 1969) never materialized. Indeed, the practicality of such an operation based on the deployment of a single mining ship at a given mine

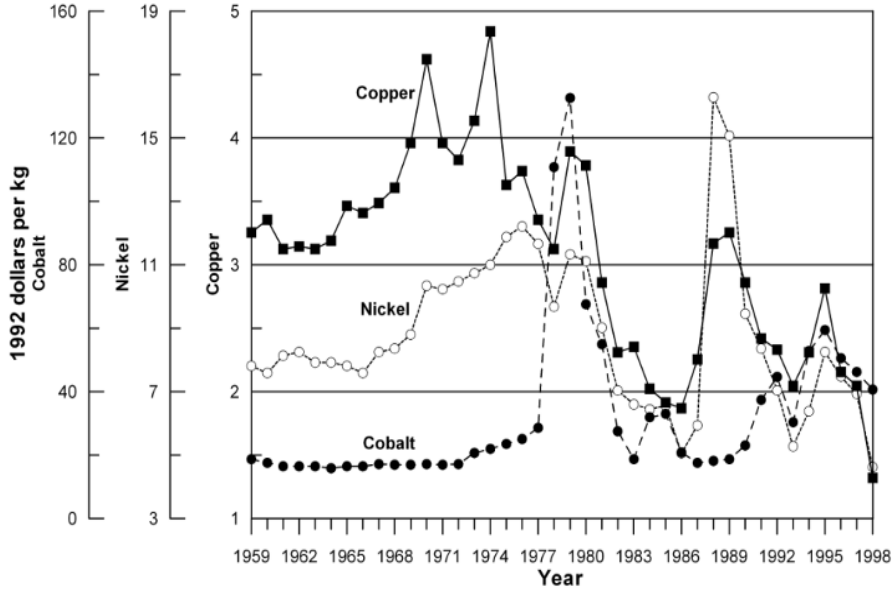

Fig. 11.25 Variation in the prices of Co, Ni and Cu in the United States from 1959-1998 expressed in constant 1992 dollars per kg (after Plunkert and Jones 1999). The prices of Co, Ni and Cu in 1999 in current dollar prices were Co $US 21, Ni $US 2 and Cu $US 0.75. Co is therefore easily the most valuable metal in deep-sea nodules and Co-rich crusts after Pt.

site was questioned by Glasby (1983). The feasibility of developing a reliable mining system was also cast into doubt when the testing of deep-sea nodule mining at the pilot-plant stage in 1978 ended abruptly with the loss of the entire mining system over the stern of the ship after about 800 t of nodules had been recovered from the seafloor. False expectations were also raised by the development of a deep-sea mining system by the Lockhead/OMCO consortium using the *Hughes Glomar Explorer* as the mother ship. The system developed was considered to be one of the greatest innovations in ship design and deep-sea technology in the twentieth century. Only later was it revealed that the *Hughes Glomar Explorer* had been built specifically to recover the K-129, a sunken Soviet nuclear submarine, and that the building of this ship had been funded entirely by the CIA at a cost of about $500 million in current dollars.

Nonetheless, the key problem was undoubtedly the provisions of the Third United Nations Convention on the Law of the Sea (UNCLOS III) which lasted from 1973 until 1982 and was the largest ever forum for international diplomacy (Anon 1982). These provisions were considered so onerous that several countries with an interest in deep-sea mining (including the U.S.A., U.K. and Germany) refused to sign the initial Law of the Sea Treaty in 1982. One provision that the United States, in particular, found unacceptable was the requirement to transfer technology to the Enterpise (representing Third World countries). Nonetheless, these countries eventually signed the convention in 1994 after a new agreement on deep-seabed mining was reached. This led to the International Seabed Authority (ISA) being set up in Kingston, Jamaica, to mangage the mineral resources of the International Seabed Area (http//:www.isa.org.jm). However, it was the marked drop in the price of Ni and Cu from 1979 to 1982 (Fig. 11.25) which essentially ended all commercial and almost all scientific interest in deep-sea manganese nodules in these countries in 1982.

Concurrently, there was a marked surge in the world price of Co in 1979 and 1980 (Fig. 11.25) following the invasion of the Shaba Province of Zaire by insurgents in 1978 (Manheim 1986). Cobalt is essential for the production of the superalloys used in jet aircraft engines. As a result, President Reagan created a strategic materials task force in 1980 to evaluate the availability of strategic minerals such as Co, Mn and the Pt metals. This stimulated interest in marine resources of cobalt, manganese and platinum. Although the cost of mining these deposits was considered to be too high to be practical, it was thought that an increase in demand (and therefore in price) for these minerals or technological innovations which would reduce the cost of mining could make these deposits an economically viable source of these minerals. In 1983, President Reagan proclaimed a 200 n.m. Exclusive Economic Zone (EEZ) around the United States and the US-controlled islands in the Pacific and Caribbean. This paved the way for research on Co-rich manganese crusts around Johnson Island and the Hawaian Archipelago in the U.S. EEZ as well as within the EEZ's of the Federated States of Micronesia, Marshall Islands, Kiribati and from international waters in the Mid-Pacific Mountains. Hein (2004) has listed 36 cruises dedicated to the study of Co-rich crusts in the Pacific between 1981 and 1999 undertaken by groups from the USA, Japan, Korea, Germany, Russia, Australia, France and New Zealand. Since then, China has become a major player in Co-rich crust investigations. One of the advantages of mining Co-rich Mn crusts compared to deep-sea manganese nodules is that they mostly lie within the EEZ's of island nations and therefore outside the juridiction of the ISA. Mining rights could therefore be negotiated with the host government. However, the price of Co in 1998 was less than 30% of its peak value in 1979 in real terms (Fig. 11.25) and there is no serious talk of mining these deposits yet.

Following the adoption of the Law of the Sea Treaty in 1982, a new phase was initiated to assess the commercial potential of manganese nodules and a number of countries registered claims to deep-sea mining areas as „pioneer investors" through the United Nations on the basis of UNCLOS. These countries committed themselves to long-term programmes to establish the viability of nodule mining including nodule surveys, the development of mining systems, nodule processing and environmental surveys. So far, the following countries have registered, France, Russia, India and Japan (1987), People's Republic of China (1991), InterOceanMetal (1992) and Republic of Korea (1994). Fig 11.26 shows the locations of the mine site areas allocated to each of these countries within the C-C F.Z. India has registered its claim to an area within the Central Indian Ocean Basin (CIOB) south of India (Juahari and Pattan 2000; Mukhopadhyay et al. 2002). However, the commercial viability of nodules mining is by no means assured and no consortium is building a nodule mining system at present. This reflects the fact that world metal prices are too low for nodule mining to be profitable. As can be seen in Fig. 11.25, the price of both Ni and Cu in 1998 was less than 40% of their peak values in the 1970s in real terms. It would therefore appear that those countries still interested in the possibility of exploiting nodules are

looking for a strategic source of metals rather than a resource that is economically cost competitive.

For deep-sea nodules, only those nodules with Cu+Ni+Co >2.5% and abundance >10 kg m^{-2} can be considered to be a potential economic resource. This represents only a small percentage of total quantity of nodules worldwide (i.e. diagenetic nodules from the C-C F.Z. and Central Indian Ocean Basin). To be economic, a 20 year-mine-site would be required to produce 3 Mt of nodules per year. This would cover an area >6,000 km^2. According to Lenoble (2004), the estimated total number of potential mine sites varies from 8 to 225 corresponding to a total of between 480-13,500 Mt of nodules. However, if the capacity of world metal markets to absorb production from the deep sea is taken into account, a more realistic assessment was taken to be 3-10 mine sites with a total tonnage of 100-600 Mt over this period. This reflects the marked differences in the ratios of the amounts of metals in nodules (Ni 7: Cu 6: Co 1) compared to the ratios of their consumption (Ni 27: Cu 267: Co 1) (Bernhard and Blissenbach 1988). As a result, if large tonnages of nodules were to be mined for Ni and Cu, it would lead to overproduction of Co with an associated drop in its world price. The markets would therefore have to be manipulated to avoid such disruptions. Based on an annual worldwide production rate of Ni of 0.9 Mt in 1998; Morgan (2000) considered Ni to be the primary metal of commercial interest in deep-sea nodules. Because deep-sea nodules occur at great depths in the oceans (greater than 4,000 m), they require sophisticated capital-intensive technology to mine and are in direct competition with land-based mineral resources. A decision to mine them must therefore ultimately be based on economic rather than technological considerations.

For Co-rich manganese crusts, the crusts should contain >0.8% Co and be >40 mm thick to be considered economically viable. The crusts occur in shallower water depths (1,000-2,500 m) than deep-sea nodules (>4,000 m) and could be mined within national Exclusive Economic Zones (EEZs) and therefore under national jurisdiction. Excellent accounts of the distribution and composition of Co-rich crusts in the world ocean have been presented by Andreev and Gramberg (1998) and Hein (2000) and several authors have attempted to assess of their economic potential (Wiltshire et al. 1999; Hein 2000, 2004; Wiltshire 2000). Andreev and Gramberg (2002) have estimated the total abundance of Co-rich crusts in the world ocean to be about $21 \cdot 10^9$ t.

The types of mining systems likely to be used for the recovery of deep-sea nodules and Co-rich Mn crusts are not well known. For nodules, Lenoble (2004) has described a system to mine the French area. This

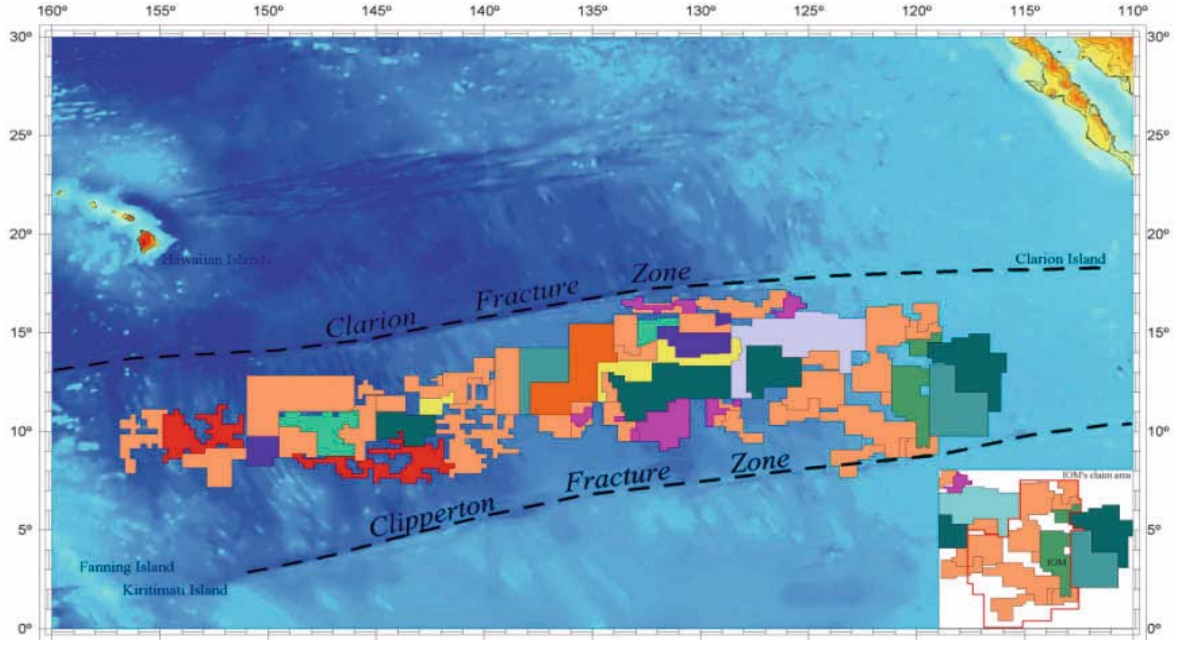

Fig. 11.26 Schematic map showing the distribution of the allocated sectors of registered pioneer investors and applicants for pioneer investor status in the C-C F.Z. Most of the consortia interested in deep-sea mining have already made extensive studies of their future 'mine sites' in the C-C F.Z. The economic potential of this region is reflected in the large proportion of the area already under claim. Areas not subject to claims are often topographically unsuitable (too mountainous). The map is an updated version of the original version appearing in Kotlinski (1995).

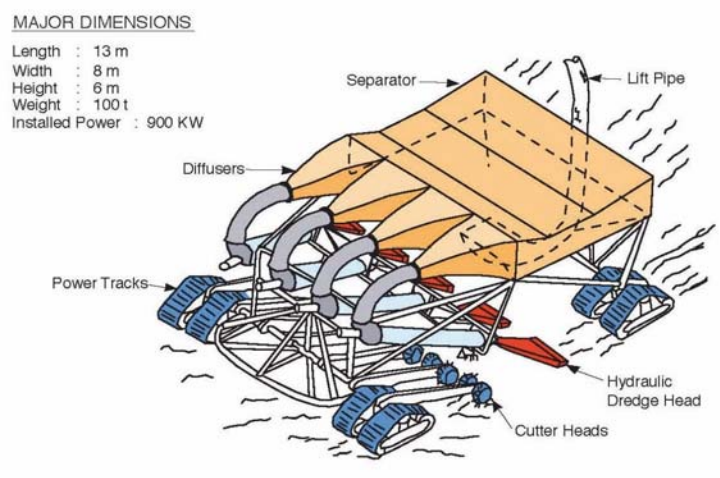

Fig. 11.27 Sketch of a proposed vehicle for mining Co-rich Mn crusts (after Hein et al. 2004, Fig. 9).

involves the deployment of a self-propelled dredge which crawls along the bottom, collects the nodules, crushes them and introduces them to a 600 m long flexible hose connected to a rigid pipe. The crushed nodules are then lifted to a semi-submersible surface platform in a 4,800 m rigid steel pipe by airlift or pumps. They are then transferred from the platform to the ore carrier through a flexible hose as thick slurry. The recovery rate using this method would be of the order of 1.5 Mt of nodules on a dry-weight basis per year.

Mining systems for the recovery of Co-rich Mn crusts have been described by Hein (2004). According to this author, mining crusts is technically much more difficult than mining nodules because the crusts are attached to a substrate and occur in undulating terrain. It is therefore necessary to separate the crust from the underlying substrate at the seafloor. One proposed mining system consists of a bottom crawling vehicle attached to the surface mining vessel by a hydraulic pipe lift system. The mining machine provides its own propulsion and travels at a speed of about 20 cm sec^{-1}. The miner has articulated cutters that would fragment the crusts and reduce the amount of substrate material collected. This system could possibly mine 1 Mt of crust with a 25% dilution by substrate on a dry-weight basis per year. Fig. 11.27 shows a possible design of a vehicle for mining Co-rich Mn crusts.

Both Hein (2004) and Lenoble (2004) have considered the profitability of mining deep-sea nodules and Co-rich Mn crusts in some detail and concluded that mining of these deposits is not commercially viable at current world metal prices. Mining these deposits therefore remains a matter for the future.

11.4.12 Future Prospects

The geochemistry of manganese in the marine environment is defined by the following characteristics: its relatively high abundance in the earth's crust, its availability in two valency states whose stability boundary lies within the range of the natural environment and the high adsorption capacity of its oxides for cationic species, especially Ni^{2+}, Co^{3+} and Cu^{2+}. As such, manganese naturally migrates to zones with the highest redox potential within the marine environment. The modern, well-oxygenated deep-sea is therefore the ultimate repository for manganese.

Manganese can also fractionate from iron and other transition metals to form shallow-marine ferromanganese concretions and submarine hydrothermal crusts under conditions in which iron and the associated transition metals are trapped as sulphides prior to the deposition of the manganese oxide minerals. Mn can also form deposits enriched in elements such as Co, Ni, Cu and Zn under conditions in which these elements can be adsorbed from seawater and sediment pore water onto the surfaces of manganese oxide minerals. The most favourable conditions for this to occur require extremely low growth rates of the manganese oxide minerals. These are usually to be found in low sedimentation regimes in the deep sea as with deep-sea manganese nodules or associated with the oxygen-minimum zone at mid-depths in the open ocean as with Co-rich manganese crusts. These factors are responsible for the formation of potential economic deposits of manganese in the deep oceans, namely deep-sea manganese nodules and Co-rich manganese crusts.

In addition, the rate of formation of marine manganese deposits in the deep ocean is extremely slow. The formation of these deposits therefore takes place over long periods of time. Deposition of manganese oxides in the deep oceans is also a function of the degree of oxygenation of the oceans. This in turn is controlled by the ventilation of the deep ocean which varies according to the climate. Deep-sea manganese nodules and Co-rich Mn crusts therefore record variations in the degree of oxygenation and pattern of circulation of the deep ocean. Mn crusts can therefore be considered to be condensed stratigraphic sections which can be used to elucidate variations in paleoceanographic conditions on timescales from Milankovitch cycles to geological era on the basis of their isotopic ratios. As a result, both deep-sea manganese nodules and Co-rich manganese crusts may be thought of as archives of paleoenvironmental data and therefore important targets for paleoceanographic studies. Because of their much longer period of formation, Co-rich manganese crusts are more useful than deep-sea manganese nodules in this respect.

Although the boom period of research into deep-sea Mn nodules and Co-rich Mn crusts associated with the drive to establish these deposits as an economic resource in the 1970s and 1980s is over, there remain many interesting topics which have been neglected over the last two decades. These include the study of shallow-marine concretions, lake concretions, hydrothermal Mn crusts and fossil manganese deposits. Each of these deposits has its own characteristic modes of formation. In addition, much of the work on deep-sea manganese nodules has focussed on areas of potential economic interest. There remains considerable scope for studying nodules from a much wider range of settings than has previously been attempted, especially for investigating their internal characteristics in much greater detail using modern instrumental techniques.

The economic potential of marine manganese deposits and the potential of these deposits as paleoenvironmental indicators are directly related to the chemistry of manganese, its associated transition metals and other key elements adsorbed on to the surface of these deposits. It is this complex interplay of these factors which makes the study of marine manganese deposits so intriguing. Unfortunately, research on deep-sea manganese nodules and crusts has been held hostage to the economic potential of these deposits. Time will tell if these deposits are to become a major source of metals for the world as was once thought.

11.5 Problems

Problem 1

Figure 11.28 is a simplified E_H-pH diagram for Mn at 25°C, 1 atmosphere pressure and in pure water for a limited number of aqueous species and solid phases of Mn taken from Garrels and Christ (1965 Fig 7.28a). The boundaries between the dissolved species and solid phases are taken to be at a total activity of the dissolved species of 10^{-6} and 10^{-2}. The total dissolved carbonate species is taken to be $10^{-1.4}$.

In your opinion, what are the advantages of plotting an E_H, pH diagram of Mn of the type shown in Fig. 11.2 compared with this older type of Eh, pH diagram pioneered by Garrels and Christ (1965)? How do you account for the fact that solid manganese oxide minerals do not appear to be thermodynamically stable under seawater conditions in the diagram of Glasby and Schulz (1999; Fig. 11.2).

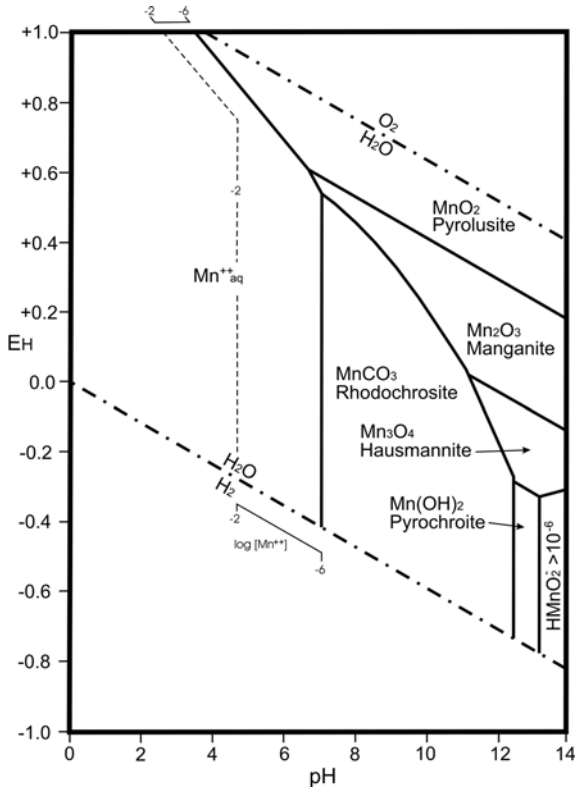

Figs 11.28 Simplified E_H-pH diagram for Mn at 25°C, 1 atmosphere pressure and in pure water for a limited number of aqueous species and solid phases of Mn (after Garrels and Christ 1965 Fig 7.28a).

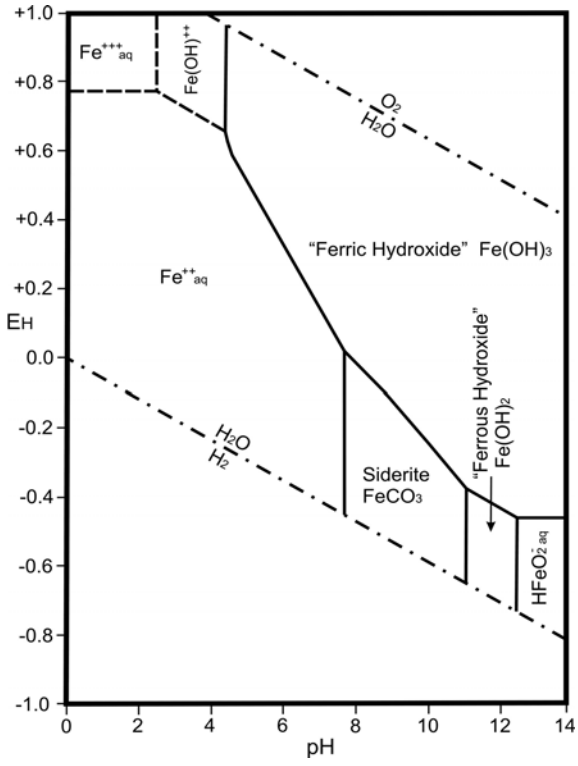

Figs 11.29 Simplified E_H-pH diagram for Fe at 25°C, 1 atmosphere pressure and in pure water for a limited number of aqueous species and solid phases of Fe (after Garrels and Christ 1965 Fig 7.14).

Problem 2

Figure 11.29 is a simplified E_H-pH diagram for Fe at 25°C and 1 atmosphere pressure showing the relations between the aqueous Fe species and metastable iron hydroxides and siderite. The boundaries between the dissolved species and solid phases are taken to be at a total activity of the dissolved species of 10^{-6}. The total dissolved carbonate species is taken to be 10^{-2} (Garrels and Christ 1965 Fig 7.14).

In your opinion, what are the advantages of plotting an E_H, pH diagram of the type shown in Fig. 11.4 compared with this older type of E_H, pH diagram pioneered by Garrels and Christ (1965)? What are the limitations of Fig. 11.4 in deducing the form of Fe in deep-sea manganese nodule?

Problem 3

Estimate the flux of Mn^{2+} from marine sediments from Loch Etive, Scotland. Some marine sediments, particularly in hypoxic fjord environments and in some hemipelagic environments, contain elevated concentrations of manganese. The sediments receive this manganese in the form of solid MnO_2 through the water column. In return, they release some Mn^{2+} in solution back to the water column. The extent of this exchange needs to be measured in order to determine the importance of Mn in oxidation-reduction processes in the sediment quantitatively. The flux of Mn^{2+} within the sediment and from the sediment to the water column can be calculated from the Mn^{2+} gradient using Fick's first law.

The following is a table (Tab. 11.7, Fig. 11.30) of measured pore water manganese concentrations in reducing sediment at the deepest station in the upper basin of Loch Etive, Scotland, where Mn^{2+} diffuses up to the surface of the sediment following the concentration gradient. The temperature of the sediment is 10°C and the porosity 0.84 (Overnell 2002; Overnell et al. 2002).

a) Calculate the maximum upward flux of Mn^{2+} towards the sediment surface (J_{Mn}) in the reducing sediments of the upper basin of Loch Etive. Use the depth interval with the steepest upward gradient for the calculation. The Mn^{2+} diffusion coefficient for sediment along with the in situ porosity and temperature are given in chapter 3 together with the necessary equations.

b) At what depth below the sediment surface are the Mn-oxides reduced and Mn^{2+} ions released to the pore water?

c) Are there indications that precipitation of Mn oxides is already taking place in the uppermost few millimeters of the sediment?

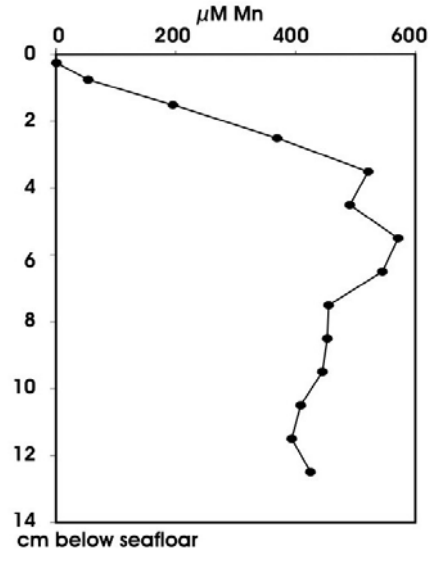

Figs 11.30 Measured pore water manganese concentrations in reducing sediment at the deepest station in the upper basin of Loch Etive, Scotland.

Table 11.7 Measured pore water manganese concentrations in reducing sediment at the deepest station in the upper basin of Loch Etive, Scotland.

Depth cm	Mn^{2+} µM	Depth cm	Mn^{2+} µM
0.25	1.5	6.5	544.9
0.75	54.2	7.5	455.1
1.5	195.6	8.5	453.1
2.5	369.1	9.5	444.7
3.5	521.4	10.5	408.4
4.5	490.6	11.5	393.8
5.5	571.2	12.5	425.0

Problem 4

Plot the NASC-normalized REE distribution patterns (Table 11.8) for the following types of submarine and subaerial Mn deposits. Remember to include all REE on the x-axis, even those elements that have not been analyzed. What do these REE patterns tell us about the modes of formation of these various manganese deposits?

Problem 5

Radiometric dating has revealed wide variations (by four orders of magnitude) for the growth rates of marine manganese deposits: Co-rich Mn crusts (0.8 mm Ma^{-1}; Puteanus and Halbach 1988), deep-sea manganese nodules on red clay substrates (1-2 mm Ma^{-1}; Hu and Ku 1984), deep-sea manganese nodules on siliceous ooze substrates (3-8 mm Ma^{-1}; Hu and Ku 1984), deep-sea manganese nodules on hemipelagic clay substrates (20-50 mm Ma^{-1}; Hu and Ku 1984), Baltic Sea concretions from 1,700-21,000 mm Ma^{-1}; Liebetrau et al. 2002) and submarine hydrothermal manganese crusts >1,000 mm Ma^{-1}. These growth rates vary by a four orders of magnitude. How do you account for such wide variations in growth rates?

Table 11.8 REE distribution patterns for submarine and subaerial Mn deposits.
Source of data: a Kunzendorf et al. (1993), b Glasby et al. (1987), c De Carlo and McMurtry (1992), d Szefer et al. (1998), e Glasby et al. (1997), f Glasby et al. (2004), g Gromet et al. (1984) n.a. = not analyzed.

	Deep-sea nodule SW Pacific	Deep-sea nodule CC FZ	Deep-sea nodule Peru Basin	Co-rich Mn crust	Baltic Sea ferroman-ganese concretion	Submarine hydro-thermal crust	Vani Mn deposit	NASC
source of data	a	b	b	c	d	e	f	g
La	167	93	55	287	24.1	38.1	19.2	31.1
Ce	952	344	112	1277	40.8	80.8	28	66.7
Nd	183	134	46	260	20.9	39.1	11.2	27.4
Sm	40	33.3	12.3	50.5	4.58	8.44	2.2	5.59
Eu	10.7	7.8	3.0	14.0	1.08	2.51	3.3	1.18
Gd	n.a.	n.a.	n.a.	60.8	4.46	7.54	2.9	5.5
Tb	6.5	4.0	1.9	n.a.	0.63	1.09	0.2	0.85
Dy	n.a.	n.a.	n.a.	48.7	3.42	6.38	2.4	5.54
Er	n.a.	n.a.	n.a.	26.5	1.92	3.15	1.6	3.27
Yb	19.5	12.9	8.7	25.3	2.1	2.64	1.6	3.06
Lu	2.9	1.8	1.4	3.57	0.29	0.36	0.2	0.456

Acknowledgements

The author would like to thank Professor G.M. McMurtry (University of Hawaii), Dr C.L. Morgan (Planning Solutions, Hawaii), Professor A. Usui (Koichi University) and Dr U. von Stackelberg (BGR) for their reviews of the manuscript. The author is also greatly indebted to Dr S.I. Andreev, Dr J. Fenner, Professor M. Frank, Dr J.R. Hein, Dr J. Overnell, Dr I. Pulyaeva, Dr V.V. Shilov, Dr I.M. Varentsov and Dr J. Wiltshire for their helpful contributions.

References

Abouchami, W., Goldstein, S.L., Galer, S.J.G., Eisenhauer, A. and Mangini, A., 1997. Secular changes in lead and neodymium in central Pacific seawater recorded in a Fe-Mn crust. Geochimica et Cosmochimica Acta, 61: 3957-3974.

Albarède, F. and Goldstein, S.L., 1992. World map of Nd isotopes in sea-floor ferromanganese deposits. Geology, 20: 761-763.

Aller, R.C., 1990. Bioturbation and manganese cycling in hemipelagic sediments. Philosophical Transactions of the Royal Society of London, A331: 51-68.

Amos, A.F., Roels, O.A., Garside, C., Malone, T.C. and Paul, A.Z., 1977. Environmental aspects of nodule mining. In: Glasby, G.P. (ed), Marine manganese deposits. Elsevier, Amsterdam, pp. 391-437.

Andreev, S.I. and Gramberg, I.S., 1998. The explanatory note to the metallogenic map of the world ocean. VNIIOkeanologia (St Petersburg) and InterOceanMetall (Szczecin), 212 pp. + illustrations (in English and Russian)

Andreev, S.I. and Gramberg, I.S., 2002. Cobalt-rich ores of the world ocean. Ministry of Natural Resources of the Russian Federation and All-Russian Research Institute for Geology and Mineral Resources of the World Ocean, St. Petersburg, 167 pp. + appendix (in Russian with English abstract)

Anon, 1979. La Genèse des nodules de manganese. Colloques Internationaux du Centre National de la Recherche Scientifique (CNRS), 287: 410 pp.

Anon 1982. United Nations Convention on the Law of the Sea of 10 Dcember 1982 (http://www.un.org/Depts/los/index.htm.Convention_agreements/texts/unclos/unclos_e.pdf)

Aplin, A.C. and Cronan, D.S., 1985. Ferromanganese deposits from the central Pacific Ocean, II. Nodules and asso-ciated sediments. Geochimica et Cosmochmica Acta, 49: 437-451.

Banerjee, R., 2000. A documentation of burrows in hard substrates of ferromanganese crusts and associated soft sediments from the Central Indian Ocean Basin. Current Science, 79: 517-521.

Barnes, S.S. and Dymond, J., 1967. Rates of accumulation of ferro-manganese nodules. Nature, 213: 1218-1219.

Baturin, G.N., 1988. The geochemistry of manganese and manganese nodules in the ocean. D. Reidel, Dordrecht, 342 pp.

Beard, D.L., Johnson, C.M., Von Damm, K.L. and Poulson, R.L., 2003. Iron isotope constraints on Fe cycling and mass balance in oxygenated Earth oceans. Geology, 31: 629-632.

Bender, M.L., Klinkhammer, G.P. and Spencer, D.W., 1977. Manganese in seawater and the marine manganese balance. Deep-Sea Research, 24: 799-812.

Berger, W.H., Fischer, K., Lai, C. and Wu, G., 1987. Ocean productivity and organic carbon flux. Scripps Institution of Oceanography Reference Series 87-30.

Bernhard, H.-H. and Blissenbach, E., 1988. Economic importance. In: Halbach, P., Friedrich, G. and von Stackelberg, U. (eds), The manganese nodule belt of the Pacific Ocean Geological environment, nodule formation, and mining aspects. Enke Verlag, Stuttgart, pp. 4-9.

Bischoff, J.L. and Piper, D.Z., 1979. Marine geology and oceanography of the Pacific manganese nodule province. Plenum Press, NY, 842 pp.

Bischoff, J.L., Heath, G.R. and Leinen, M.L., 1979. Geochemistry of deep-sea sediments from the Pacific manganese nodule province: DOMES Sites A, B, and C. In: Bischoff, J.L. and Piper, D.Z. (eds), Marine geology and oceanography of the Pacific manganese nodule province. Plenum Press, NY, pp. 397-436.

Böllhofer, A., Eisenhauer, A., Frank, N., Pech, D. and Mangini, A., 1996. Thorium and uranium isotopes in a manganese nodule from the Peru basin determined by alpha spectrometry and thermal ionization mass spectrometry (TIMS): Are manganese supply and growth related to climate? Geologische Rundschau, 85: 577-585.

Böllhofer, A., Frank, N., Rohloff, S., Mangini, A. and Scholten, J.C., 1999. A record of changing redox conditions in the northern Peru Basin during the Late Quaternary deduced from Mn/Fe and growth rate variations in two diagenetic manganese nodules. Earth and Planetary Science Letters, 170: 403-415.

Bruland, K.W., 1983. Trace elements in sea-water. In: Riley, J.P. and Chester, R. (eds), Chemical oceanography. Academic Press, London, pp. 157-220.

Bruland, K.W., Orians, K.J. and Cowen, J.P., 1994. Reactive trace metals in the stratified central North Pacific. Geochimica et Cosmochimica Acta, 58: 3171-3182.

Bruland, K.W. and Lohan, M.C., 2004. Controls of trace metals in seawater. In: Elderfield, H. (ed.), Treatise on geochemistry volume 6 The oceans and marine geochemistry. Elsevier, Amsterdam, pp. 23-47.

Burgarth, K.P. and von Stackelberg, U., 1995. Sulfide - impregnated volcanics and ferromanganese incrustations from the southern Lau Basin (Southwest Pacific). Marine Georesources and Geotechnology, 13: 263-308.

Burns, R.G. and Burns, V.M., 1977. Mineralogy. In: Glasby, G.P. (ed.), Marine manganese deposits. Elsevier, Amsterdam, pp. 185-248.

Burns, R.G. and Burns, V.M., 1980. Manganese oxides. Reviews in Mineralogy, 6: 1-46.

Burton, J.D. and Statham, P.J., 1988. Trace metals as tracers in the ocean. Philosophical Transactions of the Royal Society of London, A325: 127-145.

Burton, K.W., Ling, H.-F. and O'Nions, R.K., 1997. Closure of the central American Isthmus and its effect on deep-water foand lacustrine nodules: Distribution and geochemistry. In: Glasby, G.P. (ed.), Marine manga-nese deposits. Elsevier, Amsterdam, pp. 45-86.

Calvert, S.E. and Piper, D.Z., 1984. Geochemistry of ferromanganese nodules from DOMES Site A, Northern Equatorial Pacific: Multiple diagentic metal sources in the deep sea. Geochim. et Cosmochim. Acta, 48: 1913-1928.

Calvert, S.E.., Piper, D.Z. and Baedecker, P.A., 1987. Geochemistry of the rare earth elements of ferromanganese nodules from DOMES Site A, northern equatorial Pacific.

Geochimica et Cosmochimica Acta, 51: 2331-2338.

Chabaux, F., Cohen, A.S., O'Nions, R.K. and Hein, J.R., 1995. ^{238}U - ^{234}U - ^{230}Th chronometry of Fe-Mn crusts: Growth processes and recovery of thorium isotopic ratios of seawater. Geochimica et Cosmochimica Acta, 59: 633-638.

Chabaux, F., O'Nions, R.K., Cohen, A.S. and Hein, J.R., 1997. ^{238}U - ^{234}U - ^{230}Th disequilibrium in hydrogenous oceanic Fe-Mn crusts: Paleoceanographic record or diagenetic alteration? Geochimica et Cosmochimica Acta, 61: 3619-3632.

Chen, J.C. and Owen, R.M., 1989. The hydrothermal component in ferromanganese nodules from the southeast Pacific Ocean. Geochimica et Cosmochimica Acta, 53: 1299-1305.

Chester, R., 1990. Marine geochemistry. Chapman & Hall, London, 698 pp.

Christensen, J.N., Halliday, A,.N., Godfrey, L.V., Hein, J.R. and Rea, D.K., 1997. Climate and ocean dynamics of lead isotope records in Pacific ferromanganese crusts. Science, 277: 913-918.

Chukhrov, F.V., Gorshkov, A.I., Ermilova, L.P. et al., 1982. On mineral forms of manganese and iron occurrences in oceanic sediments. International Geological Review, 24: 466-480.

Chukhrov, F.V., Gorshkov, A.I., Drits, V.A., Shterenberg, L.Ye., Sivtsov, A.V. and Sakharov, B.A., 1983. Mixed-layered asbolite-buserite minerals and asbolite in oceanic iron-manganese nodules. International Geological Review, 25: 838-847.

Chukhrov, F.V., Gorshkov, A.I., and Drits, V.A., 1989. Supergene manganese oxides. Nauka, Moscow, 208 pp. (In Russian)

Clarke, A., Church, J. and Gould, J., 2001. Ocean processes and climate phenomena. In: Siedler, G., Church, J. and Gould, J.J. (eds), Ocean circulation & climate observation and modeling of the global ocean. Academic Press, San Diego, pp. 11-30.

Cowen, J.P. and Bruland, K.W., 1985. Metal deposits associated with bacteria: implications for Fe and Mn marine geochemistry. Deep-Sea Research, 32A: 253-272.

Cowen, J.P., DeCarlo, E.H. and McGee, D.L., 1993. Calcareous nannofossil biostratigraphic dating of a ferromanganese crust from Schumann Seamount. Marine Geology, 115: 289-306.

Cronan, D.S., 1977. Deep-sea nodule: distribution and chemistry. In: Glasby, G.P. (ed.), Marine manganese deposits. Elsevier, Amsterdam, pp. 11-44.

Cronan, D.S., 1980. Underwater minerals. Academic Press, London, 362 pp.

Cronan, D.S., 1987. Controls on the nature and distribution of manganese nodules in the western equatorial Pacific Ocean. In: Teleki, P.G., Dobson, M.R., Moore, J.R. and von Stackelberg, U. (eds), Marine minerals Advances in research and resource assessment. D. Reidel, Dordrecht, pp. 177-188.

Cronan, D.S., 1997. Some controls on the geochemical variability of manganese nodules with particular reference to the tropical South Pacific. In: Nicholson, K., Hein, J.R., Bühn, B. and Dasgupta, S. (eds), Manganese mineralization: Geochemistry and mineralogy of terrestrial and marine deposits. Geological Society Special Publication, 119: 139-151.

Cronan, D.S. (ed.), 2000. Handbook of marine minerals. CRC Press, Boca Raton, Florida, 406 pp.

Cronan, D.S. and Hodkinson, R.A., 1994. Element supply to surface manganese nodules along the Aitutaki-Jarvis Transect, South Pacific. Journal of the Geological Society of London, 151: 392-401.

David, K., Frank, M., O'Nions, R.K., Belshaw, N.S. and Arden, J.W., 2001. The Hf isotopic composition of global seawater and the evolution of Hf isotopes in deep Pacifc Ocean from Fe-Mn crusts. Chemical Geology, 178: 23-42.

Davies, T.A., 1985. Mesozoic and Cenozoic sedimentation in the Pacific Ocean Basin. In: Nairn, A.E.M., Stehli, F.G. and Uyeda, S. (eds), The ocean basins and margins 7A The Pacific Ocean. Plenum Press, NY, pp. 65-88.

de Baar, H.W., Bacon, M.P., Brewer, P.G. and Bruland, K.W., 1985. Rare earth elements in the Pacific and Atlantic Oceans. Geochimica et Cosmochimica Acta, 49: 1943-1959.

de Baar, H.J.W., de Jong, J.T.M., Bakker, D.C.E., Löscher, B.M., Veth, C., Bathmann, U. and Smetacek, V., 1995. Importance of iron for pankton blooms and carbon dioxide drawdown in the Southern Ocean. Nature, 373: 412-415.

De Carlo, E.H., 1991. Paleoceanographic implications of the rare earth element variabiliy within a Fe-Mn crust from the central Pacific Ocean. Marine Geology, 98: 449-467.

De Carlo, E.H. and McMurtry, G.M., 1992. Rare-earth element geochemistry of ferromanganese crusts from the Hawaiian Archipelago, central Pacific. Chemical Geology, 95: 235-250.

Dekov, V.M., Marchig, V., Rajita, I. and Uzonyi, I., 2003. Fe-Mn micronodules born in the metalliferous sediments of two spreading centres: the East Pacific Rise and Mid-Atlantic Ridge. Marine Geology, 199: 101-121.

Dickens, G.R. 2004. Hydrocarbon-driven warming. Nature, 429: 513-515.

Dillard, J.G., Crowther, D.L. and Calvert, S.E., 1984. X - ray photoelectron spectroscopic study of ferromanganese nodules: Chemical speciation for selected transition metals. Geochimica et Cosmochimica Acta, 48: 1565-1569.

Dorgan, K.M., Jumars, P.A., Johnson, B., Boudreau, B.P. and Landis, E., 2005. Burrow extension by crack propagation. Nature, 433: 475.

Drits, V.A., Silvester, E., Gorshkov, A.I. and Manceau, A., 1997. Structure of synthetic monoclinic Na-rich birnessite and hexagonal birnessite: I. Results from X-ray diffraction and selected-area electron diffraction. American Mineralogist, 82: 946-961.

Dymond, J. and Eklund, W., 1978. A microprobe study of metalliferous sediment components. Earth and Planetary Science Letters, 40: 243-251.

Dymond, J., Lyle, M., Finney, B., Piper, D.Z., Murphy, K., Conard, R. and Pisias, N., 1984. Ferromanganese nodules from MANOP Sites H, S, and R - Control of mineralogical and chemical composition by multiple accretionary processes. Geochimica et Cosmochimica Acta, 48: 931-949.

Earney, F.F.C., 1990. Marine mineral resources. Routledge, London, 387 pp.

Eckhardt, J.D., Glasby, G.P., Puchelt, H. and Berner, Z., 1997. Hydrothermal manganese crusts from Enareta and Palinuro seamounts in the Tyrrhenian Sea. Marine Georesources and Geotechnology, 15: 175-209.

Edmond, J.M., Chung, Y. and Sclater, J.G., 1971. Pacific bottom

water: Penetration east around Hawaii. Journal of Geophysical Research, 76: 8089-8097.

Ehrlich, H.L., 1996. Geomicrobiology. Marcel Dekker, NY, 719 pp.

Eisenhauer, A., Gögen, K., Pernicka, E. and Mangini, A., 1992. Climatic influences on the growth rates of Mn crusts during the Late Quaternary. Earth and Planetary Science Letters, 109: 25-36.

Elderfield, H. and Schulz, A., 1996. Mid-ocean ridge hydrothermal fluxes and the chemical composition of the ocean. Annual Review of Earth and Planetary Sciences, 24: 191-224.

Finney, B., Heath, G.R. and Lyle, M., 1984. Growth rates of manganese-rich nodules at MANOP Site H (Eastern North Pacific). Geochimica et Cosmochimica Acta, 48: 911-919.

Fitzwater, S.E., Coale, K.H., Gordon, M., Johnson, K.S. and Ondrusek, M.E., 1996. Iron deficiency and plankton growth in the equatorial Pacific. Deep-Sea Research, 43: 995-1015.

Fleet, A.J. 1983. Hydrothermal and hydrogenous ferro-manganese deposits: Do they form a continuum? In: Rona, P., Boström, K., Laubier, L. and Smith, K.L. (eds) Hydrothermal processes at seafloor spreading centers. NATO Conference Series, 12: 535-555.

Frank, M., 2002. Radiogenic isotopes: Tracers of past ocean circulation and erosional input. Reviews of Geophysics, 40(1): Article number 1001.

Frank, M., O'Nions, R.K., Hein, J.R. and Banakar, V.K., 1999a. 60 Myr records of major elements and Pd-Nd isotopes from hydrogenous ferromanganese crusts: reconstruction of seawater paleoceanography. Geochimica et Cosmochimica Acta, 63: 1689-1708.

Frank , M., Reynolds, B.C. and O'Nions, R.K., 1999b. Nd and Pb isotopes in Atlantic and Pacific water masses before and after closure of the Panama gateway. Geology, 27: 1147-1150.

Friedrich, G., Glasby, G.P., Thijssen, T. and Plüger, W.L., 1983. Morphological and geochemical characteristics of manganese nodules collected from three areas on an equatorial Pacific transect by R.V. *Sonne*. Marine Mining, 4: 167-253.

Friedrich, G. and Schmitz-Wiechowski, A., 1980. Mineralogy and chemistry of a ferromanganese crust from a deep-sea hill, central Pacific, „VALDIVIA" Cruise VA 13/2. Marine Geology, 37: 71-90.

Froelich, P.N., Klinkhammer, G.P., Bender, M.L., Luedtke, N.A., Heath, G.R., Cullen, D., Dauphin, P., Hammond, D., Hartmann, B. and Maynard, V., 1979. Early oxidation of organic matter in pelagic sediments of the eastern equatorial Atlantic: suboxic diagenesis. Geochimica et Cosmochimica Acta, 43: 1075-1090.

Futa, K., Peteman, Z.E. and Hein, J.R., 1988. Sr and Nd isotopic variations in ferromanganese crusts from the Central Pacific: Implications for age and source provenance. Geochimica et Cosmochimica Acta, 52: 2229-2233.

Garrels, R.M. and Christ, C.L., 1965. Solutions, minerals, and equilibria. Harper & Row, N.Y. 450 pp.

German, C.R. and Angel, M.V., 1995. Hydrothermal fluxes of metal to the oceans: a comparison with anthropogenic discharges. In: Parson, L.M., Walker, C.L. and Dixon, D.R. (eds), Hydrothermal vents and processes. Geological Society Special Publication, 87: 365-372.

German, C.R. and Von Damm, K.L., 2004. Hydrothermal processes. In: Elderfield, H. (ed.), Treatise on geochemistry volume 6 The oceans and marine geochemistry. Elsevier, Amsterdam, pp. 181-222.

Gingele, F.X. and Kasten, S., 1994. Solid-phase manganese in Southeast Atlantic sediments: Implications for the paleoenvironment. Marine Geology, 121: 317-332.

Giovanoli, R., 1980. On natural and synthentic manganese nodules. In: Varentsov, I.M. and Grasselly, Gy. (eds), Geology and geochemistry of manganese, volume 1. Hungarian Academy of Sciences, Budapest, pp. 159-202.

Giovanoli, R., 1985. A review of the todorokite-buserite problem; implications to the mineralogy of marine manganese nodules: discussion. American Mineralogist, 70: 202-204.

Giovanoli, R. and Bürki, P., 1975, Comparison of X-ray evidence of marine manganese nodules and non-marine manganese ore deposits. Chimia, 29: 266-269.

Giovanoli, R. and Arrhenius, G., 1988. Structural chemistry of marine manganese and iron minerals and synthetic model compounds. In: Halbach, P., Friedrich, G. and von Stackelberg, U. (eds), The Manganese Nodule Belt of the Pacific Ocean Geological environment, nodule formation and mining aspects. Enke Verlag, Stuttgart, pp. 20-37.

Glasby, G.P., 1972. The mineralogy of manganese nodules from a range of marine environments. Marine Geology, 13: 57-72.

Glasby, G.P., 1973. Mechanism of enrichment of the rarer elements in marine manganese nodules. Marine Chemistry, 1: 105-125.

Glasby, G.P., 1974. Mechanism of incorporation of manganese and associated trace elements in marine manganese nodules. Oceanography and Marine Biology: An Annual Review, 12: 11-40.

Glasby, G.P. (ed), 1977. Marine manganese deposits. Elsevier, Amsterdam, 523 pp.

Glasby, G.P., 1978. Deeep-sea manganese nodules in the stratigraphic record: Evidence from DSDP cores. Marine Geology, 28: 51-64.

Glasby, G.P., 1983. The Three-Million-Tons-Per-Year Manganese Nodule „Mine Site": An optimistic assumption? Marine Mining, 4: 73-77.

Glasby, G.P., 1984. Manganese in the marine environment. Oceanography and Marine Biology: An Annual Review, 22: 169-194.

Glasby, G.P., 1988. Manganese deposition through geological time: Dominance of the Post-Eocene environment. Ore Geology Reviews, 4: 135-144.

Glasby, G.P., 1991. Mineralogy and geochemistry of Pacific red clays. N.Z. Journal of Geology and Geophysics, 34: 167-176.

Glasby, G.P., 2000. Lessons learned from deep-sea mining. Science, 289: 551, 553.

Glasby, G.P., 2002. Deep-seabed mining: Past failures and future prospects. Marine Georesources and Geotechnology, 20: 161-176.

Glasby, G.P., Meylan, M.A., Margolis, S.V. and Bäcker, H., 1980. Manganese deposits of the Southwestern Pacific Basin. In: Varentsov, I.M. and Grasselly, Gy. (eds), Geology and geochemistry of manganese, volume 3. Hungarian Academy

of Sciences, Budapest, pp. 137-183.

Glasby, G.P. and Thijssen, T., 1982. Control of the mineralogy and composition of the manganese nodules by the supply of divalent transition metal ions. Neues Jahrbuch für Mineralogie Abhandlung, 145: 291-307.

Glasby, G.P., Friedrich, G.; Thijssen, T.; Plüger, W.L., Kunzendorf, H., Ghosh, A.K. and Roonwal, G.S., 1982: Distribution, morphology, and geochemistry of manganese nodules from the *Valdivia* 13/2 area, equatorial North Pacific. Pacific Science, 36: 241-263.

Glasby, G.P., Stoffers, P., Sioulas, A., Thijssen, T. and Friedrich, G., 1983. Manganese nodule formation in the Pacific Ocean: a general theory. Geo-Marine Letters, 2: 47-53.

Glasby, G.P., Gwozdz, R., Kunzendorf, H., Friedrich, G. and Thijssen, T., 1987. The distribution of rare earth and minor elements in manganese nodules and sediments from the equatorial and S.W. Pacific. Lithos, 20: 97-113.

Glasby, G.P., Uscinowicz, S.Z. and Sochan, J.A., 1996. Marine ferromanganese concretions from the Polish exclusive economic zone: Influence of Major Inflows of North Sea Water. Marine Georesources and Geotechnology, 14: 335-352.

Glasby, G.P., Emelyanov, E.M., Zhamoida, V.A., Baturin, G.N., Leipe, T., Bahlo, R. and Bonacker, P., 1997a. Environments of formation of ferromanganese concretions in the Baltic Sea: a critical review. In: Nicholson, K., Hein, J.R., Bühn B. and Dasgupta, S. (eds), Manganese mineralization: Geochemistry and mineralogy of terrestrial and marine deposits. Geological Society Special Publication, 119: 213-237.

Glasby, G.P., Stüben, D., Jeschke, G., Stoffers, P. and Garbe-Schönberg, C.-D., 1997b. A model for the formation of hydrothermal manganese crusts from the Pitcairn Island hotspot. Geochim. et Cosmochim. Acta, 61: 4583-4597.

Glasby, G.P. and Schulz, H.D., 1999. E_H, pH diagrams for Mn, Fe, Co, Ni, Cu and As under seawater conditions: Application of two new types of E_H, pH diagrams to the study of specific problems in marine geochemistry. Aquatic Geochemistry, 5: 227-248.

Glasby, G.P., Papavassiliou, C.T., Mitsis, J., Valsami-Jones, E., Liakopoulos, A. and Renner, R.M., 2004. The Vani manganese deposit, Milos island, Greece: A fossil stratabound Mn-Ba-Pb-Zn-As-Sb-W-rich hydrothermal deposit. In: Fytikas, M. and Vougioukalakis, G. (eds), The South Aegean Volcanic Arc Present knowledge and future perspectives. Developments in Volcanology, Elsevier, Amsterdam (in press)

Gordon, A.L. and Gerard, R.D., 1970. North Pacific bottom potential temperatures. In: Hayes, J.D. (ed.), Geological investigations of the North Pacific. Geological Society of America Memoir, 126, pp. 23-39.

Graham, I.J., Carter, R.M., Ditchburn, R.G. and Zondervan, A., 2004. Chronostratigraphy of ODP 181, Site 1121 sediment core (Southwest Pacific Ocean), using $^{10}Be/^{9}Be$ dating of trapped ferromanganese nodules. Marine Geology, 205: 227-247.

Gromet, L.P., Dymek, R.F., Haskin, L.A., and Korotev, R.L., 1984. The „North American Shale Composite“: its compilation, major and trace element characteristics. Geochimica et Cosmochimica Acta, 48: 2469-2482.

Halbach, P., Marchig, V. and Scherhag, C., 1980. Regional variations in Mn, Cu, and Co of ferromanganese nodules from a basin in the Southeast Pacific. Marine Geology, 38: M1-M9.

Halbach, P., Scherhag, C., Hebisch, U. and Marchig, V., 1981. Geochemical and mineralogical control of different genetic types of deep-sea nodules from Pacific Ocean. Mineral Deposita, 16: 59-84.

Halbach, P. and Puteanus, D., 1984. The influence of the carbonate dissolution rate on the growth and composition of Co-rich ferromanganese crusts from the central Pacific seamount areas. Earth and Planetary Science Letters, 68: 73-87.

Halbach, P., Friedrich, G. and von Stackelberg, U. (eds), 1988. The Manganese Nodule Belt of the Pacific Ocean geological environment, nodule formation, and mining aspects. Enke Verlag, Stuttgart, 254 pp.

Halbach, P., Kriete, C., Prause, B. and Puteanus, D., 1989. Mechanism to explain the platinum concentration in ferromanganese seamount crusts. Chemical Geology, 76: 95-106.

Han, X., Jin, X., Yang, S., Fietzke, J. and Eisenhauer, A., 2003. Rhythmic growth of Pacific ferromanganese nodules and their Milankovitch climatic origin. Earth and Planetary Science Letters, 211: 143-157

Harada, K. and Nishida. S. 1976. Biostratigraphy of some marine manganese nodules. Nature, 260: 770-771.

Harada, K. and Nishida. S. 1976. Biochronology of some Pacific manganese nodules and their growth histories. Colloques Internationaux du C.N.R.S. N° 289 – La Genèse des Nodules de Manganèse, pp. 211-216.

Hastings, D. and Emerson, M., 1986. Oxidation of manganese by spores of a marine bacillus: Kinetics and thermodynamic considerations. Geochimica et Cosmochimica Acta, 50: 1819-1824.

Hayes, S.P., 1979. Benthic currents observations at DOMES sites A, B, and C in the tropical North Pacific Ocean. In: Bischoff, J.L. and Piper, D.Z. (eds), Marine geology and oceanography of the Pacific manganese nodule province. Plenum Press, NY, pp. 83-112.

Hayes, S.P., 1988. Benthic currents in the deep ocean. In: Halbach, P., Friedrich, G. and von Stackelberg, U. (eds), The manganese nodule belt of the Pacific Ocean Geological environment, nodule formation, and mining aspects. Enke Verlag, Stuttgart, pp. 99-102.

Heath, G.R., 1981. Ferromanganese nodules of the deep sea. Economic Geology, 75: 736-76

Hein, J.R., 2004. Cobalt-rich ferromanganese crusts: Global distribution, composition, origin and research activities. In: Minerals other than polymetallic nodules of the international seabed area Proceedings of a workshop held on 26-30 June 2000 in Kingston, Jamaica Volume 1, pp.188-272 (http//:www.isa.org.jm)

Hein, J.R., Morgenson, L.A., Clague, D.A. and Koski, R.A., 1987. Cobalt-rich ferromanganese crusts from the exclusive economic zone of the United States and nodules from the oceanic Pacific. In: Scholl, D.W., Grantz, A. and Vedder, J.G. (eds), Geology and resource potential of the continental margin of western North America and the adjacent oceans-Beaufort Sea to Baja California. Circum-Pacific Council for Energy and Mineral Recources, Earth Science Series, Houston, Texas, pp. 753-771.

Hein, J.R., Schwab, W.C. and Davis, A.S., 1988. Cobalt- and platinum-rich ferromanganese crusts and associated substrate rocks from the Marshall Islands. Marine Geology, 78: 255-283.

Hein, J.R., Yeh, H.-W., Gunn, S.H., Sliter, W.H., Benninger,

L.M. and Wang, C.-H., 1993. Two major episodes of Cenozoic phosphogenesis recorded in equatorial Pacific seamount deposits. Paleoceanography, 8: 292-311.

Hein, J.R., Gibbs, A.E., Clague, D.A. and Torresan, M., 1996. Hydrothermal mineralization along submarine rift zones, Hawaii. Marine Georesources and Geotechnology, 14: 177-203.

Hein, J.R., Koschinsky, A., Bau, M., Manheim, F.T., Kang, J.-K., and Roberts, L., 2000. Cobalt-rich ferromanganese crusts in the Pacific. In: Cronan, D.S. (ed), Handbook of marine minerals. CRC Press, Boca Raton, Florida, pp. 239-279.

Hem, J.D., Roberson, C.E. and Lind, C.J., 1985. Thermodynamic stability of CoOOH and its coprecipitation with manganese. Geochim. et Cosmochim. Acta, 49: 801-810.

Heye, D., 1978. Changes in the growth rate of manganese nodules from the Central Pacific in the area of a seamount as shown by the Io nethod. Marine Geology, 28: M59-M65.

Hlawatsch, S., 1999. Mn-Fe-Akkumulate als Indikator für Schad- und Nährstoffflüsse in der westlichen Ostsee. Geomar Report 85, Geomar Research Center, Kiel (with English abstract)

Hlawatsch, S., Neumann, T., van der Berg, C.M.G., Kersten, M., Harff, J., and Suess, E., 2002. Fast-growing shallow-water ferro-manganese nodules from the western Baltic Sea: origin and modes of trace element incorporation. Marine Geology, 182: 373-387.

Hodge, V.F., Stallard, M., Koide, M. and Goldberg, E.D., 1985. Platinum and platinum anomaly in the marine environment. Earth and Planetary Science Letters, 72: 158-162.

Hogg, N.G., 2001. Quantification of the deep circulation. In: Siedler, G., Church, J. and Gould, J.J. (eds), Ocean circulation & climate observation and modeling of the global ocean. Academic Press, San Diego, pp. 259-270.

Horn, D.R. (ed.), 1972. Ferromanganese deposits of the ocean floor. National Science Foundation, Washington, D. C., 293 pp.

Huh, C-A. and Ku, T.-L. 1984. Radiochemical observations on manganese nodules from three sedimentary environments in the North Pacific. Geochimica et Cosmochimica Acta, 48: 951-963.

Ito, T., Usui, A., Kajiwara, Y., Nakano, T., 1998. Strontium isotopic composition and paleoceanographic implcation of fossil manganese nodules in DSDP/ODP cores, Leg 1-126. Geochimica et Cosmochimica Acta, 62: 1545-1554.

Jauhari, P. and Pattan, J.N., 2000. Ferromanganese nodules from the Central Indian Ocean Basin. In: Cronan, D.S. (ed.), Handbook of marine minerals. CRC Press, Boca Raton, Florida, pp. 171-195.

Jeong, K.S., Kang, J.K. and Chough, S.K., 1994. Sedimentary processes and manganese nodule formation in the Korea Deep Ocean Study (KODOS) area, western part of Clarion-Clipperton fracture zones, northeast equatorial Pacific. Marine Geology, 122: 125-150.

Jeong, K.S., Kang, J.K., Lee, K.Y. Jung, H.S., Chi, S.B. and Ahn, S.J., 1996. Formation and distribution of manganese nodule deposits in the western margin of Clarion-Clipperton fracture zones, northeast equatorial Pacific. Geo-Marine Letters, 16: 123-131.

Jeong, K.S., Jung, H.S., Kang, J.K., Morgan, C.L. and Hein, J.R., 2000. Formation of ferromanganese crusts on northwest intertropical Pacific seamounts: electron photomicrography and microprobe chemistry. Marine Geology, 162: 541-559.

Johnson, C.E. and Glasby, G.P., 1969. Mössbauer Effect determination of particle size in microcrystalline iron-manganese nodules. Nature, 222: 376-377.

Johnson, D.A., 1972. Eastward-flowing bottom currents along the Clipperton Fracture Zone. Deep-Sea Research, 19: 253-257

Johnson, K.S., Coale, K.H., Berelson, W.M. and Gordon, R.M., 1996. On the formation of the manganese maximum in the oxygen minimum. Geochimica et Cosmochimica Acta, 60: 1291-1299.

Johnson, K.S., Gordon, R.M. and Coale, K.H., 1997. What controls dissolved iron concentrations in the world ocean? Marine Chemistry, 57: 137-161.

Johnston, J.H. and Glasby, G.P., 1978. The secondary iron oxidehydroxide mineralogy of some deep sea and fossil manganese nodules: A Mössbauer and X-ray study. Geochemical Journal, 12: 153-164.

Johnston, J.H. and Glasby, G.P., 1982. A Mössbauer spectroscopic and X-ray diffraction study of the iron mineralogy of some sediments from the Southwest Pacific Basin. Marine Chemistry, 11: 437-448.

Jung, H.-S. and Lee, C.-P., 1999. Growth of diagenetic ferromanganese nodules in an oxic deep-sea environment, northeast Pacific. Marine Geology, 157: 127-144.

Kadko, D. and Burckle, L.H., 1980. Manganese growth rates determined by fossil diatom dating. Nature, 287: 725-726.

Kasten, S., Glasby, G.P., Schulz, H., Friedrich, G. and Andreev, S.I., 1998. Rare earth elements in manganese nodules from the South Atlantic Ocean as indicators of oceanic bottom water flow. Marine Geology, 146: 33-52.

Knie, K., Korschinek, G., Faestermann, T., Dorfi, E.A., Rugel, G and Wallner, A., 2004. ^{60}Fe anomaly in a deep-sea manganese crust and implications for a nearby supernova source. Physical Review Letters, 93: 171103.

Knoop, P.A., Owen, R.M. and Morgan, C.L., 1998. Regional variability in ferromanganese nodule composition: north-eastern tropical Pacific Ocean. Marine Geology, 147: 1-12.

Köning, I., Drodt, M., Suess, E. and Trautwein, A.X., 1997. Iron reduction through the tan-green color transition in deep-sea sediments. Geochimica et Cosmochimmica Acta, 61: 1679-1683.

Kontar, E.A. and Sokov, A.V., 1994. A benthic storm in the northeastern tropical Pacific over fields of manganese nodules. Deep-Sea Research I, 41: 1069-1089.

Koschinsky, A. and Halbach, P., 1995. Sequential leaching of marine ferromanganese precipitates: Genetic implications. Geochimica et Cosmochimica Acta, 59: 5113-5132.

Koschinsky, A. and Hein, J.R., 2003. Uptake of elements from seawater by ferromanganese crusts: solid-phase associations and seawater speciation. Marine Geology, 198: 331-351.

Koschinsky, A., Halbach, P., Hein, J.R. and Mangini, A., 1996. Ferromanganese crusts as indicators for paleoceanographic events in the NE Atlantic. Geologische Rundschau, 85: 567-576.

Koschinsky, A., Stascheit, A.-M., Bau, M. and Halbach, P., 1997. Effects of phosphatization on the geochemical and

mineralogical composition of marine ferromanganese crusts. Geochimica et Cosmochimica Acta, 61: 4079-4094.

Kotlinski, R., 1995. InterOceanMetal Joint Organization: Archievements and Challenges. Proceedings of the ISOPE (The International Society of Offshore and Polar Engineers)-Ocean Mining Symposium, Tsukuba, Japan, November 21-22, 5-7.

Krishnaswamy, S., 1976. Authigenic transition elements in Pacific pelagic clays. Geochimica et Cosmochimica Acta, 40: 425-435.

Ku, T.-L. and Glasby, G.P., 1972. Radiometric evidence for the rapid growth rates of shallow-water, continental margin manganese nodules. Geochimica et Cosmochimica Acta, 36: 699-703.

Ku, T.-L., 1977. Rates of accretion. In: Glasby, G.P. (ed.) Marine manganese deposits. Elsevier, Amsterdam, pp. 249-267.

Kuma, K., Usui, A., Paplawsky, W., Gedulin, B. and Arrhenius, G., 1994. Crystal structures of synthetic 7 Å and 10 Å manganates substituted by mono - and divalent cations. Mineralogical Magazine, 58: 425-447.

Kunzendorf, H., Glasby, G.P., Stoffers, P. and Plüger, W.L., 1993. The distribution of rare earth and minor elements in manganese nodules, micronodules and sediments along an east-west transect in the southern Pacific. Lithos, 30: 45-56.

Kusukabe, M. and Ku, T.L., 1984. Incorporation of Be isotopes and other trace metals into marine ferromanganese deposits. Geochimica et Cosmochimica Acta, 48: 2187-2193.

Lalou, C., Brichet, E., Jehanno, C. and Perez-Leclaire, H., 1983. Hydrothermal manganese oxide deposits from Galapagos mounds, DSDP Leg 70, hole 509B and „Alvin“ dives 729 and 721. Earth and Planetary Science Letters, 63:63-75.

Lavasseur, S., Frank, M., Hein, J.R. and Halliday, A.N., 2004. The global variation in the iron isotope composition of marine hydrogenetic ferromanganese deposits: impliations for seawater chemistry? Earth and Planetary Science Letters, 224: 91-105.

Lavelle, J.W., Cowen, J.P. and Massoth, G.J., 1992. A model for the deposition of hydrothermal manganese near mid-ocean ridge crests. Journal of Geophysical Research, 97: 7413-7427.

Lee, D.-C., Halliday, A.N., Hein, J.R., Burton, K.W., Christensen, J.N. and Günther, D., 1999. Hafnium isotope stratigraphy of ferromanganese crusts. Science, 285: 1052-1054.

Lei, G., 1996. Crystal structure and metal uptake capacity of 10 Å-manganates: An overview. Marine Geology, 133: 103-112.

Lenoble, J.-P., 2004. A comparison of the possible economic returns from mining deep-sea polymetallic nodules, sea floor massive sulphides and cobalt-rich crusts. Proceedings of a workshop held on 26-30 June 2000 in Kingston, Jamaica Volume 1, pp. 424-465 (http//: www.isa.org.jp)

Liebetrau, V., Eisenhauer, A., Gussone, N., Wörner, G., Hansen, B.T., Leipe, T., 2002. Ra/Ba growth rates and U-Th-Ba systematics of Baltic Fe-Mn crusts. Geochimica et Cosmochimica Acta, 66 : 73-83.

Lilley, M.D., Feely, R.A. and Trefry, J.H., 1995. Chemical and biochemical transformations in hydrothermal plumes. In: Humphris, S.E. Zierenberg, R.A., Mullineaux, L.S. and Thompson, R.E. (eds), Seafloor Hydrothermal systems: Physical, chemical, biological, and geological interactions. American Geophysical Union Geophysical Monogrograph, 91: 369-391.

Ling, H.F., Burton, K.W., O'Nions, R.K., Kamber, B.S., von Blanckenberg, F., Gibb, A.J. and Hein, J.R., 1997. Evolution of Nd and Pb isotopes in central Pacific seawater from ferromanganese crusts. Earth and Planetary Science Letters, 146: 1-12.

Lonsdale, P., 1976. Abyssal circulation of the southeastern Pacific and some geological implications. Journal of Geophysical Research, 81: 1163-1176.

Lonsdale, P., 1981. Drifts and ponds of reworked pelagic sediment in part of the Southwest Pacific. Marine Geology, 43: 153-193.

Lupton, J., 1998. Hydrothermal helium plumes in the Pacific Ocean. Journal of Geophysical Research, 103: 15,835-15,868.

Lyle, M., 1983. The brown-green color transition in marine sediments: A marker of the Fe(III)-Fe(II) redox boundary. Limnology and Oceanography 28: 1026-1033.

Lyle, M., Owen, R.M. and Leinen, M., 1986. History of hydrothermal sedimentation at the East Pacific Rise, 19°S. In: Initial Reports of the Deep Sea Drilling Project. U.S. Government Printing Office, Washington, D.C., 92: 585-596.

McCave, I.N., 1988. Biological pumping upwards of the coarse fraction of deep-sea sediments. Journal of Sedimentary Petrology, 58: 148-158.

Macdonald, K.C. and Hollister, C.D., 1973. Near-bottom thermocline in the Samoan Passage, west equatorial Pacific. Nature, 241: 461-462.

McMurtry, G.M., von der Haar, D.L., Eisenhauer, A., Mahoney, J.J. and Yeh, H.W., 1994. Cenozoic accumu-lation history of a Pacific ferromanganese crust. Earth and Planetary Science Letters, 125: 105-118.

Manceau, A., Llorca, S. and Calas, G., 1987. Crystal chemistry of cobalt and nickel in lithiophorite and asbolane from New Caledonia. Geochimica et Cosmochimica Acta, 51: 105-113.

Manceau, A., Gorshkov, A.I. and Drits, V.A., 1992a. Structural chemistry of Mn, Fe, Co, and Ni in manganese hydrous oxides: Part I. Information from EXAFS spectroscopy. American Mineralogist, 77: 1133-1143.

Manceau, A., Gorshkov, A.I. and Drits, V.A., 1992b. Structural chemistry of Mn, Fe, Co, and Ni in manganese hydrous oxides: Part II. Information from EXAFS spectroscopy and electron and X-ray diffraction. American Mineralogist, 77: 1144-1157.

Manceau, A., Drits, V.A., Silvester, E., Bartoli, C. and Lanson, B., 1997. Structural mechanism of Co^{2+} oxida-tion by the phyllomanganate buserite. American Mine-ralogist, 82: 1150-1175.

Manceau, A., Lanson, B. and Drits, V.A., 2002. Structure of heavy metal sorbed birnessite. Part III. Results from powder and polarized extended X-ray absorption fine structure spectroscopy. Geochimica et Cosmochimica Acta, 66: 2639-2663.

Mandernack, K.W., Post, J. and Tebo, B.M., 1995. Manganese mineral formation by bacterial spores of the marine Bacillus, strain SG-1: Evidence for the direct oxidation of Mn(II) to Mn(IV). Geochimica et

Cosmochimica Acta, 59: 4393-4408.

Mangini, A., 1988. Growth rates of manganese nodules and crusts. In: Halbach, P., Friedrich, G. and von Stackelberg, U. (eds), The Manganese Nodule Belt of the Pacific Ocean Geological environment, nodule formation, and mining aspects. Enke Verlag, Stuttgart, pp. 142-151.

Mangini, A., Dominik, J., Muller, P.J and Stoffers, P., 1982. Pacific deep circulation: A velocity increase at the end of the interglacial stage 5? Deep-Sea Research, 29A: 1517-1530.

Mangini, A., Halbach, P., Puteanus, D. and Segl, M., 1987. Chemistry and growth history of Central Pacific Mn - crusts and their economic importance. In: Teleki, P.G., Dobson, M.R., Moore, J.R. and von Stackelberg, U. (eds), Marine minerals Advances in research and resource assessment. D. Reidel, Dordrecht, pp. 205-220.

Mangini, A., Eisenhauer, A. and Walter, P., 1990a. Response of manganese in the ocean to climate change in the Quaternary. Paleoceanography, 5: 811-821.

Mangini, A., Segl, M., Glasby, G.P, Stoffers, P. and Plüger, W.L., 1990b. Element accumulation rates in and growth histories of manganese nodules from the Southwestern Pacific Basin. Marine Geology, 94: 97-107.

Manheim, F.T., 1986. Marine cobalt resources. Science, 232: 600-608.

Manheim, F.T. and Lane-Bostwick, C.M., 1988. Cobalt in ferromanganese crusts as a monitor of hydrothermal discharge on the Pacific sea floor. Nature, 335: 59-62.

Mantyla, A.W., 1975. On the potential temperature in the abyssal Pacific Ocean. Journal of Marine Research, 33: 341-354.

Marchig, V., 2000. Hydrothermal activity on the southern, ultrafast-spreading segment of the East Pacific Rise. In: Cronan, D.S. (ed.), Handbook of marine minerals. CRC Press, Boca Raton, Florida, pp. 309-325..

Marchig, V. and Erzinger, J., 1986. Chemical composition of Pacific sediments near 20°S: changes with increasing distance from the East Pacific Rise. In: Initial Reports of the Deep Sea Drilling Project. U.S. Government Printing Office, Washington, D.C., pp. 371-381.

Marcus, M.A., Manceau, A. and Kersten, M., 2004. Mn, Fe, Zn and As speciation in a fast growing ferromanganese marine nodule. Geochimica et Cosmochimica Acta, 68: 3125-3136.

Martin, J.H., Knauer, G.A. and Broenkow, W.W., 1985. VERTEX: the lateral transport of manganese in the northeast Pacific. Deep-Sea Research, 32: 1405-1427.

Medford, R.D., 1969. Marine mining in Britain. Mining Magazine, 121(5): 369-381 and 121(6): 474-480.

Mellin, T.A. and Lei, G., 1993. Stabilization of 10 Å-manganates by interlayer cations and hydrothermal treatment: Implications for the mineralogy of marine manganese concretions. Marine Geology, 115: 67-83.

Mero, J.L., 1965. Mineral resources of the sea. Elsevier, Amsterdam, 312 pp.

Mero, J.L., 1977. Economic aspects of nodule mining. In: Glasby, G.P. (ed.), 1977. Marine manganese deposits. Elsevier, Amsterdam, pp. 327-355.

Meylan, M.A., Glasby, G.P., McDougall, J.C. and Kumbalek, S.C., 1982. Lithology, colour, mineralogy, and geochemistry of marine sediments from the Southwestern Pacific and Samoan Basin. New Zealand Journal of Geology and Geophysics, 25: 437-458.

Meylan, M.A., Glasby, G.P., Hill, P.J., McKelvey, B.C., Walter, P. and Stoffers, P., 1990. Manganese crusts and nodules from the Manihiki Plateau and adjacent areas: Results of HMNZS Tui cruises. Marine Mining, 9: 43-72.

Michard, G. and Albarède, F. 1986.The REE content of some hydrothermal fluids. Chemical Geology, 55: 51-60.

Miller, S. and Cronan, D.S., 1994. Element supply to surface sediments and interrelationships with nodules along the Aitutaki-Jarvis Transect, South Pacific. Journal of the Geological Society of London, 151: 403-412.

Moore, J.G. and Clague, D.A., 2004. Hawaiian submarine manganese-iron oxide crusts — A dating tool? GSA Bulletin, 116: 337-347.

Morgan, C.L., 2000. Resource estimates of the Clarion - Clipperton manganese nodule deposits. In: Cronan, D.S. (ed.), Handbook of marine minerals. CRC Press, Boca Raton, Florida, pp. 145-170.

Morgan, J.J., 2005. Kinetics of reaction between oxygen and Mn(II) species in aqueous solutions. Geochimica et Cosmochimica Acta, 69: 35-48.

Mukhopadhyay, R., Iyer, S.D. and Ghosh, A.K., 2002. The Indian Ocean Nodule Field: petrotectonic evolution and ferromanganese deposits. Earth-Science Reviews, 60: 67-130.

Müller, P.J., Hartmann, M. and Suess, E., 1988. The chemical environment of pelagic sediments. In: Halbach, P., Friedrich, G. and von Stackelberg, U. (eds), The manganese nodule belt of the Pacific Ocean Geological environment, nodule formation, and mining aspects. Enke Verlag, Stuttgart, pp. 70-99.

Murray, J.W. and Brewer, P.G., 1977. Mechanism of removal of manganese, iron and other trace metals from seawater. In: Glasby, G.P. (ed), Marine manganese deposits. Elsevier, Amsterdam, pp. 291-325.

Murray, J.W., Balistrieri, L.S. and Paul, B., 1984. The oxidation state of manganese in marine sediments and ferromanganese nodules. Geochimica et Cosmochimica Acta, 48: 1237-1247.

Nemoto, K. and Kroenke, L.W., 1981. Marine geology of the Hess Rise 1. Bathymetry, surface sediment distribution and environment of deposition. Journal of Geophysical Research, 86: 10734-10752.

Nicholson, K., Hein, J.R., Bühn, B. and Dasgupta S. (eds), 1997. Manganese mineralization: Geochemistry and mineralogy of terrestrial and marine deposits. Geological Society Special Publication, 119: 370 pp.

Norris, R.D. and Röhling, U., 1999. Carbon cycling and chronology of climate warming at the Palaeocene/Eocene transition. Nature, 401: 775-778.

Nozaki, Y., 1997. A fresh look at element distribution in the North Pacific. EOS Transactions of the American Geophysical Union, 78: 221.

O'Nions, R.K., Frank, M., von Blanckenburg, F. and Ling, H.F., 1998. Secular variation of Nd and Pb isotopes in ferromanganese crusts from the Atlantic, Indian and Pacific Oceans. Earth and Planetary Science Letters, 155: 15-28.

Overnell, J., 2002. Manganese and iron profiles during early diagenesis in Loch Etive, Scotland. Application of two diagenetic models. Estuarine, Coastal and Shelf Science, 54: 33-44.

Overnell, J., Harvey, S.M. and Parkes, R.J., 1996. A biogeochemical comparison of sea loch sediments: Manganese and iron contents, sulphate reduction rates and oxygen uptake rates. Oceanologica Acta, 19: 41-55.

Overnell, J., Brand, T., Bourgeois, W. and Statham, P.J., 2002. Manganese dynamics in the water column of the upper basin of Loch Etive, a Scottish fjord. Estuarine, Coastal and Shelf Science, 55: 481-492.

Piper, D.Z. and Williamson, M.E., 1977. Composition of Pacific Ocean ferromanganese nodules. Marine Geology., 23: 285-303.

Piper, D.Z. and Blueford, J.R., 1982. Distribution, mineralogy, and texture of manganese nodules and their relation to sedimentation at the DOMES Site A in the equatorial North Pacific. Deep-Sea Research, 29A: 927-952.

Piper, D.Z., Basler, J.R. and Bischoff, J.L., 1984. Oxidation state of marine manganese nodules. Geochimica et Cosmochimica Acta, 48: 2347-2355.

Piper, D.Z., Swint, T.R., Sullivan, L.G. and McCoy, F.W., 1985. Manganese nodules, seafloor sediment, and sedimentation rates in the Circum-Pacific region. Circum-Pacific Council for Energy and Mineral Resources Circum-Pacific Map Project. American Association of Petroleum Geologists, Tulsa, Oklahoma.

Piper, D.Z., Swint-Iki, T.R. and McCoy, F.W., 1987. Distribution of ferromanganese nodules in the Pacific Ocean. Chemie der Erde, 46: 171-184.

Plüger, W.L., Friedrich, G. and Stoffers, P., 1985. Environmental controls of the formation of deep-sea ferromanganese concretions. Monograph Series on Mineral Deposits, 25: 31-52.

Plunkert, P.A. and Jones, T.S, 1999. Metal prices in the United States through 1998. USGS. 181 pp. (http://minerals.usgs.gov/minerals/pubs/metal_prices)

Post, J.E., 1999. Manganese oxide minerals: crystal structures and environmental significance. Proceedings of the National Academy of Science of the USA, 96: 3447-3454.

Pulyaeva, I., 1997. Stratification of ferromanganese crusts on the Magellan seamounts. Proceedings of the 30th International Geological Congress, Vol. 13: 111-128.

Puteanus, D., and Halbach, P., 1988. Correlation of Co concentration and growth rate-a model for age determination of ferromanganese crusts. Chemical Geology, 69: 71-85.

Raab, W.J. and Meylan, M.A., 1977. Morphology. In: Glasby, G.P. (ed.), Marine manganese deposits. Elsevier, Amsterdam, pp. 109-146.

Rehkämper, M., Frank, M., Hein, J.R. and Halliday, A.N., 2004. Cenozoic marine geochemistry of thallium deduced from isotopic studies of ferromanganese crusts and palagic sediments. Earth and Planetary Science Letters, 219: 77-91.

Reid, J.L. and Lonsdale, P.F., 1974. On the flow of water through the Samoan Passage. Journal of Physical Oceanography, 4: 58-73.

Reyss, J.L., Lemaitre, N., Ku, T.L., Marchig, V., Southon, J.R., Nelson, D.E. and Vogel, J.S., 1985. Growth of manganese nodule from the Peru Basin: A radiochemical anomaly. Geochimica et Cosmochimica Acta, 49: 2401-2408.

Roemmich, D., Huatala, S. and Rudnick, D.L., 1996. Northward abyssal transport through the Samoan Passage and adjacent regions. Journal of Geophysical Research, 101: 14,039-14,055.

Roy, S., 1981. Manganese deposits. Academic Press, London, 458 pp.

Rudnick, D.L., 1997. Direct velocity measurements in the Samoan Passage. Journal of Geophysical Research, 102: 3293-3303.

Sanderson, B., 1985. How bioturbation supports manganese nodules at the sediment-water interface. Deep-Sea Research, 32A: 1281-1285.

Sawlan, J.J. and Murray, J.W., 1983. Trace metal remobilization in the interstitial waters of red clay and hemipelagic marine sediments. Earth and Planetary Science Letters, 64: 213-230.

Schlosser, P., Bullister, J.L., Fine, R., Jenkins, W.J., Key, R., Roether, W. and Smethie, W.M., 2001. Transformation and age of water masses. In: Siedler, G., Church, J. and Gould, J.J. (eds), Ocean circulation & climate observation and modeling of the global ocean. Academic Press, San Diego, pp. 431-452 + Plate 5.8.17 (P. 428)

Schmitz, W., Mangini, A., Stoffers, P., Glasby, G.P. and Plüger, W.L., 1986. Sediment accumulation rates in the southwestern Pacific Basin and Aitutaki Passage. Marine Geology, 73: 181-190.

Schmitz, W.J., 1995. On the interbasin-scale thermohaline circulation. Reviews of Geophysics, 33: 151-173.

Scholten, J.C., Scott, S.D., Garbe-Schönberg, D., Fietze, J., Blanz, T and Kennedy, C.B., 2004. Hydrothermal manganese crusts from the Pitcairn region. In: Hekinian, R., Stoffers, P. and Cheminée, J.-L., (eds), Oceanic hotspots intraplate submarine magmatism and tectonism. Springer-Verlag, Berlin, pp.375-405.

Segl, M., Mangini, A., Bonani, G., Hofmann, H.J., Nessi, M., Suter, M., Wölfli, W., Friedrich, G., Plüger, W.L., Wiechowski, A. and Beer, J., 1984. ^{10}Be-dating of a manganese crust from the central North Pacific Ocean and implications for ocean palaeocirculation. Nature, 309: 540-543.

Segl, M., Mangini, A., Beer, J., Bonani, G., Suter, M. and Wölfli, W., 1989. Growth rate variations of manganese nodules and crusts induced by paleoceanographic events. Paleoceanography, 4: 511-530.

Shaw, T.J., Gieskes, J.M. and Jahnke, R.A., 1990. Early diagenesis in differing depositional environments: The response of transition metals in pore waters. Geochimica et Cosmochimica Acta, 54: 1233-1246.

Shevenell, A.E., Kennett, J.P. and Lea, D.W., 2004. Middle Miocene Southern Ocean cooling and Antarctic cryosphere expansion. Science, 305: 1766-1770.

Shilov, V.V., 2004. Stratigraphy of Upper Cenozoic deposits in the Clarion-Clipperton Fracture Zone (Pacific Ocean). Unpublished Candidate thesis, VSEGEI (All-Russian Institute of Geology), St. Petersburg. 158 pp. (In Russian)

Silvester, E., Manceau, A., Drits, V.A., 1997. Structure of synthetic monoclinic Na-rich birnessite: II. Results from chemical studies and EXAFS spectroscopy. American Mineralogist, 82: 962-978.

Skornyakova, N.S. and Murdmaa, I.O., 1992. Local variation in distribution and composition of ferromanganese nodules

in the Clarion - Clipperton Nodule Province. Marine Geology, 103: 381-405.

Sorem, R.K. and Fewkes, R.H., 1979. Manganese nodule research data and methods of investigation. IFI/ Plenum Press, NY, 723 pp.

Stoffers, P., Glasby, G.P., Thijssen, T., Shrivastava, P.C. and Melguen, M., 1981. The geochemistry of co - existing manganese nodules, micronodules, sediments and pore waters from five areas in the equatorial and South - West Pacific. Chemie der Erde, 40: 273-297.

Stoffers, P., Glasby, G.P. and Frenzel, G., 1984. Comparison of the characteristics of manganese micronodules from the equatorial and south - west Pacific. TMPM Tschermaks Mineralogische und Petrographische Mitteilungen, 33: 1-23.

Stoffers, P., Schmitz, W., Glasby, G.P., Plüger, W.L. and Walter, P., 1985. Mineralogy and geochemistry of sediments in the Southwestern Pacific Basin: Tahiti - East Pacific Rise - New Zealand. New Zealand Journal of Geology and Geophysics, 28: 513-530.

Stüben, D., Glasby, G.P., Eckhardt, J.-D., Berner, Z., Mountain, B.W. and Usui, A., 1999. Enrichments of platinum-group elements in hydrogenous, diagenetic and hydrothermal marine manganese and iron deposits. Exploration and Mining Geology, 8: 233-250.

Sverjensky, D.A. 1984. Equilibrium redox equilibria in aqueous solution. Earth and Planetary Science Letters, 67: 70-78.

Szefer, P., Glasby, G.P., Kunzendorf, H., Görlich, E.A., Latka, K., Ikuta, K., and Ali, A.A., 1998. Distribution of rare earth and other elements, and the mineralogy of the iron oxyhydroxide phase in marine ferromanganese concretions from within Slupsk Furrow southern Baltic Sea, off Poland. Applied Geochemistry, 13: 305-312.

Taft, B.A., Hayes, S.P., Friederich, G.E, Codispoti, A, 1991. Flow of abyssal water into the Samoan Passage. Deep-Sea Research, 38, Supplement 1: S103-S128.

Tebo, B.M., Ghiorse, W.C., van Waasbergen, L.G., Siering, P.L. and Caspi, R., 1997. Bacterially-mediated mineral formation: Insights into manganese (II) oxidation from molecular genetic and biochemical studies. Reviews in Mineralogy, 35: 225-266.

Tebo, B.M., Bargar, J.R., Clement, B.G., Dick, G.J., Murray, K.J., Parker, D., Verity, R. and Webb, S.M., 2004. Biogenic manganese oxides: Properties and mechanisms of formation. Annual Review of Earth and Panetary Sciences, 32: 287-328.

Teleki, P.G., Dopson, M.R., Moore, J.R. and von Stackelberg, U. (eds), 1987. Marine minerals Advances in research and resource assessment. D. Reidel, Dordrecht, 588 pp.

Thamdrup, B. and Canfield, D.E., 1996. Pathways of carbon oxidation in continental margin sediments off central Chile. Limnology and Oceanography, 41: 1629-1650.

Thiel, H. (ed.), 2001. Environmental impact studies for the mining of polymetallic nodules from the deep sea. Deep-Sea Research II, 48: 3427-3882.

Thijssen, T., Glasby, G.P., Friedrich, G., Stoffers, P. and Sioulas, A., 1985. Manganese nodules in the central Peru Basin. Chemie der Erde, 44: 1-46.

Thomson, J., Higgs, N.C., Hydes, D.J., Wilson, T.R.S. and Sorensen, J., 1987. Geochemical oxidation fronts in NE Atlantic distal turbidites and their effects in the sedimentary record. In: Weaver, P.P.E. and Thompson, J. (eds), Geology and geochemistry of abyssal plains. Geological Society Special Publication, 31: 167-177.

Turekian, K.K. and Bacon, M.P., 2004. Geochronometry of marine deposits. In: Elderfield, H. (ed.), Treatise on geochemistry vol. 6 The oceans and marine geochemistry. Elsevier, Amsterdam, pp. 321-341,

Turner, S. and Buseck, P.R., 1981. Todorokites: A new family of naturally occuring manganese oxides. Science, 212: 1024-1027.

Usui, A., 1979. Nickel and copper accumulation as essential elements in 10Å manganite of deep-sea manganese nodules. Nature, 279: 411-413.

Usui, A., 1992. Hydrothermal manganese minerals in Leg 126 cores. Proceedings of Ocean Drilling Program Scentific Results, Volume 126: 113-123.

Usui, A. and Nishimura, A., 1992. Submersible observations of hydrothermal manganese deposits on the Kaikata Seamount, Izu-Ogasawara (Bonin) Arc. Marine Geology, 106: 203-216

Usui, A. and Ito, T., 1994. Fossil manganese deposits buried within DSDP/ODP cores, Leg 1-126. Marine Geology, 119: 111-136.

Usui, A. and Mita, N., 1995. Geochemistry and mineralogy of a modern buserite deposit from a hot spring in Hokkaido, Japan. Clays and Clay Minerals, 43: 116-127.

Usui, A. and Terashima, S., 1997. Deposition of hydrogenetic and hydrothermal manganese minerals in the Ogasawara (Bonin) arc area, northwest Pacific. Marine Georecources and Geotechnology, 15: 127-154.

Usui, A. and Glasby, G.P., 1998. Submarine hydrothermal manganese deposits in the Izu-Bonin-Mariana arc: An overview. The Island Arc, 7: 422-431.

Usui, A., Yuasa, M., Yokota, S., Nohara, M. and Nishimura, A., 1986. Submarine hydrothermal manganese deposits from the Ogasawara (Bonin) Arc, off the Japanese islands. Marine Geology, 73: 311-322.

Usui, A., Mellin, T.A., Nohara, M. and Yuasa, M., 1989. Structural stability of marine 10 Å manganates from the Ogasawara (Bonin) Arc: Implications for low-temperature hydrothermal activity. Marine Geology, 86: 41-56.

Usui, A., Nishimura, A. and Mita, N., 1993. Composition and growth history of surficial and buried manganese nodules in the Penrhyn Basin, Southwest Pacific. MarineGeology, 114: 133-153.

Usui, A., Bau, M. and Yamazaki, T., 1997. Manganese microchimneys buried in Central Pacific Pacific pelagic sediments: evidence of intraplate water circulation. Marine Geology, 141: 269-285.

van Andel , Tj.H., Heath, G.R. and Moore, T.C., 1975. Cenozoic history and paleoceanography of the central equatorial Pacific Ocean. Geological Society of America Memoir, 143: 134 pp.

van de Fliert, T., Frank, M., Halliday, A.N., Hein, J.R., Hattendorf, B., Günther, D. and Kubik, P.W., 2003. Lead isotopes in North Pacific deep - water implications for past changes in input sources and circulation patterns. Earth and Planetary Science Letters, 209: 149-164.

van de Fliert, T., Frank, M., Halliday, A.N., Hattendorf, B.,

Günther, D. and Kubik, P.W., 2004a. Tracing the history of submarine hydrothermal inputs and the significance of hydrothermal hafnium for the seawater budget—a combined Pb-Hf-Nd approach. Earth and Planetary Science Letters, 222: 259-273.

van de Fliert, T., Frank, M., Halliday, A.N., Hein, J.R., Hattendorf, B., Günther, D. and Kubik, P.W., 2004b. Deep and bottom water export from the Southern Ocean to the Pacific over the past 38 million years. Paleoceanograpy, 19: PA1020

van de Fliert, T., Frank, M., Lee, D.-C., Halliday, A.N., Reynolds, B.C. and Hein, J.R., 2004c. New constraints on the sources and behavior of neodymium and hafnium in seawater from Pacifc Ocean ferromanganese crusts. Geochimica et Cosmochimica Acta, 68: 3827-3843.

Varentsov, I.M. and Grasselly, Gy. (eds), 1980. Geology and geochemistry of manganese. Hungarian Academy of Sciences, Budapest, 3 volumes.

Varentsov, I.M., Drits, V.A., Gorshkov, A.I., Sivtsov, A.V. and Sakharov, B.A., 1991a. Mn-Fe oxyhydroxide crusts from Krylov Seamount (Eastern Atlantic): Mineralogy, geochemistry and genesis. Marine Geology, 96: 53-70.

Varentsov, I.M., Drits, V.A. and Gorshkov, A.I., 1991b. Rare earth element indicators of Mn-Fe oxyhydroxide crust formation on Krylov Seamount, Eastern Atlantic. Marine Geology, 96: 71-84.

von Blanckenburg, F. O'Nions, R.K. and Hein, J.R., 1996a. Distribution and source of pre-anthropogenic lead isotopes in deep ocean water from Mn-Fe crusts. Geochimica et Cosmochimica Acta, 60: 4957-4963.

von Blanckenburg, F., O'Nions, R.K., Belshaw, N.S., Gibb, A. and Hein, J.R., 1996b. Global distribution of beryllium isotopes in deep ocean water as derived from Fe-Mn crusts. Earth and Planetary Science Letters, 141: 213-226.

von der Haar, D.L., Mahoney, J.J. and McMurtry, G.M., 1995. An evaluation of strontium isotopic dating of ferromanganese oxides in a marine hydrogenous crust. Geochimica et Cosmochimica Acta, 59: 4267-4277.

von Langen, P., Johnson, K.S., Coale, K.H. and Elrod, V.A., 1997. Oxidation kinetics of manganese (II) in seawater in nanomolar concentrations. Geochimica et Cosmochimica Acta, 61: 4945-4954.

von Stackelberg, U., 1997. Growth history of manganese nodules and crusts of the Peru Basin. In: Nicholson, K., Hein, J.R., Bühn, B. and Dasgupta S. (eds), Manganese mineralization: Geochemistry and mineralogy of terrestrial and marine deposits. Geological Society Special Publication, 119: 153-176.

von Stackelberg, U., 2000. Manganese nodules of the Peru Basin. In: Cronan, D.S. (ed.), Handbook of marine minerals. CRC Press, Boca Raton, Florida, pp. 197-238.

von Stackelberg, U., Kunzendorf, H., Marchig, V. and Gwozdz, R., 1984. Growth history of a large manganese crust from the Equatorial North Pacific Nodule Belt. Geologishes Jahrbuch, 75A: 213-235.

von Stackelberg, U. and Marchig, V., 1987. Manganese nodules from the equatorial North Pacific Ocean. Geologishes Jahrbuch, 87D: 123-227.

von Stackelberg, U. and Beiersdorf, H., 1991. The formation of manganese nodules between the Clarion and Clipperton fracture zones southeast of Hawaii. Marine Geology, 98: 411-423.

Wallace, H.E., Thomson, J., Wilson, T.R.S., Weaver, P.P.E., Higgs, N.C., Hydes, D.J., 1988. Active diagenetic formation of metal-rich layers in N.E. Atlantic sediments. Geochimica et Cosmochimica Acta, 52: 1557-1569.

Wallner, C., Faestermann, T., Gerstmann, U., Knie, K., Korschinek, G., Lierse, C. and Rugel, G., 2003. Supernova produced and anthropogenic ^{244}Pu in deep sea manganese encrustations. New Astronomy Reviews, 48: 145-150.

Waychunas, G.A., 1991. Crystal chemistry of oxides and oxyhydroxides. Reviews in Mineralogy, 25: 11-68.

Wiltshire, J.C., 2000. Innovations in marine ferromanganese oxide tailings disposal. In: Cronan, D.S. (ed.), Handbook of marine minerals. CRC Press, Boca Raton, Florida, pp. 281-305.

Wiltshire, J.C., Wen, X.Y and Yao, D., 1999. Ferromanganese crusts near Johnson Island: Geochemistry, stratigraphy and economic potential. Marine Georesources and Geotechnology, 17: 257-270.

Xu, D., 1997. Paleo-ocean events and mineralization in the Pacific. Proceedings of the 30th International Geological Congress, Vol. 13: 129-144.

Yeats, P.A. and Strain, P.M., 1990. The oxidation rate of manganese in seawater: Rate constants based on field data. Estuarine Coastal and Shelf Science, 31: 11-24.

Zachos, J., Pagani, M., Sloan, L., Thomas, E., and Billups, K., 2001. Trends, rhythms, and aberrations in global climate 65 Ma to present. Science, 292: 686-693.